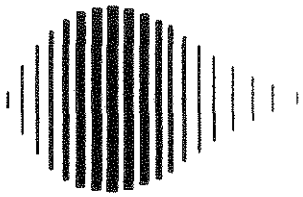

NATIONAL CENTER FOR EARTHQUAKE ENGINEERING RESEARCH

State University of New York at Buffalo

DAMAGE ASSESSMENT OF REINFORCED CONCRETE STRUCTURES IN EASTERN UNITED STATES

by

A.M. Reinhorn, M.J. Seidel, S.K. Kunnath and Y.J. Park

Department of Civil Engineering
State University of New York at Buffalo
Buffalo, New York 14260

Technical Report NCEER-88-0016

June 15, 1988

This research was conducted at the State University of New York at Buffalo and was partially supported by the National Science Foundation under Grant No. ECE 86-07591.

NOTICE

This report was prepared by the State University of New York at Buffalo as a result of research sponsored by the National Center for Earthquake Engineering Research (NCEER). Neither NCEER, associates of NCEER, its sponsors, the State University of New York at Buffalo, nor any person acting on their behalf:

a. makes any warranty, express or implied, with respect to the use of any information, apparatus, method, or process disclosed in this report or that such use may not infringe upon privately owned rights; or

b. assumes any liabilities of whatsoever kind with respect to the use of, or for damages resulting from the use of, any information, apparatus, method, or process disclosed in this report.

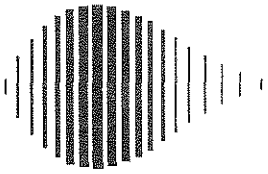

DAMAGE ASSESSMENT OF REINFORCED CONCRETE STRUCTURES IN EASTERN UNITED STATES

by

Andrei M. Reinhorn[1], Michael J. Seidel[2], Sashi K. Kunnath[3] and Young J. Park[4]

June 15, 1988

Technical Report NCEER-88-0016

NCEER Contract Numbers 86-1033 and 87-1005

NSF Master Contract Number ECE 86-07591

1 Associate Professor, Dept. of Civil Engineering, State University of New York at Buffalo
2 Research Assistant, Dept. of Civil Engineering, State University of New York at Buffalo
3 Graduate Research Assistant, Dept. of Civil Engineering, State University of New York at Buffalo
4 Senior Research Associate, Brookhaven National Laboratory

NATIONAL CENTER FOR EARTHQUAKE ENGINEERING RESEARCH
State University of New York at Buffalo
Red Jacket Quadrangle, Buffalo, NY 14261

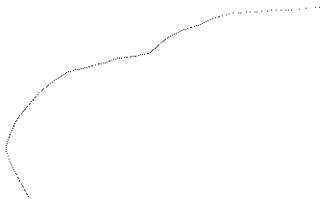

PREFACE

The National Center for Earthquake Engineering Research (NCEER) is devoted to the expansion of knowledge about earthquakes, the improvement of earthquake-resistant design, and the implementation of seismic hazard mitigation procedures to minimize loss of lives and property. Initially, the emphasis is on structures and lifelines of the types that would be found in zones of moderate seismicity, such as the eastern and central United States.

NCEER's research is being carried out in an integrated and coordinated manner following a structured program. The current research program comprises four main areas:

- Existing and New Structures
- Secondary and Protective Systems
- Lifeline Systems
- Disaster Research and Planning

This technical report pertains to Program 1, Existing and New Structures, and more specifically to Evaluation Methods and Risk Assessment.

The long term goal of research in Existing and New Structures is to develop methods for rational probabilistic risk assessment for damage or collapse of structures, mainly existing buildings, especially in regions of moderate seismicity. The work will rely on improved definitions of seismicity and site response, experimental and analytical evaluations of systems response, and more accurate assessment of risk factors. This technology will be incorporated in expert systems tools and improved code formats for existing and new structures. Methods of retrofit will also be developed. When this work is completed, it should be possible to characterize and quantify societal impact of seismic risk in various geographical regions and large municipalities. Toward this goal, the program has been divided into five components, as shown in the figure below:

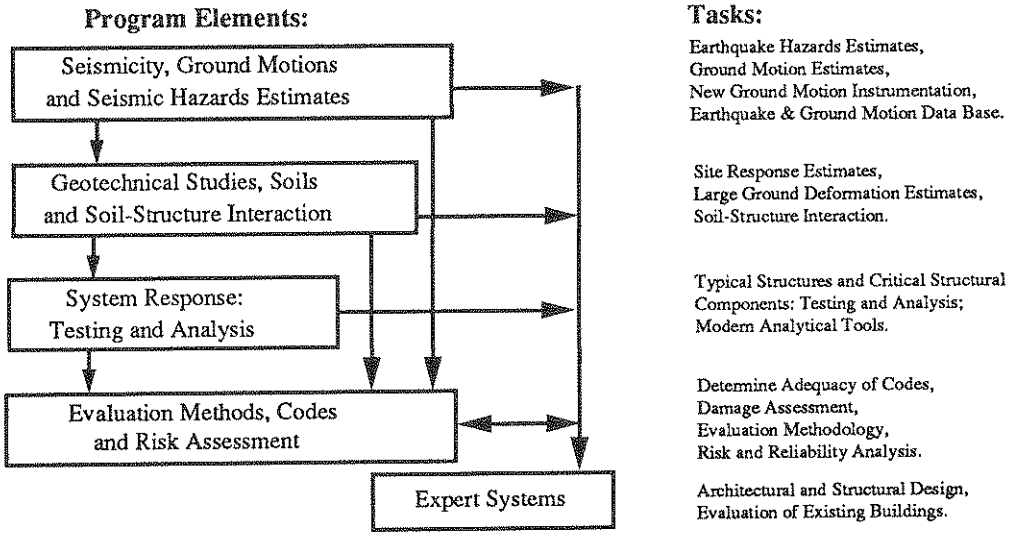

Evaluation Methods and Risk Assessment Studies constitute one of the important areas of research in Existing and New Structures. Current research activities include the following:

1. Development of a damage estimation procedure for the eastern United States.
2. Evaluation of Response Modification Factor (RMF) for buildings and bridges.
3. Development of a probabilistic procedure to determine load and resistance factors.
4. Development of procedures for the evaluation of seismic safety of buildings in zones of moderate seismicity.
5. Development of computer codes for identification of degree of building damage and for damage-based automated design.

The ultimate goal of projects concerned with Evaluation Methods and Risk Assessment is to provide practical tools for engineers to assess seismic risk to individual structures and thus, to estimate social impact.

This report studies damage assessment of reinforced concrete buildings which were not designed for earthquakes. However, novel ways are used to generate ground motions typical in the East and system response information is developed for reinforced concrete. Thus, this report covers topics belonging to three of the areas shown on the above chart.

A Monte Carlo simulation is employed using the simulated earthquakes and inelastic dynamic analyses. Empirical equations are developed to estimate the damage to frame or frame-wall structures as a function of earthquake magnitude and epicentral distances. This work represents one of several projects devoted to damage and risk assessment. The various experimental and analytical projects, as well as the projects in the seismicity area, contribute to improved risk assessment procedures. Some of these methods will be incorporated in the expert system design packages.

ABSTRACT

In recent years seismic hazard in eastern United States has become an important research topic. Based on past data, there is a very good chance that a significant earthquake will occur in eastern United States. Many cities have never adopted a seismic building code because of the low probability of occurrence of a major earthquake in eastern United States, thus there is a great deal of risk involved if an earthquake does occur.

The main objective of this research is to determine the seismic hazard associated with reinforced concrete structures in the eastern United States. The structures considered are medium to high rise, and are designed without consideration of seismic loading. The seismic hazard can be deduced from the resulting damage of the structures when they are subjected to strong ground motion.

Damage is quantified as an index which can be used to determine whether the structure is repairable, severely damaged, or collapsed. The damage of the structures is calculated using comprehensive inelastic dynamic analysis. For the purpose of this study, a Monte Carlo simulation approach has been chosen with simulated earthquake motion developed from spectral characteristics of earthquakes typical to eastern North America.

The study considered three similar test structures to determine the damage level associated with different types of designs. Two of the structures considered were frame type structures, one structure was a "weak beam" design and the other was a "weak column" design. Additionally, a coupled frame shear wall structure was

considered to determine the effect of the shear wall on the resulting damage index.

Monte Carlo simulations were performed for earthquakes with a variety of magnitudes and epicentral distances. The results of the simulations provide mean and expected maximum overall damage indices of the structures for each combination of magnitude and distance considered. Empirical equations were then developed to define the resulting damage as a function of the magnitude and epicentral distance of earthquakes. Thus, for a given structure and prescribed earthquake characteristics, the associated seismic hazard can be assessed.

ACKNOWLEDGMENTS

This report is part of the M.S. thesis of the second author prepared under the supervision of the other authors. The authors wish to express their appreciation to Mrs. Jane Stoyle from the National Center for Earthquake Engineering Research for editing and producing this report.

TABLE OF CONTENTS

TABLE OF CONTENTS (cont'd)

TABLE OF CONTENTS (cont'd)

LIST OF TABLES

LIST OF FIGURES

LIST OF FIGURES (cont'd)

CHAPTER 1

INTRODUCTION

1.1 Objectives

The main objective of this research is to assess the damage of reinforced concrete structures in the eastern United States when they are subjected to strong ground motion. There is a possibility that a strong motion earthquake will occur in the eastern United States, but because of the low probability of occurrence, most reinforced concrete structures are not designed to resist such earthquake motions. Therefore, the vulnerability of medium to high rise reinforced concrete structures, primarily designed for gravity loads and subjected to ground motion typical to eastern United States, is considered.

The correlation of the damage index with earthquake characteristics for reinforced concrete structures in eastern United States is considered because of the high risk of severe structural damage or collapse. If structural damage can be related to earthquake magnitude and distance, then an existing structure or a new design can be checked to determine the risk involved if an earthquake does happen to occur. For an economical design, some damage must be allowed, but excessive damage resulting in collapse or damage beyond repair should be avoided. The acceptable level of damage of a structure must be defined in relation to the risk involved and the frequency of occurrence of the earthquakes.

Additionally, the damageability of different types of structures is to be consid-

ered. A comparison between frame and coupled frame shear wall type structures will provide useful information on design options that can reduce seismic risk. For frame structures, the correlation between damage of weak-beam and weak-column type designs is sought. This correlation will provide information on the effect of member sizes on the overall distribution of damage in the structure, and thus the risk involved for the various designs.

1.2 Methods

The proposed method of evaluating structural damage of reinforced concrete structures is to use a Monte Carlo simulation process with generated earthquake motions, along with a rigorous inelastic dynamic analysis. Calculation of structural damage requires knowledge of dissipated energy and maximum deformation of each member in the structure. Thus a comprehensive inelastic dynamic analysis is required to accurately access the resulting damage due to earthquake motion.

The Monte Carlo technique is a method of simulating random processes to solve physical problems [16,33]. The Monte Carlo simulation process has been proposed because (1) earthquake accelerograms in eastern United States are rare, and (2) the inelastic dynamic response of a structure is highly dependent on the nature of the input motion. If the structure is subjected to two accelerograms with the same characteristics, the response using inelastic analysis will be different for each accelerogram due to the local variation in the acceleration pulses.

The Monte Carlo procedure consists of three phases of computations. First, a set of accelerograms are generated which have the same characteristics - magnitude, epicentral distance and duration. Even though the accelerograms have the same

characteristics, their actual appearance will be different. Next, inelastic dynamic analysis is performed for each of the generated accelerograms, and the resulting damage is computed. Finally, statistics of the resulting damage can be evaluated to determine the mean and expected maximum damage of the structure for the given earthquake characteristics.

Generation of artificial earthquakes typical of eastern United States has been proposed because of the absence of actual recorded accelerograms. In addition, it is a known fact that earthquakes in eastern and western United States do not have the same characteristics [24]. Therefore, the use of accelerograms recorded in western United States is not appropriate for this study. The earthquake generation procedure has been proposed as a random process with prescribed spectral characteristics. These characteristics are determined from ground motion relations for eastern North America as defined by Nuttli [23]. The resulting distribution of the damage index from the Monte Carlo simulation is assumed to be Gaussian because earthquake motion is modeled usually by an ergodic Gaussian process.

1.3 Scope

A survey of available damage models is presented first in chapter 2. Then, the damage index used to obtain the results, and the correlation of the damage index and the final state of the structure are discussed. The program used to perform the inelastic damage analysis of reinforced concrete structures, and the hysteretic behavior of reinforced concrete are presented.

The method developed for generating earthquakes typical to eastern United States is presented in chapter 3. Earthquakes are generated from spectral char-

acteristics of earthquakes in eastern United States. Seismicity in eastern United States is introduced and its relationship with the spectral characteristics is defined.

In chapter 4, three six story reinforced concrete test structures are designed. The design approach considered only gravity loads, and the earthquake resistant capacity of the structures was compared with building code provisions. An inelastic static analysis of the structures yields the failure modes and component properties. In addition, a comparison between the properties of the three test structures is made.

In chapter 5, the results of the Monte Carlo simulations are presented. Contour plots of mean damage and expected maximum damage for each of the test structures are developed as a function of magnitude and epicentral distance. The distribution of mean damage and expected maximum damage throughout the structures, and the final state of the structures are evaluated. Empirical equations are developed to estimate the overall structural damage as a function of magnitude and epicentral distance.

A discussion of the results is given in chapter 6. The correlation of damage, magnitude, and distance is developed, and regions of collapse, severe damage and repairable damage are defined. A discussion on the distribution of damage in the structure and the possible effects of local collapse is presented. Additionally, a comparison of the damageability of the different test structures is made and the seismic risk associated with each design is assessed.

CHAPTER 2

DAMAGE ANALYSIS AND STRUCTURAL MODELING

2.1 Introduction

The earthquake response of reinforced concrete structures is a complex problem that has been researched for many years. A simple method is required to describe the amount of potential damage of a reinforced concrete structure subjected to earthquake loading. This can be useful to check designs of reinforced concrete structures to determine how they will fair if they are subjected to strong ground motion. An economical design must allow some damage, but irreparable damage or collapse must be prevented. For large earthquakes that have long return periods, a certain level of damage may be allowed, but this damage should be limited to the reparable range. Damage should be kept to a minimal level for frequently occurring small earthquakes.

The modeling of a reinforced concrete structure is an important prerequisite for determining the damage due to an earthquake load. The structural model must be able to represent both frame and shear wall type structures, and accurately perform inelastic dynamic analysis. In addition to a correct representation of the structure, the hysteretic behavior of the concrete in shear and flexure must be correctly defined.

2.2 Damage Analysis/Index

In recent years, the study of the prediction of seismic damage in reinforced con-

crete structures has gained much attention. A method for predicting the damage of reinforced concrete structures would be useful both to determine the adequacy of existing structures and to aid in earthquake resistant design of new structures. Initially, the damage of reinforced concrete was related to a ductility index [22]. The ductility index is defined as the maximum deformation sustained by the structure to the corresponding yield deformation. Ductility ratios were extended to rotational and curvature ductility ratios and classified as damage indicators according to Banon et al [4]. Additionally, Banon and Veneziano [5] considered damage as a combination of a flexural damage ratio and a normalized cumulative rotation. The flexural damage ratio is related to the stiffness of the member, and the normalized cumulative rotation ratio considers cumulative rotations of the member. Stephens and Yao [37] developed a damage function to consider cumulative plastic deformations. Damage was also defined at the local and global level by Meyer and Roufaiel [21], where local damage was related to a stiffness ratio and global damage was related to the roof deformation of the structure. In all the damage models mentioned, damage has been defined by either a ductility ratio, stiffness ratio, or a cumulative rotation effect.

There are numerous additional damage models in the literature. A discussion and critical evaluation of a number of these damage models has been presented by Chung et al [12]. An additional survey of damage assessment and structural system identification has been performed by DiPasquale and Cakmak [14]. In this study, the dependence of the damage indicators on input parameters was considered, and it was shown that many of the damage indicators were statistically equivalent.

The damage model developed by Park and Ang [26] to quantify the damage

of reinforced concrete elements in terms of a damage index has been chosen for this study. Because reinforced concrete elements are damaged by a combination of stress reversals and large deformations, the damage index was developed to include maximum deformation and absorbed hysteretic energy. The damage index is defined as

$$D = \frac{\delta_m}{\delta_u} + \frac{\beta}{Q_y \delta_u} \int dE \tag{2.1}$$

where δ_m and dE are the maximum deformation and the incremental absorbed hysteretic energy, respectively, during the cyclic loading of the element, δ_u is the ultimate deformation of the member under monotonic loading and Q_y is the yield strength of the element. The parameter β defines the strength deterioration in the hysteretic behavior of the member.

The damage index expressed in equation 2.1 has been calibrated with information from the final state of various reinforced concrete structures that were subjected to strong motion earthquakes [28]. A damage index of 1.0 or greater indicates total collapse of the structure, and an index greater than 0.4 indicates the structure is generally beyond repair. The range of damage indices between 0.4 and 1.0 represent severe damage characterized by extensive crashing of the concrete and disclosure of buckled reinforcement. Damage indices just below 0.4 represent moderate damage with extensive large cracks and spalling of concrete. For smaller damage indices, the damage results in minor cracks and partial crushing of concrete in the columns. Structures with a damage index below 0.4 have a substantial reserve capacity before total collapse and some reserve capacity before irreparable damage.

The damage index for the entire structure, or for a group of members such as the columns on a given floor, can be determined by the weighted sum of the damage indices of the individual members. This is expressed as

$$D = \sum_{i=1}^{n} \lambda_i D_i \tag{2.2}$$

where λ_i is the energy ratio for the i^{th} member as defined by equation 2.3

$$\lambda_i = \frac{E_i}{\sum E_i} \tag{2.3}$$

where E_i represents the total absorbed energy of the i^{th} component under cyclic loading of the structure.

2.3 Inelastic Behavior of Reinforced Concrete

The hysteretic rule used to describe the behavior of reinforced concrete depends on the type of member being modeled. A three parameter model is used for the inelastic damage analysis performed in this study. This model is capable of modeling all types of members with the appropriate choice of parameters. Generally a trilinear envelope curve, figure 2.1, is used to describe the monotonic loading behavior of reinforced concrete. The two break points represent the cracking and yielding points of the member. Beyond the yielding point the additional load capacity is due to strain hardening of the reinforcement [38].

The three parameter model is using a parameter to control each of the following: (a) stiffness degradation, (b) pinching behavior, and (c) strength deterioration. As the maximum deformation of the reinforced concrete element increases under cyclic

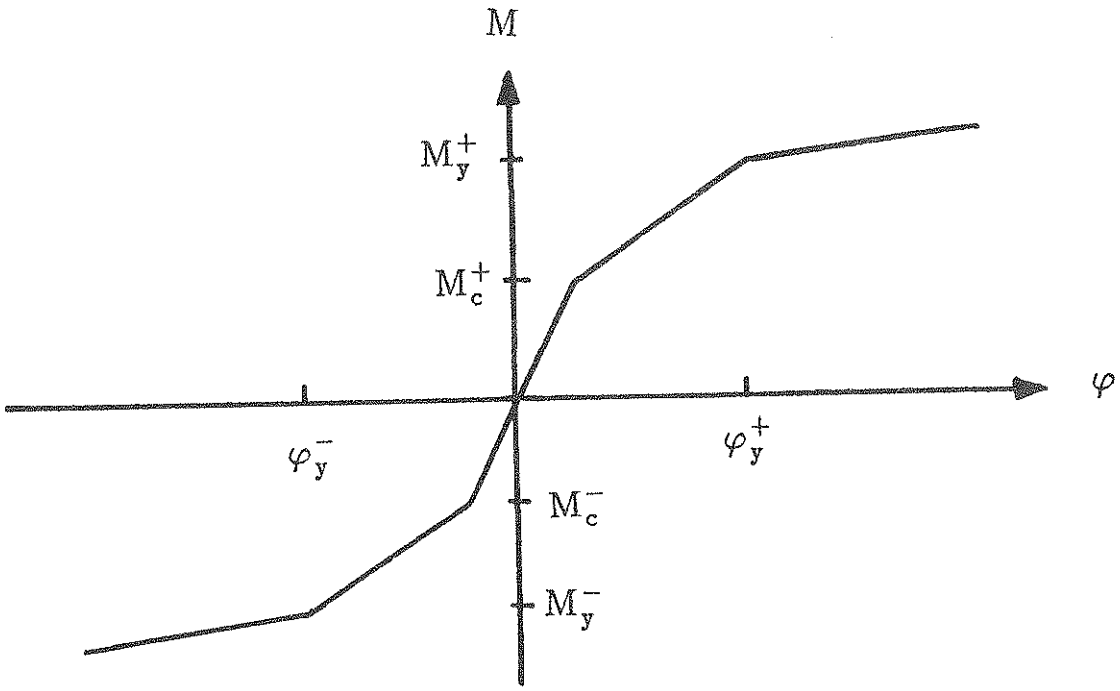

Figure 2.1
Trilinear Envelope Curve

loading, there is a trend for the stiffness of the member to reduce. The reduction of stiffness is caused by bond deterioration and cracking of the concrete around the reinforcement [31]. The energy absorbing capacity of the structure is reduced by stiffness degradation, which is accounted for by the stiffness degradation coefficient. The pinching behavior of the model is caused by the slippage of the reinforcement when there is a sudden stress reversal. When this occurs, the dissipated energy of the member is reduced, thus the hysteretic model must include this possibility. Studies of cyclic behavior of reinforced concrete members shows the maximum load capacity under cyclic loading is reduced. This deterioration of strength is partially caused by crushing and spalling of the concrete [18]. The strength deterioration parameter is used to reduce the maximum load capacity of the member as the number of cycles of inelastic load reversals increases.

2.4 IDARC - Program Organization

The inelastic damage analysis of reinforced concrete frame and shear wall structures is performed in this study by the program IDARC [25]. This program was developed to perform a complete damage analysis of a reinforced concrete structure subjected to earthquake motion. The program is organized into three phases of computations - system identification, dynamic response analysis, and damage analysis.

The first portion of the program is used for identification of the structure and its components. Input required is structural configuration, material properties and element information. The results of system identification are required for the dynamic response analysis. The system identification portion of the program determines

the component properties of the members and the fundamental natural period of the structure. An equivalent static analysis is performed using monotonic loading to determine the failure mode of the structure and the ultimate capacity of the individual members.

The dynamic analysis of the structure is evaluated using a Newmark-β algorithm to solve the equation of motion along with the three parameter hysteretic model to trace the force deformation relationship. During each step of the dynamic analysis, the total absorbed energy (used for energy ratios) and the dissipated hysteretic energy (used for damage index) of each member are updated. In addition to the energy, the maximum deformation of each member is determined.

The final portion of the program performs a comprehensive damage analysis of the structure. Damage indices for each individual member are computed. In addition, horizontal and vertical damage indices for the columns and beams on each level are produced. Finally, the overall damage index of the structure is computed.

2.5 Structural Modeling

In the program IDARC, the structure is modeled using beam, column, shear wall, edge column and transverse beam elements [42]. Many different types of reinforced concrete structures can be modeled using the appropriate combination of elements. Beams and columns are mathematically represented as flexural springs and shear walls are represented as a combination of flexural springs and shear springs. Transverse beams are represented by elastic springs with vertical and rotational degrees of freedom, and are used to interconnect the various frames. The edge columns are used to include the effect of shear walls perpendicular to the

direction of the analysis. The structure as a whole is modeled with one horizontal degree of freedom at each floor level. This is possible if the slab is treated as infinitely rigid. This assumption also makes it possible to lump the stiffness of identical frames together, thus reducing the amount of computations.

The stiffness matrix of the structure is produced using the new distribution model [25]. This model makes it possible to include the effects of local inelastic behavior of the members in the stiffness matrix. The stiffness matrix of an element is derived from the inverse of a flexibility matrix, with the flexibility distribution of the member assumed to vary linearly between the critical sections and the point of contraflexure. Critical sections are defined at the ends of the members. Thus yielding at a critical section will change the flexibility distribution in the member. Another advantage of the flexibility approach is that it can include the effect of a rigid zone at the ends of the members. This is important for reinforced concrete because of the relatively large size of the members.

During the dynamic analysis, the force deformation relationship of the critical sections of each member is traced by the three parameter hysteretic rule. When there is inelastic behavior of any member, the stiffness matrix of that member is updated to include the inelastic behavior in the response of the structure.

CHAPTER 3

GENERATION OF ARTIFICIAL EARTHQUAKES

3.1 Introduction

The number of recorded strong motion accelerograms in the eastern United States available for structural analysis and design is limited. The majority of accelerograms available have been recorded west of the Rocky Mountains, which poses a problem if the analyses of structures in the eastern United States is desired. It is also known that earthquakes in the western United States are different in many ways than their counterparts in the East [23]. A possible solution to the problem is to use artificial ground motion that has the characteristics known to earthquakes in eastern United States.

The topic of earthquake simulation has been researched for many years and numerous techniques have been developed to produce simulated earthquakes. Earthquakes have been modeled as stationary Gaussian random processes with a prescribed power spectral density function by Housner and Jennings [17]. The power spectral density function used was from actual recorded ground accelerograms. Shinozuka and Sato [35] modeled earthquake motion as a nonstationary Gaussian process. White noise has been used to generate earthquake motion by Bycroft [9]. This approach was shown to be satisfactory for engineering design purposes. Furthermore, Safak [32] has modeled earthquake motion as a band-limited, windowed, white noise process. This approach is based on the accumulation of ground motion

energy in both the time and frequency domains. The simulation of earthquakes has been extensively applied to solve problems involving earthquake response of structures.

Modeling of ground motion in the eastern United States is very important in the assessment of seismic hazards. Source scaling relations for the eastern United States were constructed by Somerville [36], and can be used for earthquake simulation. These source characteristics of the eastern United States are not fully understood, and there are some uncertainties in the relationships. Eastern United States earthquakes are known to have an energy input at higher frequencies than earthquakes in the western United States [3]. A band limited Gaussian white noise is a possible model for earthquakes that have a high frequency content. Boore [7] studied a filtered Gaussian noise to model strong ground motion, with the filter parameters based on a seismological model developed from eastern United States data.

To study the damage of structures typical in the eastern United States, it has been proposed to use a nonstationary random process with a prescribed power spectral density function to model the ground motion. The procedure requires knowledge of the power spectral density function which is characteristic of the earthquake motion being generated. Based on attenuation relations for strong ground motion in the eastern United States, a response spectrum of the ground motion can be constructed. This response spectrum can be converted to the power spectral density function characteristic to motion in the eastern United States. The duration of the strong ground motion can be determined from an expression involving the magnitude and the epicentral distance of the earthquake being generated.

3.2 Background of Earthquake Simulation

An artificial earthquake can be represented as a sum of harmonic waves with a random phase angle, and an amplitude dependent on the prescribed power spectral density function [34]. The simulation of strong ground motion consists of two steps. First, a stationary process with a zero mean is created. A stationary process is characterized by the fact that its properties do not change with time, but studies of actual accelerograms reveal that their statistical properties vary with time. Therefore, the second step in the simulation process is to convert the stationary process to a nonstationary process. This is accomplished via an intensity function. The result is a nonstationary process that resembles actual strong ground motion.

3.2.1 Formulation of Stationary Random Process

A stationary random process is created by a series of harmonic wave forms characterized by their amplitudes, frequencies and phase angles. When the harmonic waves are superimposed, they represent a stationary random process. The stationary random process, $X(t)$, is expressed as

$$X(t) = \sum_{i=1}^{n} A_i \sin(\omega_i t + \theta_i) \tag{3.1}$$

where A_i is the amplitude of the i^{th} wave form and θ_i is a random phase angle uniformly distributed between 0 and 2π. The frequency content of the process is characterized by the range of frequencies present in the summation of the harmonic waves.

The amplitude spectrum of strong ground motion earthquakes is not constant

with frequency [13]. Actually, the amplitude of each wave form is dependent on the characteristic frequency of that particular harmonic wave form. The relationship between the amplitudes and frequencies is found through the power spectral density function of the process, where the power spectral density function defines the energy per unit of time of the harmonic wave components [10].

For a single harmonic wave, $x(t) = A\sin(\omega t + \theta)$, the variance of the process is equivalent to the amplitude squared divided by two [13]. If the power spectral density function is divided into n frequency intervals according to the number of harmonic waves used in equation 3.1, then each interval contains the characteristics frequency, ω_i, of the i$^{\text{th}}$ harmonic wave. The area under the power spectral density function for a given frequency interval represents the variance of the harmonic wave with its characteristic frequency in that interval. Referring to figure 3.1, the area of the i$^{\text{th}}$ frequency interval is given by $S_x(\omega)\Delta\omega$. If this expression is set equal to the variance of the i$^{\text{th}}$ wave, $A_i^2/2$, then the amplitude of the i$^{\text{th}}$ harmonic wave is given as

$$A_i = \sqrt{2\ S_x(\omega)\Delta\omega} \tag{3.2}$$

If the upper limit of the frequency is defined as ω_u, then the frequencies of the harmonic waves are defined by,

$$\begin{aligned} \omega_i &= \left(i - \frac{1}{2}\right)\Delta\omega \\ \Delta\omega &= \frac{\omega_u}{n} \end{aligned} \tag{3.3}$$

where n is the number of harmonics prescribed in equation 3.1. The upper frequency

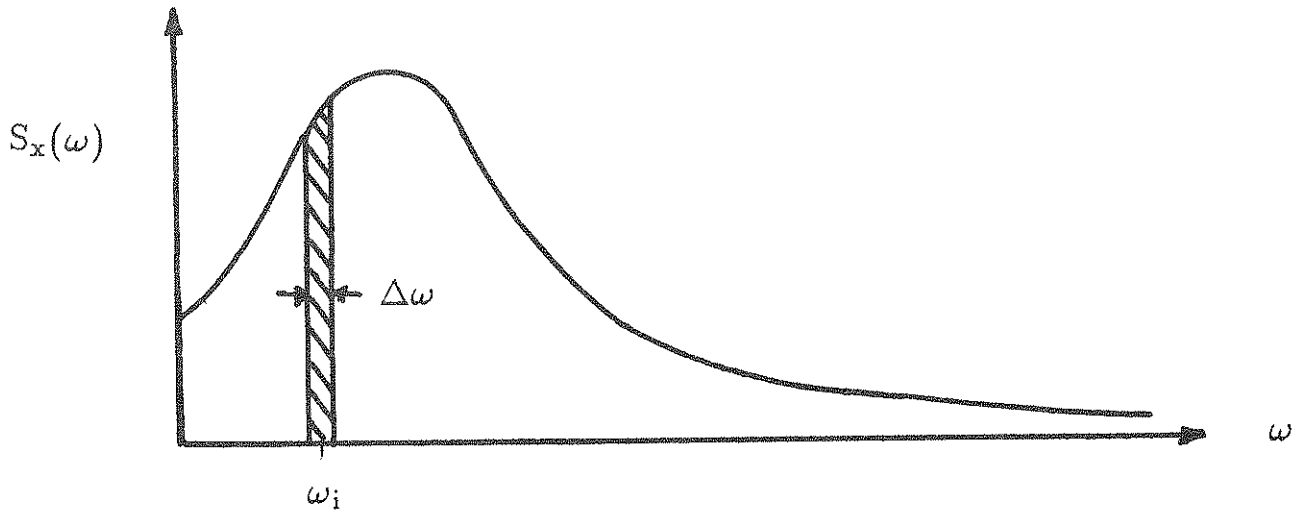

Figure 3.1
Power Spectral Density Function

of the power spectral density function shall be chosen such that the contribution of frequencies above ω_u is negligibly small.

The importance of the harmonic waves in the stationary process is dependent on the band width of the power spectral density function used to characterize the process [20]. If the power spectral density function has a narrow band, it will filter out the harmonic waves with frequencies not contained in the band. The stationary process then contains only the harmonic waves with frequencies that fall in the band of the power spectral density function. The resulting stationary process resembles a harmonic wave and not a random function. On the other hand, if the power spectral density function has a wide band, all waves with frequencies that fall in the band are present in the process. This results in a stationary process that resembles random motion.

3.2.2 Formulation of Nonstationary Random Process

Actual accelerograms are not stationary processes. In fact, they can be characterized by three distinct phases of intensity [1]. There is generally a short phase of intensity build up followed by a phase of constant intensity, after which the intensity decays in an exponential form. The stationary random process is modified by the Amin-Ang intensity function [1]. This intensity function, $I(t)$, is defined as

$$\begin{aligned} 0 \le t \le t_1 \qquad & I(t) = \left(\frac{t}{t_1}\right)^2 \\ t_1 \le t \le t_2 \qquad & I(t) = 1.0 \\ t_2 \le t \qquad & I(t) = \exp\left(\frac{-2.0(t-t_2)}{t_0}\right) \end{aligned} \tag{3.4}$$

where t_0 represents the duration of the strong ground motion, and t_1 and t_2 are taken

as $0.15t_0$ and $1.15t_0$ respectively. A plot of the intensity envelope function defined by equation 3.4 is given in figure 3.2. If the stationary random process is multiplied by the intensity function, the result is a nonstationary random process.

The procedure defined for simulation of earthquake motion can produce accelerograms with desired characteristics. The frequency content and the magnitude of the acceleration are dependent on the power spectral density function of the process. For given values of magnitude and epicentral distance, a power spectral density function can be constructed, and the duration of the strong ground motion determined. The process of earthquake simulation developed produces an accelerogram that is defined by its magnitude and epicentral distance.

3.3 Calculation of Power Spectrum

As seen in the previous section, the earthquake simulation procedure requires a power spectrum to determine the amplitude and frequency content of the generated earthquake. With the velocity response spectrum of the ground motion in eastern United States defined, section 3.4, a method has been developed by Pfaffinger [29] to calculate a response spectrum from a given power spectrum. This method will be presented in the next section.

3.3.1 Relationship Between Power Spectrum and Response Spectrum

The power spectral density function of a stationary random process can be used to characterize the process in a probabilistic sense. If the response spectrum is assumed to correspond to a stationary Gaussian process, the relationship between the response spectrum and the power spectrum can be found using a probabilistic

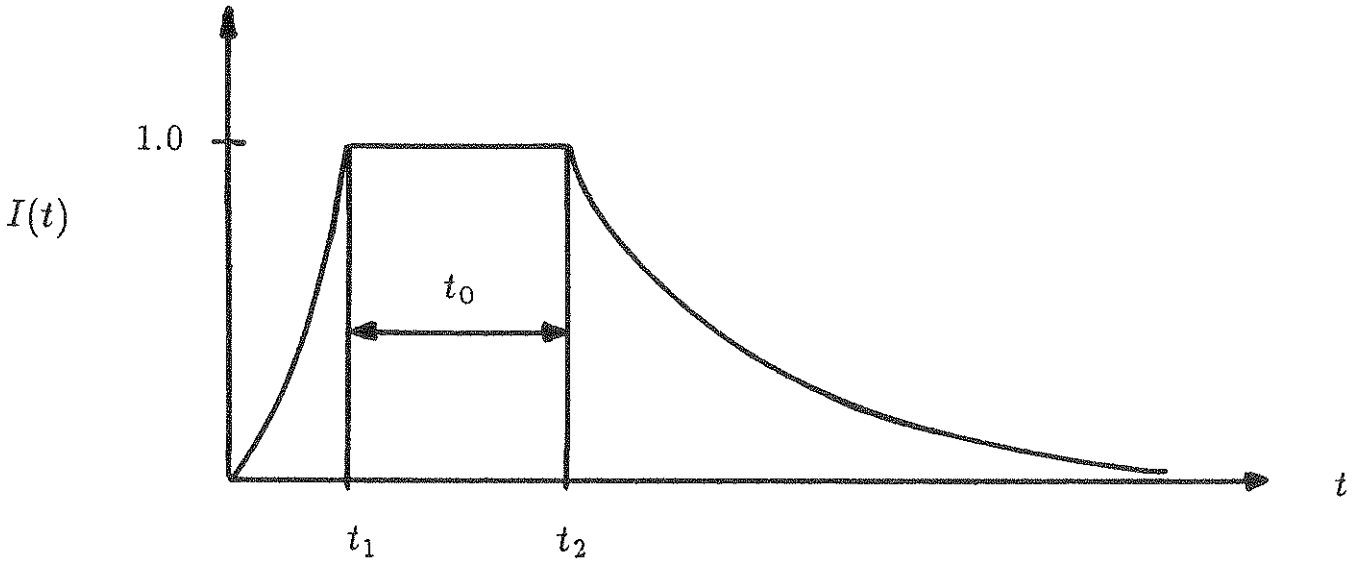

Figure 3.2
Intensity Function

approach. The probability that a random variable will fall between the limits $-x_m < x < +x_m$ is given by

$$P(x_m) = \exp(-2 f_x T_x \; e^{-1/2(x_m/\sigma_x)^2}) \tag{3.5}$$

where

$$f_x = \frac{1}{2\pi} \left(\frac{\int_0^\infty \omega^2 S_x(\omega) d\omega}{\int_0^\infty S_x(\omega) d\omega} \right)^{1/2} \tag{3.6}$$

and

$$\sigma_x = \frac{1}{2} \int_0^\infty S_x(\omega) d\omega \tag{3.7}$$

If the probability function, $P(x_m)$, is differentiated, the probability density function of maximum value, $p(x_m)$, is found. The expected extreme value of the random process is then related to the weighted average of the random process with the probability density function of maximum value as the weighting factor. The resulting expression for the maximum value of a random function is expressed in terms of the power spectral density function of the process, $S_x(\omega)$, and the duration T_x, and is expressed as

$$|x_m| = \int_0^\infty x_m p(x_m) dx_m \approx \sigma_x \left(G + \frac{\gamma}{G} \right) \tag{3.8}$$

where γ is Euler's constant, and G is defined below

$$G = \sqrt{2 \ln 2 f_x T_x} \tag{3.9}$$

Consider a single degree of freedom system excited by base motion in the form of a stationary random process. The power spectral density function of the response,

$S_q(\omega)$, is related to the power spectral density function of the input, $S_x(\omega)$, through the transfer function of the system, $H(\omega)$.

$$S_q(\omega) = |H(\omega)|^2 \; S_x(\omega) \tag{3.10}$$

The response displacement spectrum of a single degree of freedom system is defined as the maximum response of the system to a given form of excitation. If the power spectral density function of the response is known, the response spectrum is given as the maximum value of the response.

The calculation of the response spectrum from the power spectral density function of the excitation is a straightforward procedure. First, the power spectral density function of the response is found from the power spectral density function of the excitation. Then the displacement response spectrum is found from the expected maximum value, which is a function of the response power spectral density function. Thus

$$S_d(\omega, \xi) = \sigma_q \left(G + \frac{\gamma}{G} \right) \tag{3.11}$$

where q corresponds to the output process, ω and ξ are the natural frequency and damping of the SDOF system, respectively. A pseudo velocity response spectrum can easily be calculated from the displacement response spectrum.

3.3.2 Numerical Procedure

The problem at hand is the calculation of the power spectral density function from the given response spectrum. The response spectrum is related to the power spectral density function by a nonlinear equation involving integrations of the power

spectral density function, therefore a closed form solution of the power spectrum in terms of the response spectrum is not possible.

The numerical procedure developed to calculate the velocity power spectrum from the prescribed velocity response spectrum of the ground assumes that the power spectrum can be expressed as the superposition of Tajimi-Kanai power spectrums. The Tajimi-Kanai power spectrum is an approximate power spectrum used to model ground motion [20], and is expressed as

$$SX_i(\omega) = \frac{1 + 4\xi_{gi}^2(\omega/\omega_{gi})^2}{(1-(\omega/\omega_{gi})^2)^2 + 4\xi_{gi}^2(\omega/\omega_{gi})^2} \tag{3.12}$$

where ω_{gi} and ξ_{gi} are the characteristic frequency and damping of the ground respectively. For firm ground conditions, the parameters are prescribed as $\omega_{gi} = 4\pi$ and $\xi_{gi} = 0.6$ [13]. A set of Tajimi-Kanai power spectra are generated over a range of frequencies and damping values in the neighborhood of the prescribed values for firm soil conditions.

For the i^{th} Tajimi-Kanai power spectrum, $SX_i(\omega)$, the corresponding response spectrum, $RS_i(\omega)$, can be calculated based on the procedure developed by Pfaffinger [29]. With the assumption that the power spectrum of the process can be expressed as the superposition of Tajimi-Kanai power spectra, the response spectrum of the process can also be express by the superposition of the corresponding response spectra. Thus, the individual response spectra are superimposed through a set of unknown coefficients, α_i, to form a single response spectrum $RS(\omega)$.

$$RS(\omega) = \sum_{i=1}^{n} \alpha_i RS_i(\omega) \tag{3.13}$$

where n is the number of Tajimi-Kanai power spectrums desired in the superposition.

An initial estimate of the coefficients can be found by letting the superimposed response spectra, $RS(\omega)$, equal the prescribed velocity response spectrum of the ground, $S_v(\omega)$. Therefore, equation 3.13 becomes

$$\sum_{i=1}^{n} \alpha_i RS_i(\omega) = S_v(\omega) \tag{3.14}$$

Expressing equation 3.14 in matrix notation yields

$$[RS]\{\alpha\} = \{S_v(\omega)\} \tag{3.15}$$

The pseudo velocity response spectrum of the ground motion is specified at k points, where k in general does not equal n. Therefore, the order of equation 3.15 can be reduced by a least squares fit procedure, which is accomplished by premultiplying equation 3.15 by the transpose of $[RS]$. Then

$$[RS]^T[RS]\{\alpha\} = [RS]^T\{S_v(\omega)\}$$

or

$$[A]\{\alpha\} = \{B\} \tag{3.16}$$

where

$$[A] = [RS]^T[RS]$$

$$\{B\} = [RS]^T\{S_v(\omega)\}$$

Now the set of equations defined by equation 3.16 is of the order n and can be solved for the coefficients $\alpha_i, \quad i = 1, 2, \ldots, n$

With the initial values of the coefficients determined, the underlying velocity power spectrum is found by the superposition of the Tajimi-Kanai power spectra, thus

$$S_x(\omega) = \sum_{i=1}^{n} \alpha_i SX_i(\omega) \tag{3.17}$$

Generally the velocity power spectrum, $S_x(\omega)$, found from the initial estimates of the coefficients does not correspond exactly to the input velocity response spectrum. Therefore, the parameters are iteratively adjusted until the power spectrum defined by equation 3.17 produces a pseudo velocity response spectrum that is the same as the input velocity response spectrum, $S_v(\omega)$. The coefficients are adjusted by the following procedure

$$S_v(\omega) = RS(\omega) + \sum_{i=1}^{n} \frac{\partial}{\partial \alpha_i} RS(\omega)\ \Delta\alpha_i \tag{3.18}$$

and from equation 3.13 $\frac{\partial}{\partial \alpha_i} RS(\omega) = RS_i(\omega)$, therefore equation 3.18 can be express in matrix notion as

$$[RS]\{\Delta\alpha\} = \{C\} \tag{3.19}$$

where

$$\{C\} = \{S_v(\omega) - RS(\omega)\}$$

The order of equation 3.19 is reduced by the same least squares method used to find the initial values of the coefficients, and the result is a set of corrections in the coefficients α_i. The coefficients are then adjusted by the expression

$$\alpha_{i\ (\text{new})} = \alpha_{i\ (\text{old})} + \Delta\alpha_i \tag{3.20}$$

The process is repeated until superposition of the Tajimi-Kanai power spectra yields a response spectrum that is the same as the prescribed velocity response spectrum of the ground motion. An example of the fitting procedure for a magnitude of 5.7 and an epicentral distance of 20 km is shown in figure 3.3. The solid line represents the input velocity response spectrum, $S_v(\omega)$, and the symbols represent the calculated response spectrum, $RS(\omega)$.

3.4 Seismicity in Eastern United States

The procedure for the generation of earthquakes requires a power spectral density function characteristic of the earthquake record being simulated. It was shown in section 3.3 that the power spectral density function can be determined from the velocity response spectrum of the ground motion. Thus if a response spectrum typical of ground motion in the eastern United States can be defined, earthquakes can be simulated that will represent ground motion in the eastern United States.

There are many differences between the characteristics of earthquakes in the eastern and western United States [23], therefore the use of ground motion relations derived for the western United States is not adequate to describe ground motion in the east. In light of this, relationships for the peak ground motion of horizontal earthquakes in eastern North America have been developed [23]. The relationships for the peak ground motion are defined as

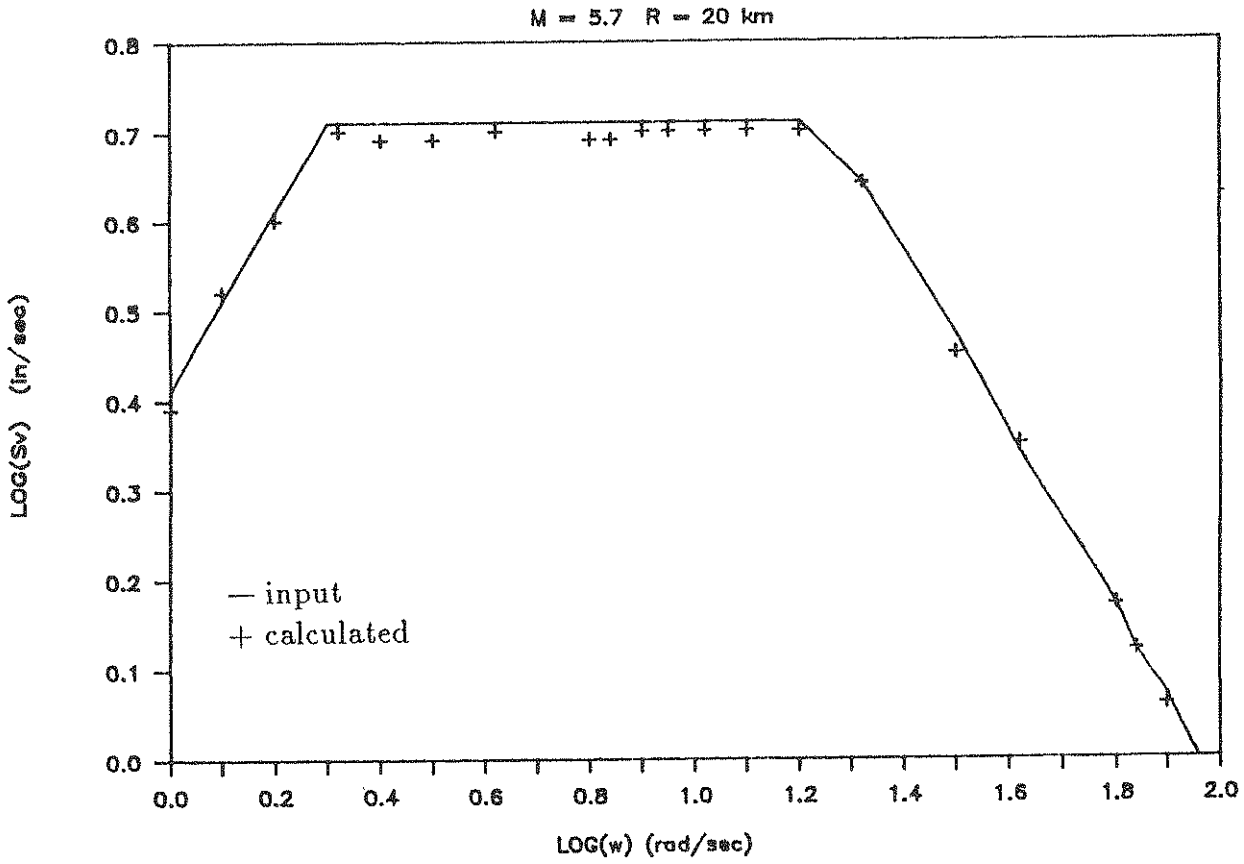

Figure 3.3
Comparison of Calculated and Given Velocity Response Spectra

$$\begin{aligned}
\log(a_h) &= \quad 0.57 + 0.50m_b - 0.83\log(R^2+h^2)^{1/2} - 0.00069R \\
\log(v_h) &= -3.60 + 1.00m_b - 0.83\log(R^2+h^2)^{1/2} - 0.00033R \\
\log(d_h) &= -6.81 + 1.50m_b - 0.83\log(R^2+h^2)^{1/2} - 0.00017R
\end{aligned} \tag{3.21}$$

where a_h is the peak ground acceleration in cm/sec^2, v_h is the peak ground velocity in cm/sec, d_h is the peak ground displacement in cm, R is the epicentral distance in km, h is the focal depth in km, and m_b is the body wave magnitude. According to Nuttli [24], for large earthquakes, the Richter magnitude, M, is synonymous to the surface wave magnitude, M_s. For earthquakes in the eastern United States, the body wave magnitude and the surface wave magnitude are related by the equation [11].

$$m_b = 2.37 + 0.6M_s \tag{3.22}$$

Unlike earthquakes in the western United States, earthquakes in the eastern United States are known not to rupture the surface of the earth. Thus a minimum focal depth must be used to calculate the peak ground motion [23].

$$\log(h) = -1.73 + 0.456m_b \tag{3.23}$$

For any set of magnitude and epicentral distance, a velocity response spectrum can be constructed to represent the motion of the earthquake. A log plot of the velocity response spectrum is given in figure 3.4. From equations 3.21, the peak ground acceleration, velocity and displacement are determined. The frequency divisions between the regions of constant displacement, velocity and acceleration

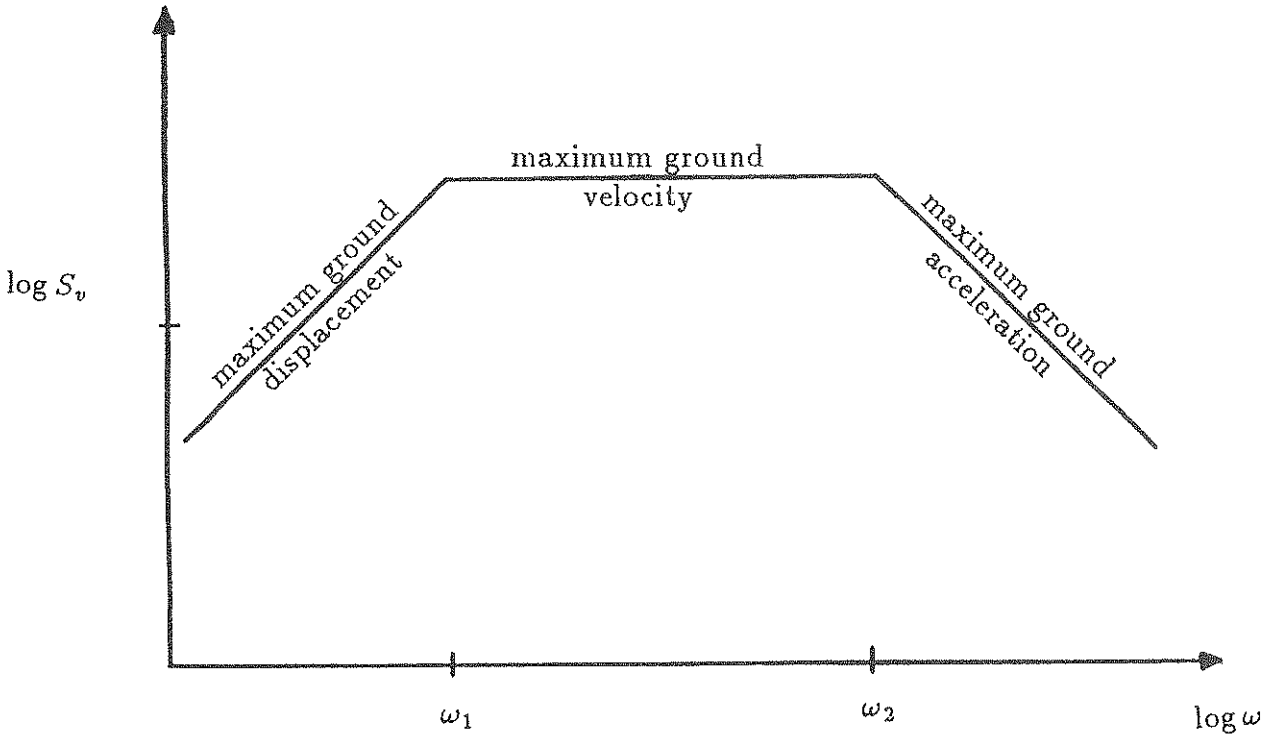

Figure 3.4
Velocity Response Spectrum

are found as

$$\omega_1 = \frac{v_h}{d_h}$$
$$\omega_2 = \frac{a_h}{v_h} \tag{3.24}$$

The velocity response spectrum, $S_v(\omega)$, is constructed from the peak ground motion and the frequency divisions defined by equations 3.24, thus

$$\begin{aligned} \omega < \omega_1 \qquad & S_v(\omega) = \omega \ d_h \\ \omega_1 < \omega < \omega_2 \qquad & S_v(\omega) = v_h \\ \omega_2 < \omega \qquad & S_v(\omega) = \frac{a_h}{\omega} \end{aligned} \tag{3.25}$$

Therefore, if the magnitude and epicentral distance of an earthquake are given, a velocity response spectrum of the ground motion can be constructed.

3.5 Duration of Strong Ground Motion

The duration of the strong ground motion has an effect on the response of a structure subjected to strong earthquake motion. The number of stress reversals the individual components of the structure will undergo is dependent on the duration of the strong ground motion. Thus the damage of the structure will depend on the duration of the strong ground motion.

The earthquake simulation procedure produces ground motion based on a given power spectral density function. In the previous sections, the power spectrum was shown to be related to the response spectrum of the ground motion, which is a function of the magnitude and epicentral distance of the earthquake being simulated. Therefore, a relationship with the duration as a function of both magnitude and

epicentral distance is desired.

There are many relationships between duration and magnitude [6,15] and between duration and epicentral distance [15,40]. A relationship for duration as a function of both magnitude and epicentral distance for earthquakes in the eastern United States is desired. Because of the lack of data on duration of earthquakes in the eastern United States, a regression analysis was performed using available data. Reference [40] presents the duration, magnitude and epicentral distance of 140 horizontal components of recorded earthquakes in California. This data was used to produce equation 3.26, which represents duration as a function of magnitude and epicentral distance.

$$t_0 = -11.321 + 3.733M + 0.079R \tag{3.26}$$

In this equation, t_0 is the strong ground motion duration in seconds required in the intensity function defined by equation 3.4. Results of the regression analysis are shown in figure 3.5.

3.6 Generation of Prototype Earthquakes

For the purpose of this study, earthquakes typical of the eastern United States with various combinations of magnitude and epicentral distance are required. Approximately 20 combinations of magnitude and distance were considered. The magnitude ranged from 4.5 to 7.0, with epicentral distances of 20, 50 and 100 kilometers for each magnitude. An infinite number of accelerograms can be produced for each combination of magnitude and epicentral distance because of the random phase

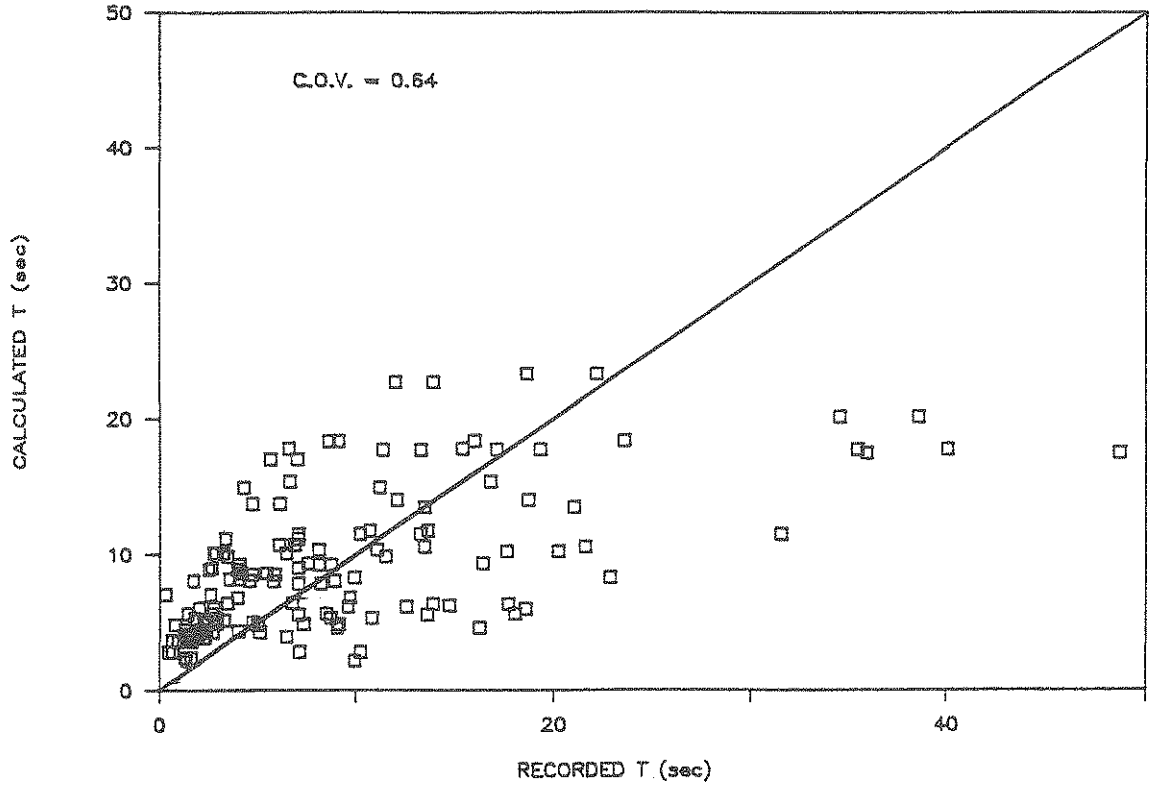

Figure 3.5
Regression Analysis for Duration

angles used in the generation process.

Velocity response spectra of the ground were produced for each combination of magnitude and epicentral distance, and then converted to velocity power spectra used to characterize the earthquakes. The frequency at which the power spectrum obtained its peak was predominately dependent on the magnitude, whereas the height of the peak was dependent on the epicentral distance. This trend is evident from a comparison of the resulting power spectral density functions for a number of combinations of magnitude and epicentral distance. Figures 3.6, 3.7 and 3.8 represent the variation of the velocity power spectra with distance for magnitudes of 5.7, 6.2 and 7.0 respectively. The energy input of the earthquakes decreases as the epicentral distance increases. This is indicated in the figures by the decrease in the peak of the power spectrum with increasing distance.

As the magnitude increased, the frequency at which the peak in the velocity power spectrum occurred decreased. For a magnitude of 5.7 the peak was at approximately 3.0 Hz, whereas the peak occurs at a frequency of 1.5 Hz for a magnitude of 7.0. Therefore, as the magnitude increases, the frequency content of the earthquakes approaches the fundamental frequency typical of medium to high rise structures.

The general appearance of the accelerograms can be summarized as follows. For a given magnitude, the peak acceleration decreases and the duration increases as the epicentral distance increases. Also, the peak acceleration increased with increasing magnitude as expected. Therefore, at large distances, the effect of low cycle fatique on the resulting damage may be important, and for short distances, the effect of excessive deformation is of primary importance in the damage of the structure.

Sample accelerograms for magnitudes of 5.7, 6.2 and 7.0 with various epicentral

distances are presented to illustrate the earthquake generation procedure. Figure 3.9 presents sample accelerograms for a magnitude of 5.7 and epicentral distances of 20, 50 and 100 km. Similarly, figures 3.10 and 3.11 present accelerograms for earthquakes with magnitudes of 6.2 and 7.0 respectively.

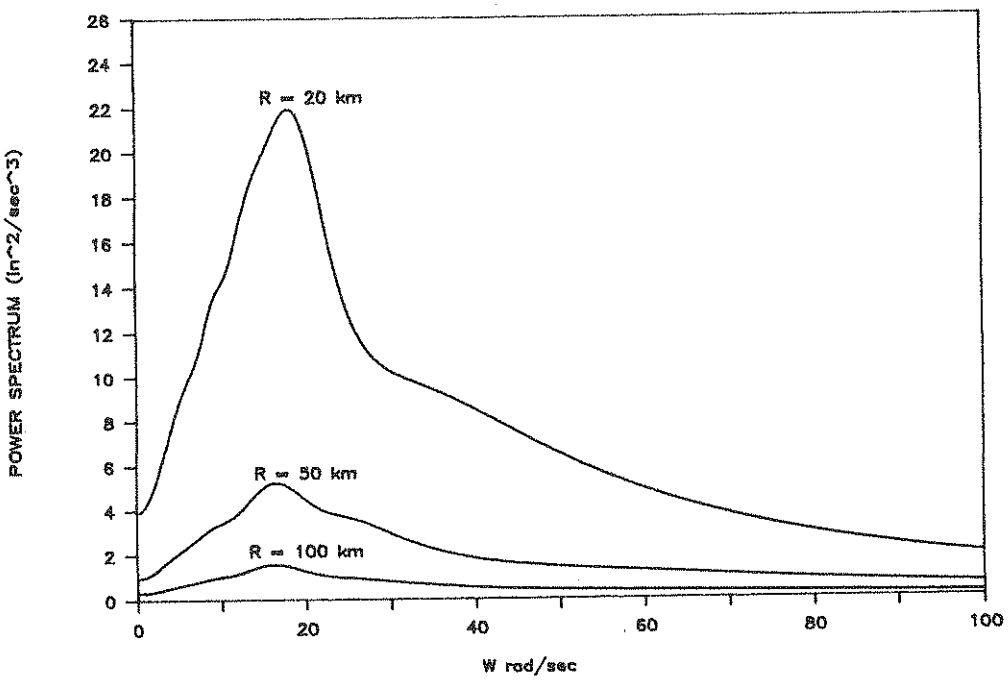

Figure 3.6
Velocity Power Spectra
Magnitude = 5.7

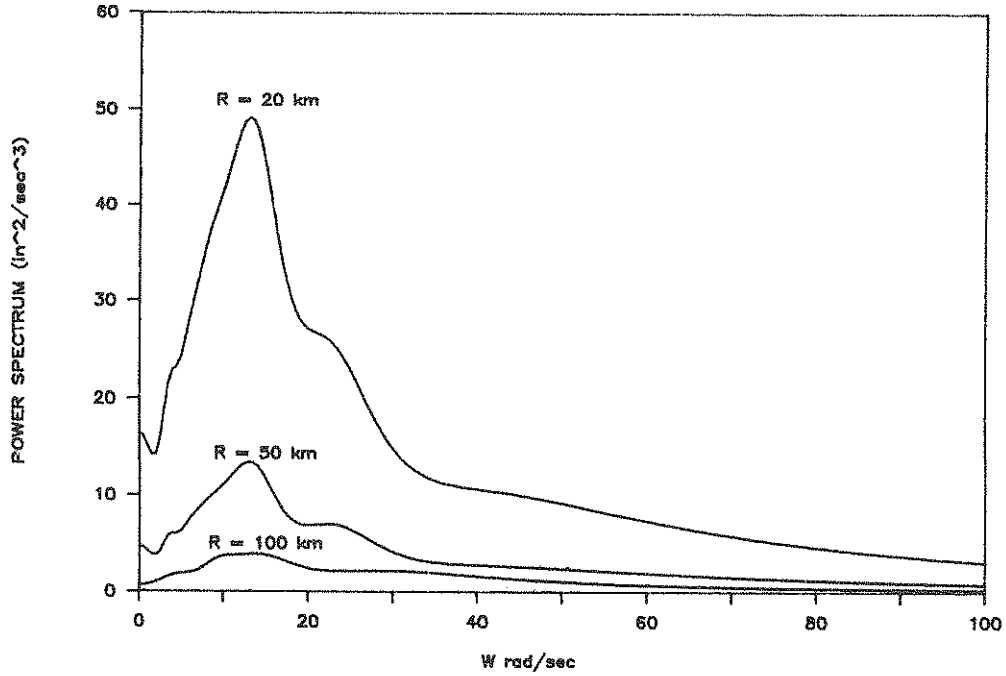

Figure 3.7
Velocity Power Spectra
Magnitude = 6.2

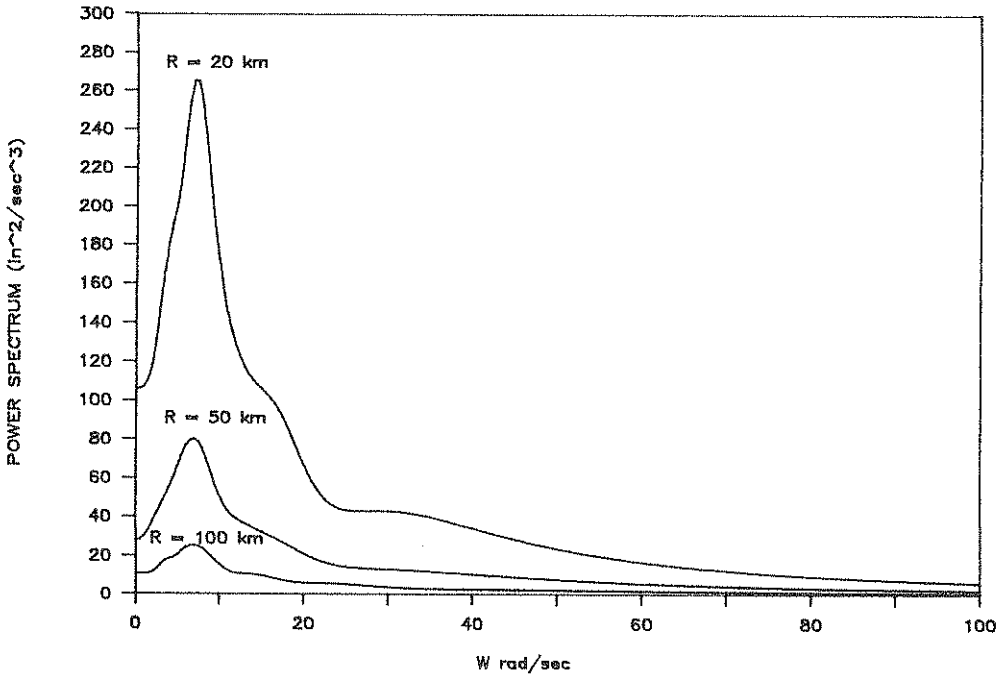

Figure 3.8
Velocity Power Spectra
Magnitude = 7.0

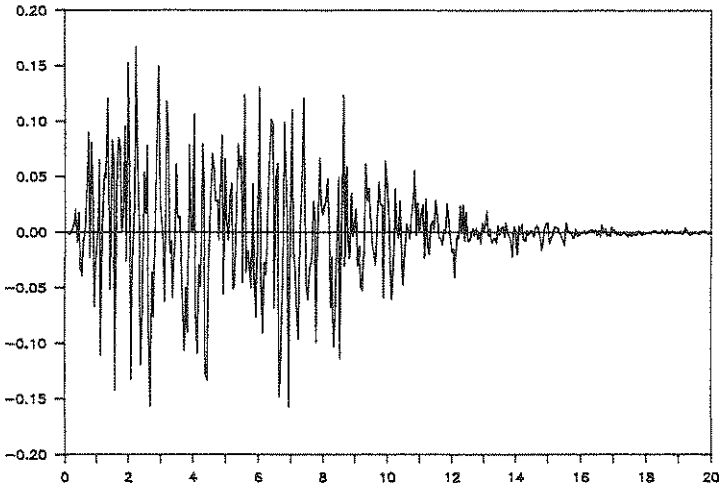

(a) Epicentral Distance = 20 km

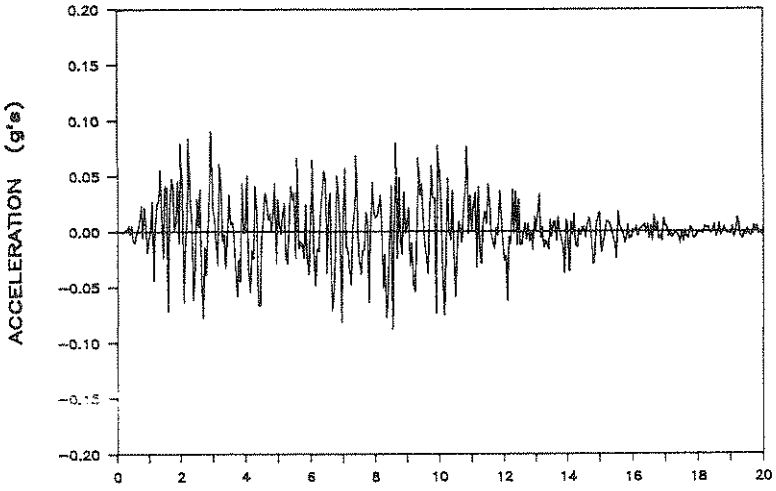

(b) Epicentral Distance = 50 km

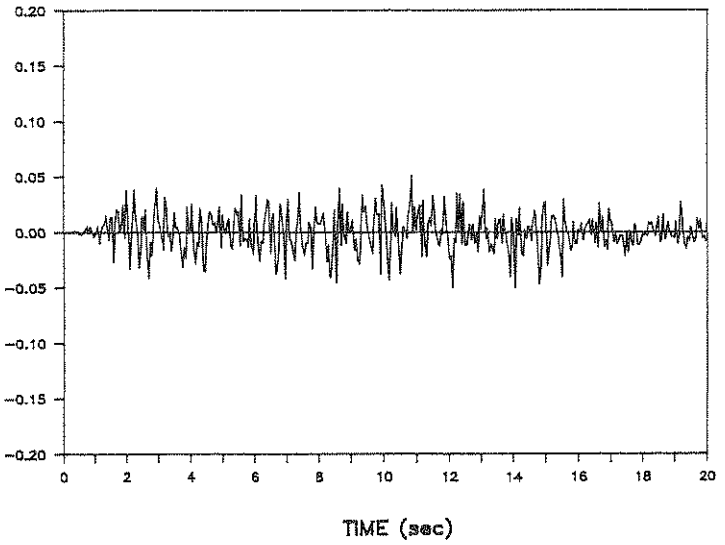

(c) Epicentral Distance = 100 km

Figure 3.9 Sample Accelerograms; Magnitude = 5.7

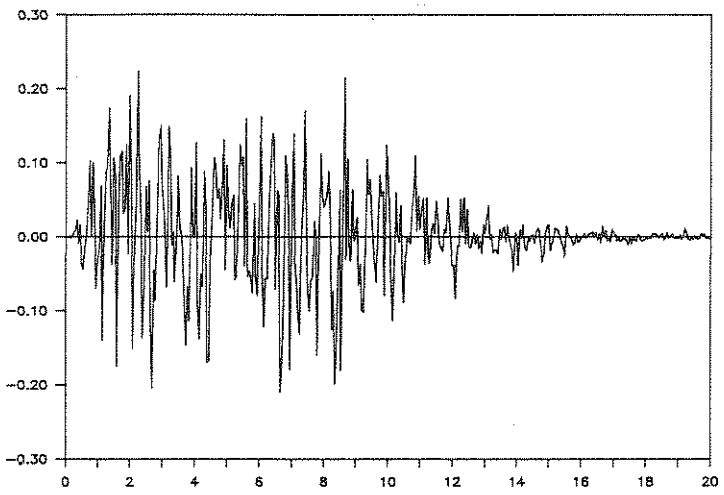

(a) Epicentral Distance = 20 km

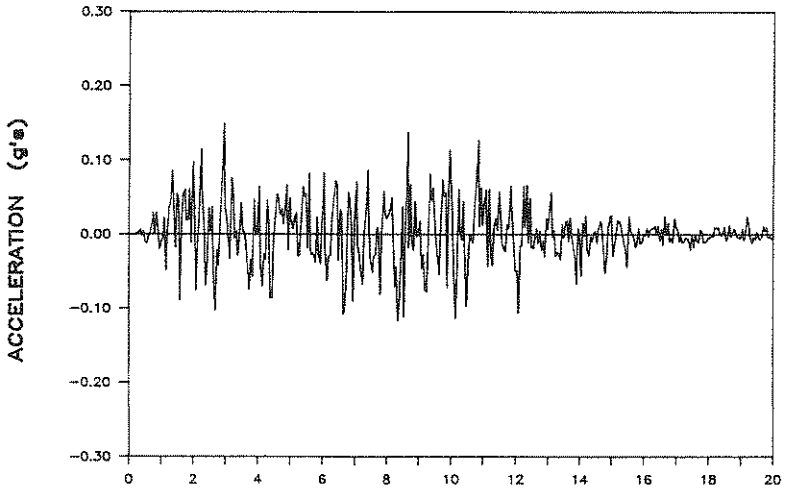

(b) Epicentral Distance = 50 km

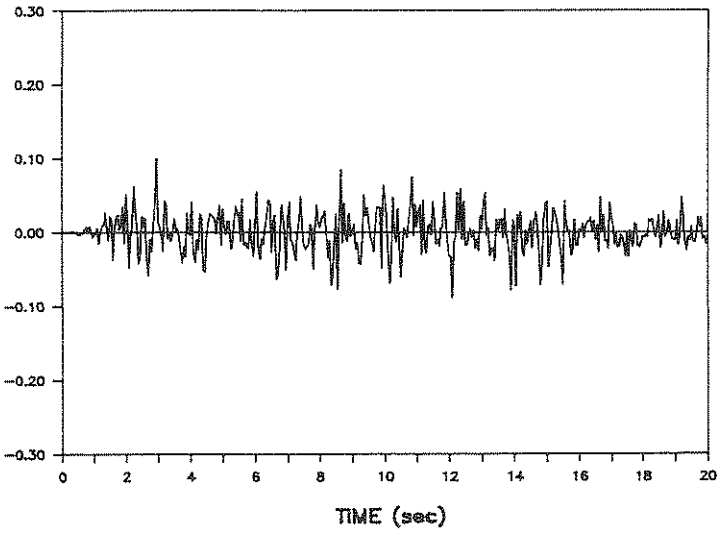

(c) Epicentral Distance = 100 km

Figure 3.10 Sample Accelerograms Magnitude = 6.2

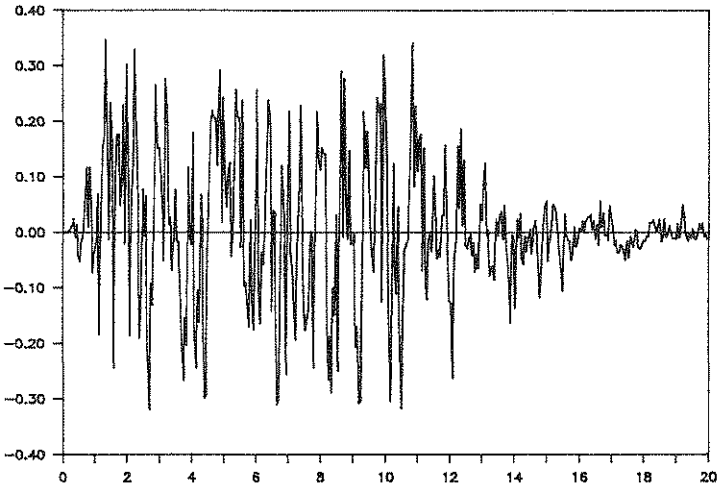

(a) Epicentral Distance = 20 km

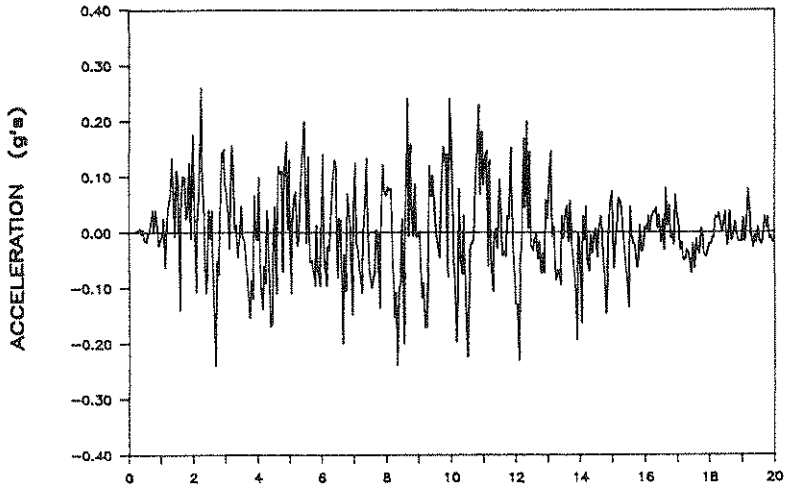

(b) Epicentral Distance = 50 km

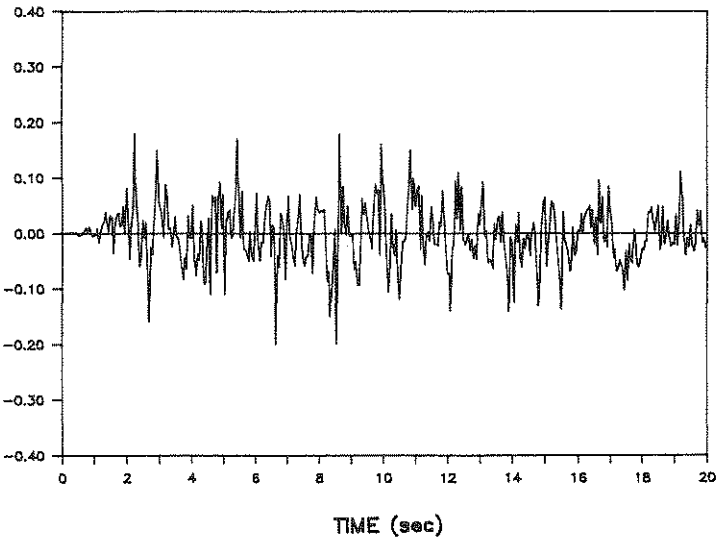

(c) Epicentral Distance = 100 km

Figure 3.11 Sample Accelerograms; Magnitude = 7.0

CHAPTER 4

TEST STRUCTURES

4.1 General

The study of seismic damageability of reinforced concrete structures typical of the eastern United States has been proposed because aseismic design of structures in this area is not a major concern to engineers. Building codes prescribe some minimum static design loads for earthquake design of structures, but do not consider actual dynamic response. Inelastic dynamic analysis of a structure is a complicated problem and is usually not considered in the design of structures, especially if the probability of occurrence of earthquakes is very small in the area of interest.

According to the Uniform Building Code (UBC), many areas in the eastern United States are in a seismic risk region of moderate to major damage [39]. A comprehensive damage analysis of reinforced concrete structures designed for these zones is considered to determine the extent of the structural damage under various size earthquakes.

4.2 Design of Test Structures

Damageability of medium to high rise reinforced concrete frame and coupled frame-shear wall structures to earthquake motion typical of eastern United States is considered. Three structures have been designed primarily for gravity loads according to the ACI 318/83 code [8]. After the designs were completed, a check was

performed to determine the seismic capacity of the structures according to the UBC [39] and ATC [2] specifications. The three test structures are (1) frame structure with "weak columns", (2) frame structure with "weak beams", and (3) coupled frame-shear wall structure.

All three test structures were designed for general office space with a uniform dead load of 100 psf. The concrete used is specified to have a 28 day compressive strength of 3000 psi. All reinforcement is prescribed as grade 40 deformed bars, with the ultimate strength taken as 70,000 psi.

4.2.1 Floor Plan and Elevations

Both of the frame structures, "weak column" and "weak beam", have the same structural configuration. The structures are six stories with a rectangular floor plan 89 feet by 125 feet. Story height is 12 feet and the overall structure height is 72 feet. A typical floor plan and elevation are given in figure 4.1. The direction of the earthquake loading is presumed to be in the longitudinal direction, which consists of four rigid parallel frames each with five bays.

The floor plan and elevation of the coupled frame-shear wall structure are shown in figure 4.2. The configuration of the structure is identical to the frame structures except for the addition of two shear walls in the principal direction of the earthquake analysis. Additionally, there are four shear walls in the direction transverse to the earthquake motion.

4.2.2 Member Sizes and Reinforcement

For frame structure I (weak columns) and the coupled frame shear wall structure, the slab was designed with a thickness of 9 inches to meet the ACI requirements

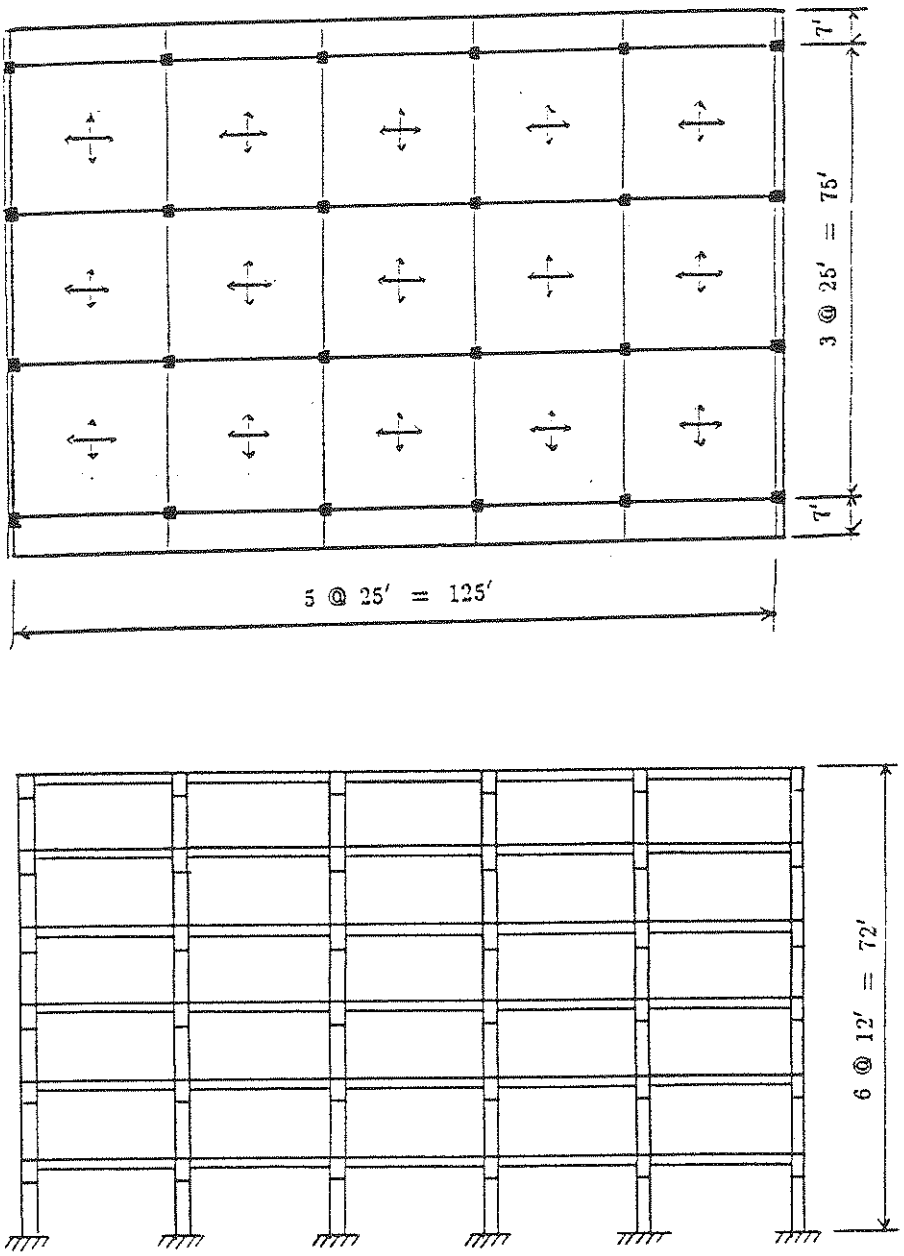

Figure 4.1
Floor plan and elevation
Frame structure I & Frame structure II

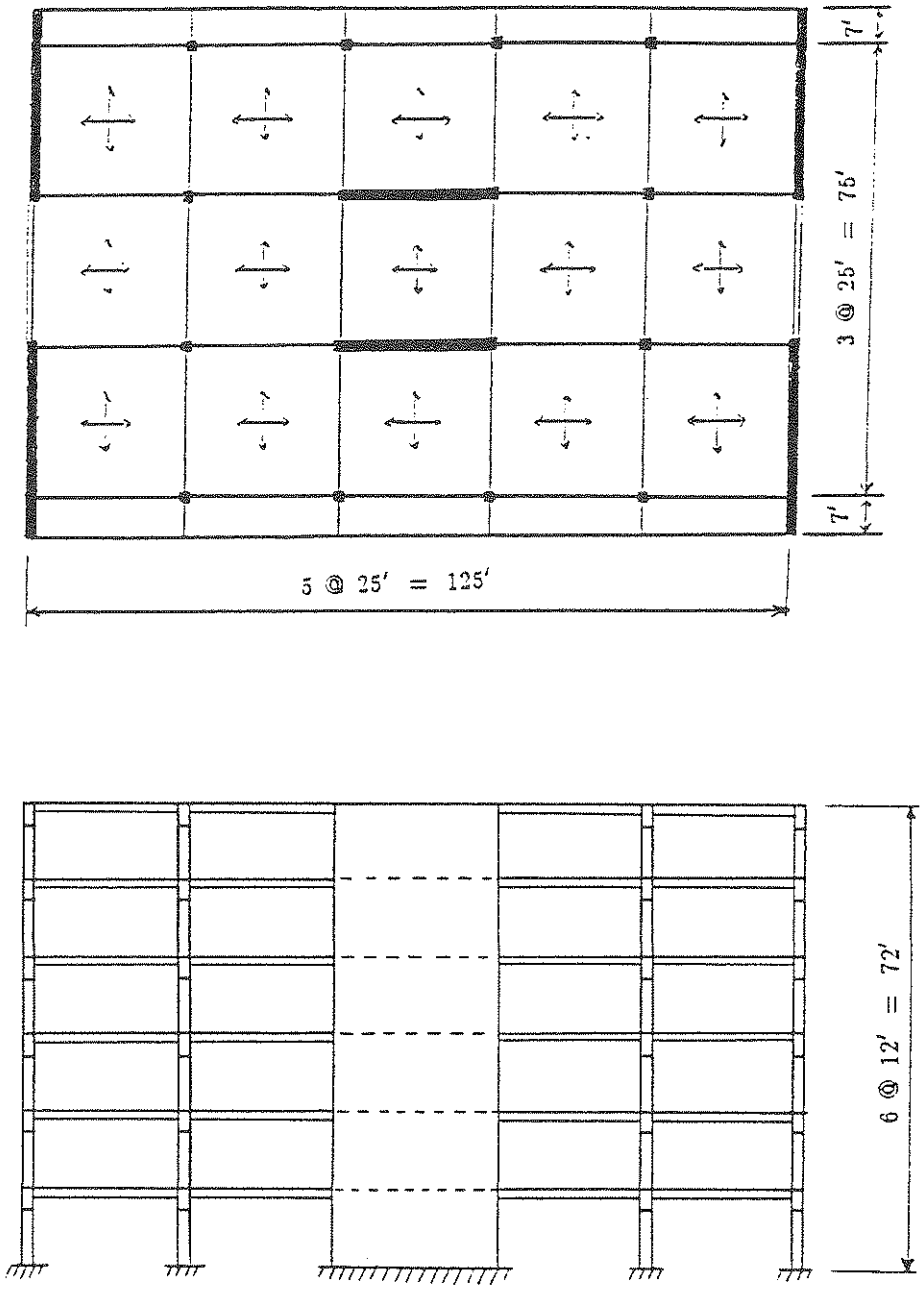

Figure 4.2
Floor plan and elevation
Shear wall structure

for deflection control. Positive moment reinforcement for the slab is #4 bars spaced at 4 inches, and negative moment reinforcement is #4 bars spaced at 3 inches. In both cases the slab has a minimum cover of 3/4 inch.

The beams of frame structure I and the coupled frame shear wall structure are identical. Beams were designed as tee sections considering the effective width of the slab, and resulted in a 15 x 21 section extending below the slab. Design moments were calculated according to the ACI approximate methods of frame analysis. For use in the dynamic analysis, section properties need to be specified at the critical sections of the member, i.e. at the ends. Design for positive moment was performed and one third of the positive reinforcement was extended to the ends of the member according to ACI code provisions. Shear reinforcement at the ends is specified as # 3 stirrups spaced at 3 inches. The resulting section has a web reinforcement ratio of 0.24% and a confinement ratio of 0.88%. The confinement ratio is defined as the ratio of the volume of the stirrups to the volume of the core, and the web reinforcement ratio is the ratio of the stirrup area to the area of the core. A cross section detail of the beam slab system is given in figure 4.3.

For frame structure II (weak beams), the slab thickness and the beam depth were reduced without causing excessive deformations. The slab thickness was reduced from 9 inches to 7 inches. The negative and positive moment reinforcement are #8 bars spaced at 10 inches and #6 bars spaced at 12 inches respectively. The beam was redesigned as a 15 x 19 section extending below the slab with the same shear reinforcement as the strong beams. Figure 4.4 shows a section detail of the reduced beam slab system. The resulting section has web reinforcement ratio of 0.49% and a confinement ratio of 1.05%.

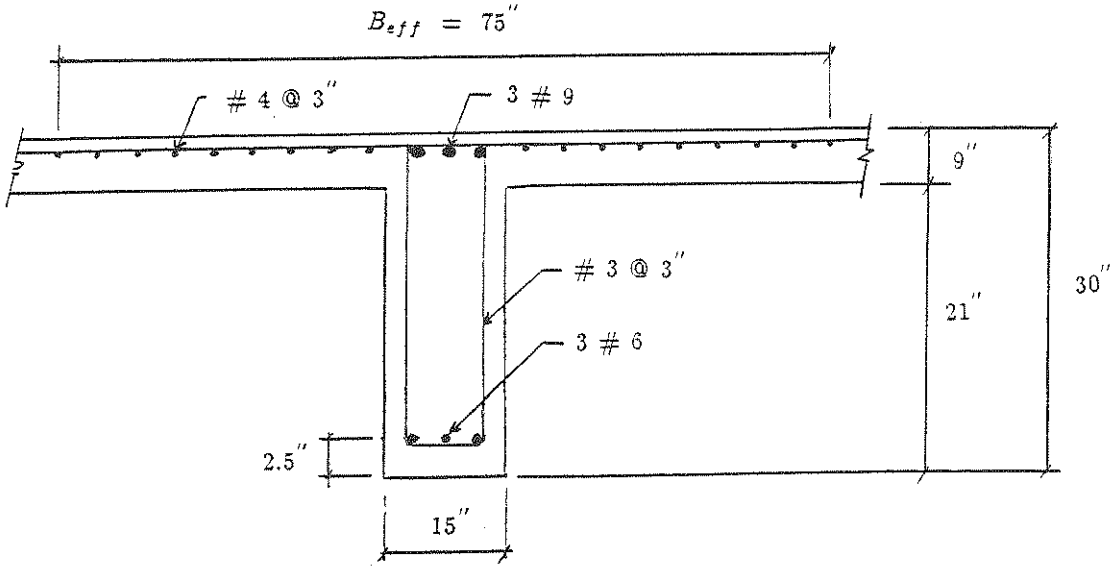

Figure 4.3
Dimensions and reinforcement of beam slab system
Frame structure I & Shear wall structure

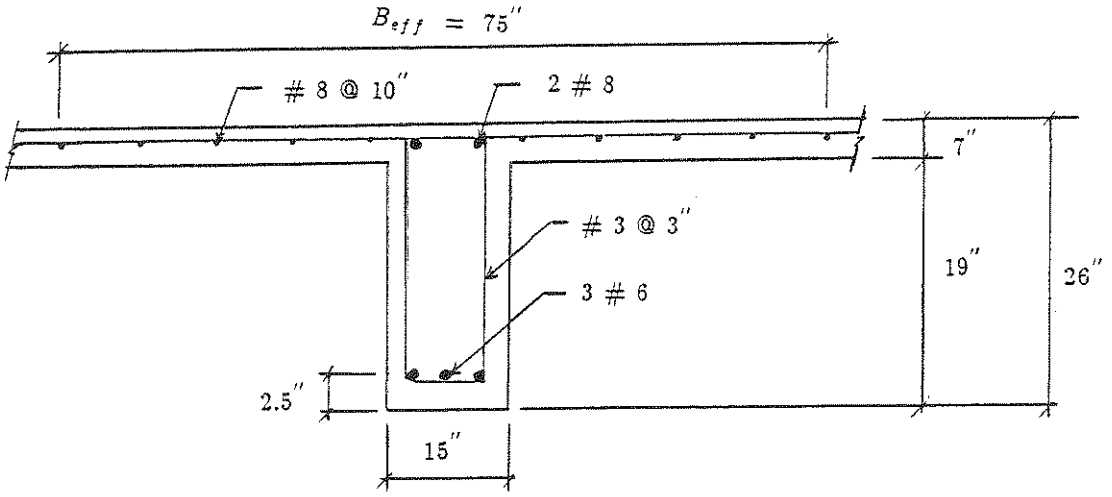

Figure 4.4
Dimensions and reinforcement of beam slab system
Frame structure II

Columns were designed as square with tied lateral reinforcement. The first three levels were divided into exterior columns and interior columns. Exterior columns are defined as the columns at the ends of the frame, and were designed differently from interior columns because of the large difference in axial load. All the columns on the top three floors are identical, and were designed for the axial load of the interior columns on their respective floors. Column sizes were generally constant for two floor levels and the reinforcement was varied to account for the change in axial load. Figure 4.5 gives column dimensions and reinforcement of all the columns.

The shear walls were designed with a thickness of 6 inches and a reinforcement ratio of 0.25% in both the vertical and horizontal directions. Edge columns of the shear wall were designed as 18 inch square tied columns. The dimensions and reinforcement details of the shear walls and edge columns are presented in figure 4.6. The shear wall properties were assumed to be uniform throughout the height of the structure.

4.2.3 Comparison of Test Structures

The member sizes and properties of the beams and columns of frame structure I and the coupled frame-shear wall structure are identical. Thus the effect of the shear wall can be directly assessed from a comparison of the results of the two structures. To study the effect of weak beams on the distribution of damage, frame structure II was designed with identical columns, but with reduced beam size.

An equivalent earthquake load analysis was performed to determine the earthquake resistant capacity of the structures according to code specifications. The Uniform Building Code defines earthquake activity in terms of seismic zones based

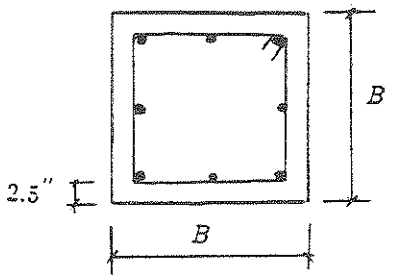

Story	Exterior			Interior		
	B	reinf.	ties	B	reinf.	ties
6	16	8 # 8	# 3 @ 16	16	8 # 8	# 3 @ 16
5	16	8 # 8	# 3 @ 16	16	8 # 8	# 3 @ 16
4	18	8 # 8	# 3 @ 16	18	8 # 8	# 3 @ 16
3	18	8 # 9	# 3 @ 18	20	8 # 14	# 4 @ 20
2	20	8 # 9	# 3 @ 18	24	8 # 14	# 4 @ 24
1	20	8 # 10	# 3 @ 20	24	8 # 14	# 4 @ 24

Figure 4.5
Column Dimensions and Reinforcement

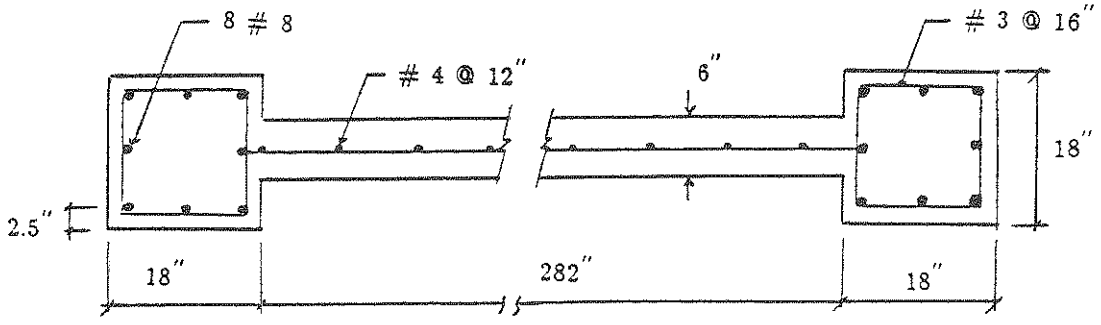

Figure 4.6
Shear Wall Dimensions and Reinforcement

on seismic risk. These zones range from 0 to 4, with 0 representing the minimum risk [39]. The structures were analyzed with lateral loads as defined by the UBC code using elastic frame analysis. The resulting moments were checked against the member capacities, with interaction of bending and axial load in the columns considered. The results showed the structures satisfied the loads corresponding to seismic zone 2. According to the UBC seismic zone map of the United States, seismic zone 2 is present in much of the eastern United States.

The Applied Technology Council (ATC) defines earthquake loading through the use of a seismicity index and a seismic design coefficient [2]. The seismic design coefficient is defined as the ratio of the total base shear force to the dead weight of the structure. A seismic design coefficient of 0.04 produces a base shear equivalent to that obtained for seismic zone 2 as defined by UBC.

According to the ATC specification, the seismicity index is used to characterize the expected severity of the earthquake ground motion. This index ranges from 1 to 4, with 4 representing the most severe ground motion expected [2]. For the structures considered, a seismicity index of 2 corresponds to a seismic design coefficient of 0.04. Much of the eastern United States is in the region characterized by a seismicity index of 2.

4.3 Structural Modeling

The structures were modeled using the various elements types available in IDARC as described in section 2.5. For the purpose of dynamic analysis, only the dead load of the structure was considered. A load factor of 1.1 was used to account for additional dead load not considered. The earthquake loading was presumed to

act in the long direction for all of the test structures.

4.3.1 IDARC Model

Both of the frame structures and the shear wall structure were modeled with two independent frames. Each structure consisted of two exterior frames and two interior frames. For the frame structures, the only difference between the exterior and interior frames was the loading, but for the shear wall structure, the interior frame was modeled with a shear wall element in its center bay. Additionally, the exterior columns of the shear wall structure were modeled as edge columns to include the effect of the transverse shear walls.

Columns were modeled with a rigid zone of 15 inches corresponding to one half of the beam depth. Only the ends of the columns on the first floor were modeled without rigid zones because of their attachment to the foundation. All the beams were modeled with a rigid zone of 10 inches corresponding to an average column width. The torsional properties of the transverse beams were calculated according to the properties of the beams in the principal direction. Beams in both directions were assumed to be identical because the span length in both directions are equal.

4.3.2 Hysteretic Properties

The hysteretic behavior of reinforced concrete was defined independently for shear and flexure. For both hysteretic rules, the post yielding stiffness was taken as 1% of the initial elastic stiffness of the member.

The three parameter hysteretic model used in IDARC requires the specification of three parameters. For the flexural hysteretic rule, the stiffness degradation coefficient was taken as 2.0. This value will reduce the stiffness, and in turn the area

of the hysteresis loops, as the cyclic behavior of the member increases. Thus as the cyclic loading progresses, the capacity of the member to dissipate energy is reduced. The pinching behavior of the reinforced concrete was not presently considered in the analysis. The strength deterioration properties of the individual members was calculated from the system identification portion of IDARC. For both the strong and weak beams, the strength deterioration parameter was 0.012. The strength deterioration of columns ranged from 0.018 to 0.107, with the lower limit of the strength deterioration parameter associated with the columns on the top floor, and the upper limit associated with the columns on the first floor. A typical hysteretic rule for a flexural element is shown in figure 4.7.

The shear behavior of the reinforced concrete was modeled with an origin oriented hysteretic rule. Once again no slipping of the reinforcement was allowed and the strength deterioration parameter was determined by the program. The resulting value of the strength deterioration parameter for the shear walls was 0.10, and the values for the columns and the beams were the same as frame structure I. Figure 4.8 shows a typical plot of the hysteretic behavior of the shear walls.

4.4 Failure Modes

The results of the system identification portion of IDARC yields the fundamental natural period, the base shear coefficient, and the ultimate failure mode of the structure. The base shear coefficient is defined as the shear force at the base divided by the weight of the structure. It is determined by applying a monotonic loading (triangular distribution) and performing inelastic analysis until the top deformation exceeds 2% of the structure's height. By this point, the structure has generally

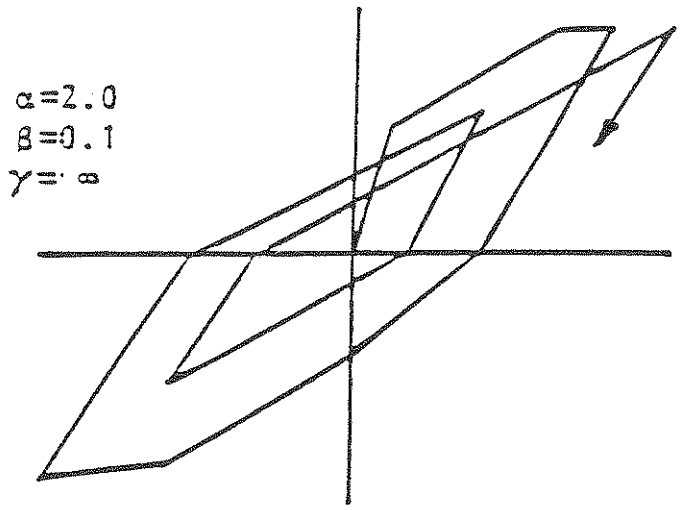

Figure 4.7
Hysteretic rule for flexure

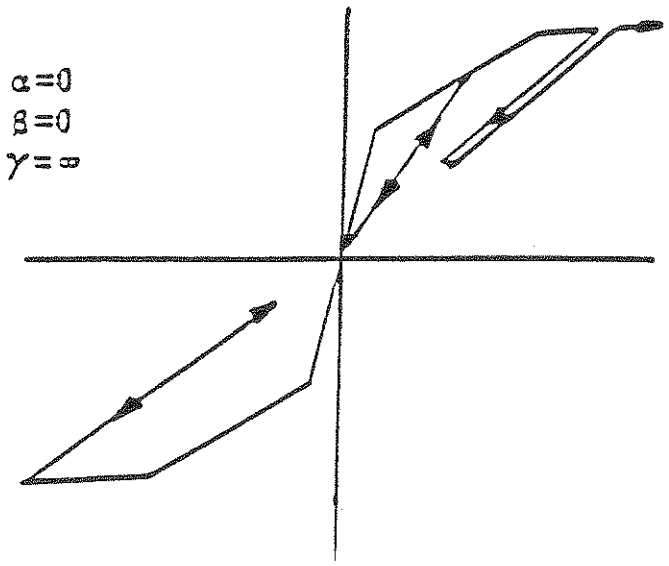

Figure 4.8
Hysteretic rule for shear

yielded and reached its ultimate capacity. The failure mode of the structure is thus defined when the top deformation exceeds 2% of the overall height of the structure.

4.4.1 Frame Structure I

Frame structure I was found to have a fundamental natural period of 0.801 seconds. A plot of the base shear coefficient versus the overall top deformation is given in figure 4.9(a). From the plot, it is evident that the maximum base shear coefficient of frame structure I is approximately 0.15. Figure 4.10 shows the failure mode of the structure when the top deformation is approximately 1% of the structure's height. Both the exterior and interior frames showed identical behavior. Generally all the beams on the first three floors yielded at their ends, whereas the columns remained elastic except at the foundation where they yielded.

The columns on the upper floors were generally much smaller than the columns at the base because the structure was designed for gravity loads. This resulted in almost a complete panel mechanism on the fifth floor with all the columns yielding at both ends, except the two exterior columns. Most likely, this mechanism developed completely at the next loading step because the next increment of load caused the top deformation to increase from 1% to over 2% of the structure's height. It is also interesting to note that the top story of both frames remained completely elastic.

4.4.2 Frame Structure II

The reduced beam size did not significantly change the fundamental natural period or the base shear coefficient. Again, the failure modes of the two frames were almost identical, but were slightly different from the failure modes of frame structure I. Plots of the failure modes of frame structure II are shown in figure

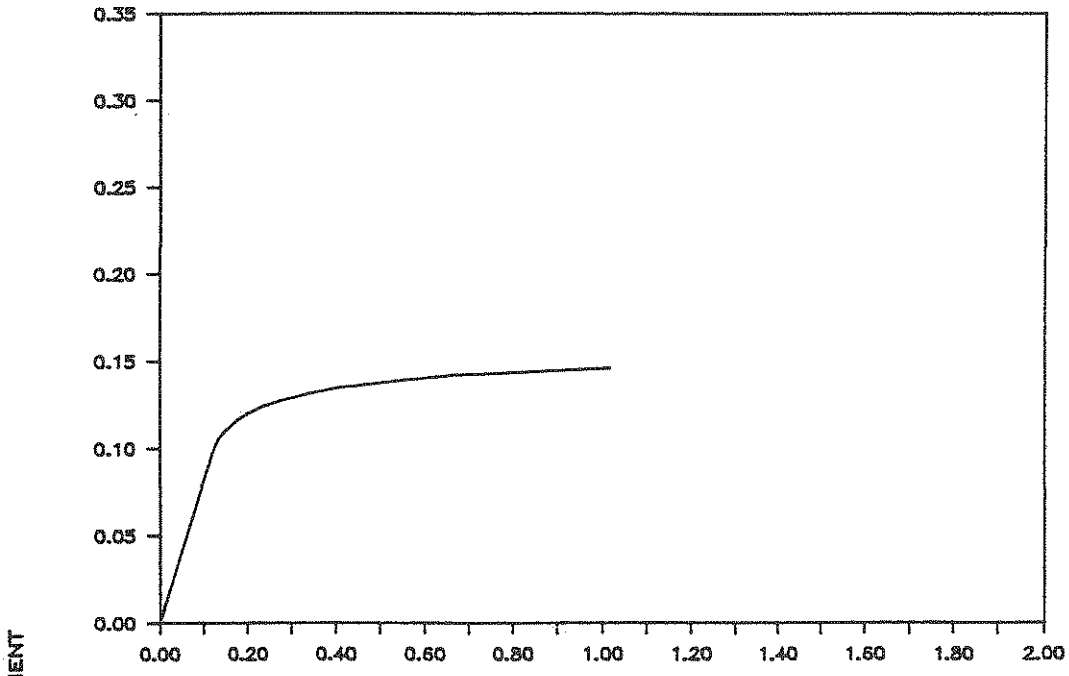

(a) Frame Structure I

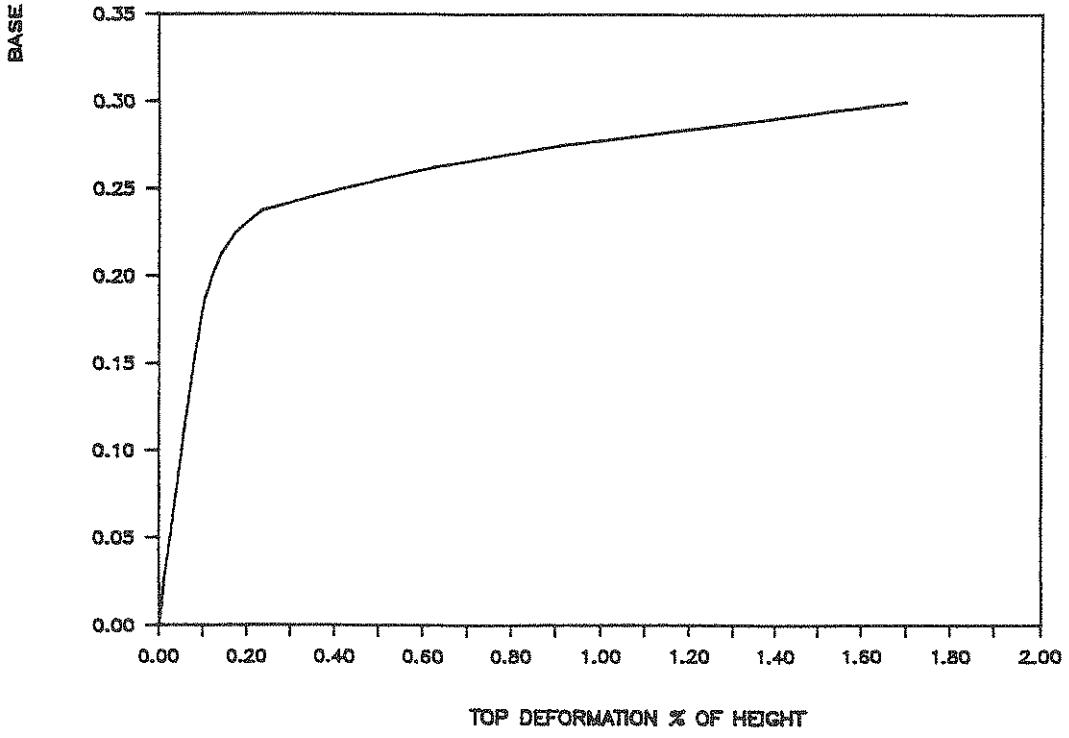

(b) Shear Wall Structure

Figure 4.9 Plots of Base Shear Coefficient

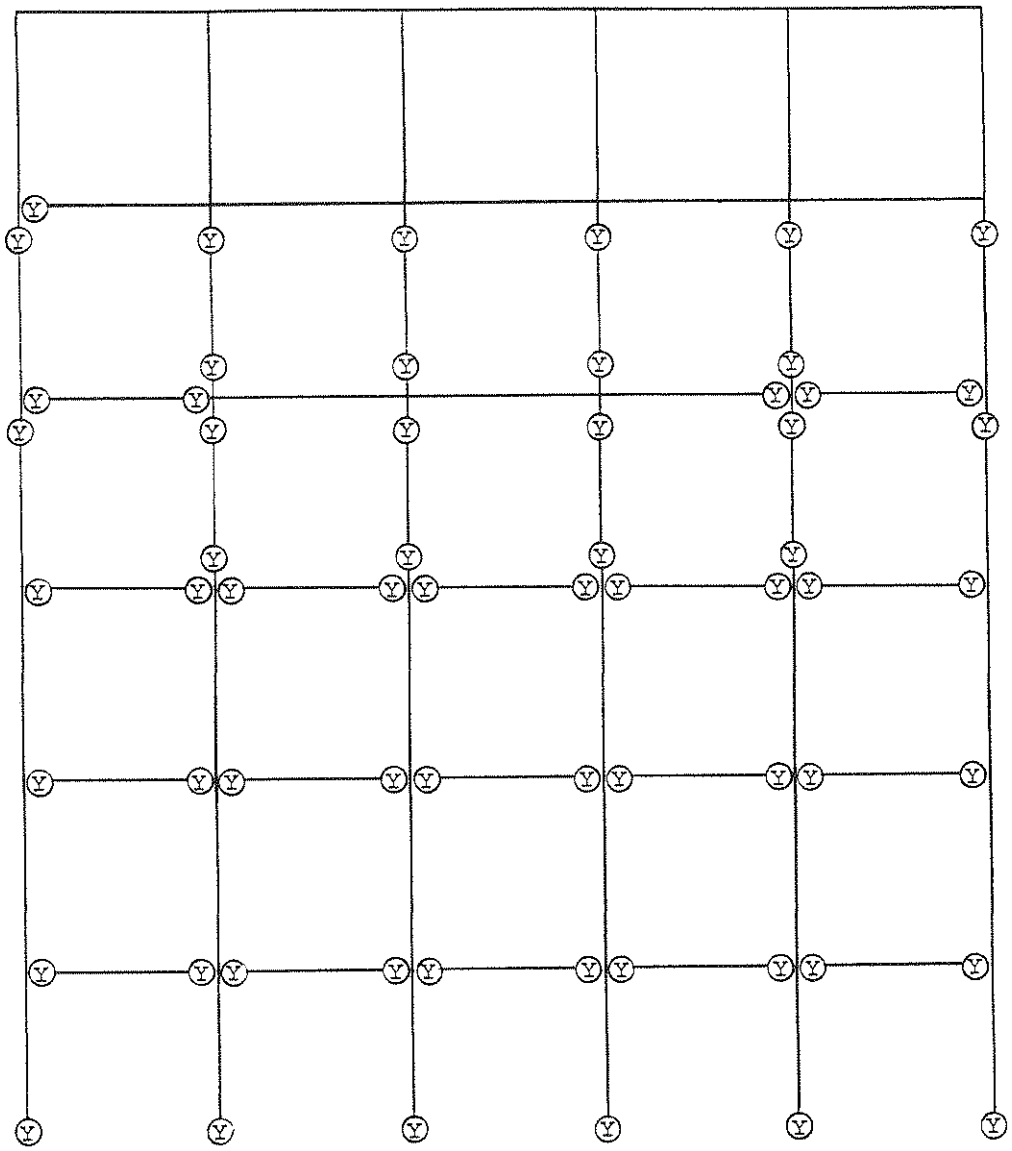

NOTATION:

⊗ = CRACK

Ⓨ = YIELD

Figure 4.10 (a)
Failure Mode of Exterior Frame
Frame Structure I

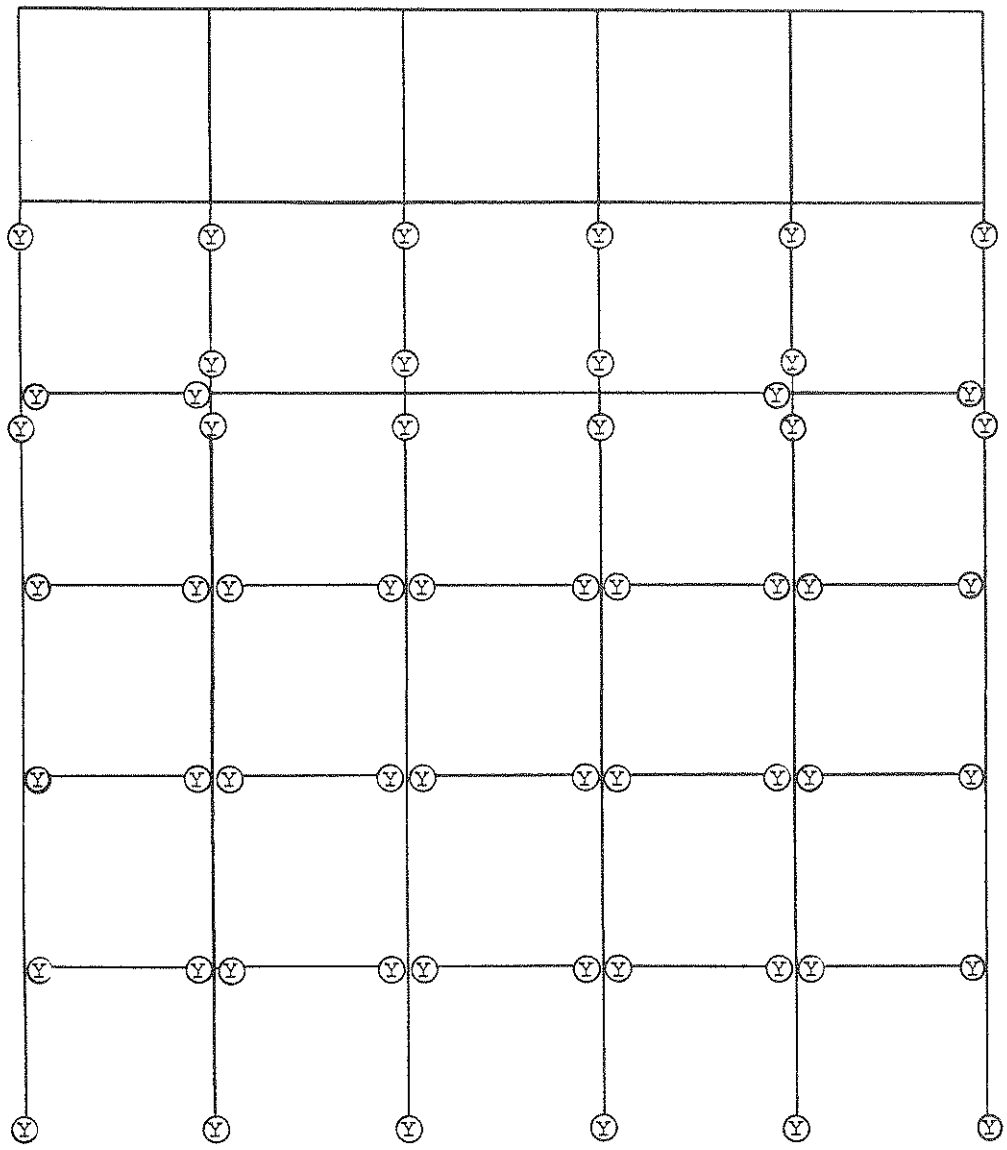

NOTATION:

⊗ = CRACK

Ⓨ = YIELD

Fig. 4.10 (b)
Failure Mode of Interior Frame
Frame Structure I

4.11 when the top deformation was 1.9% of the structures height. The effect of the reduced beams was to decrease the amount of yielding in the columns on the fourth and fifth stories, and subsequently increase the amount of yielding in the beams on these floors. As a result, the top deformation of the weak beam structure was less than the top deformation of the strong beam structure for the same ultimate load.

4.4.3 Shear Wall Structure

The results of the analysis shows that a fundamental natural period of 0.515 seconds was evaluated for the shear wall structure. The base shear coefficient was found to be 0.30, which is approximately twice that of the frame structures. Note that the shear wall structure was identical to frame structure I except for the addition of the shear walls. Figure 4.9(b) shows the variation of the base shear coefficient of the shear wall structure for the monotonic loading.

The presence of the shear wall drastically changed the failure mode of the exterior frame, see figure 4.12(a). All the columns on the top floor have yielded at both ends and all but two columns on the fourth and fifth floors have yielded. In addition to increased column yielding, there is a significant amount of yielding in the beams on the upper floors. This was not present in frame structure I. The lower three floors essentially behaved the same as those of frame structure I.

The failure mode of the interior frame, figure 4.12(b), showed that the only yielding of the shear wall was at the foundation. All the beams connected to the shear wall yielded at their connections, due to the increased stiffness of the shear wall. Generally, the edge columns on the outside of the frames connected to the transverse shear walls remained elastic, and the beams framing into the edge columns

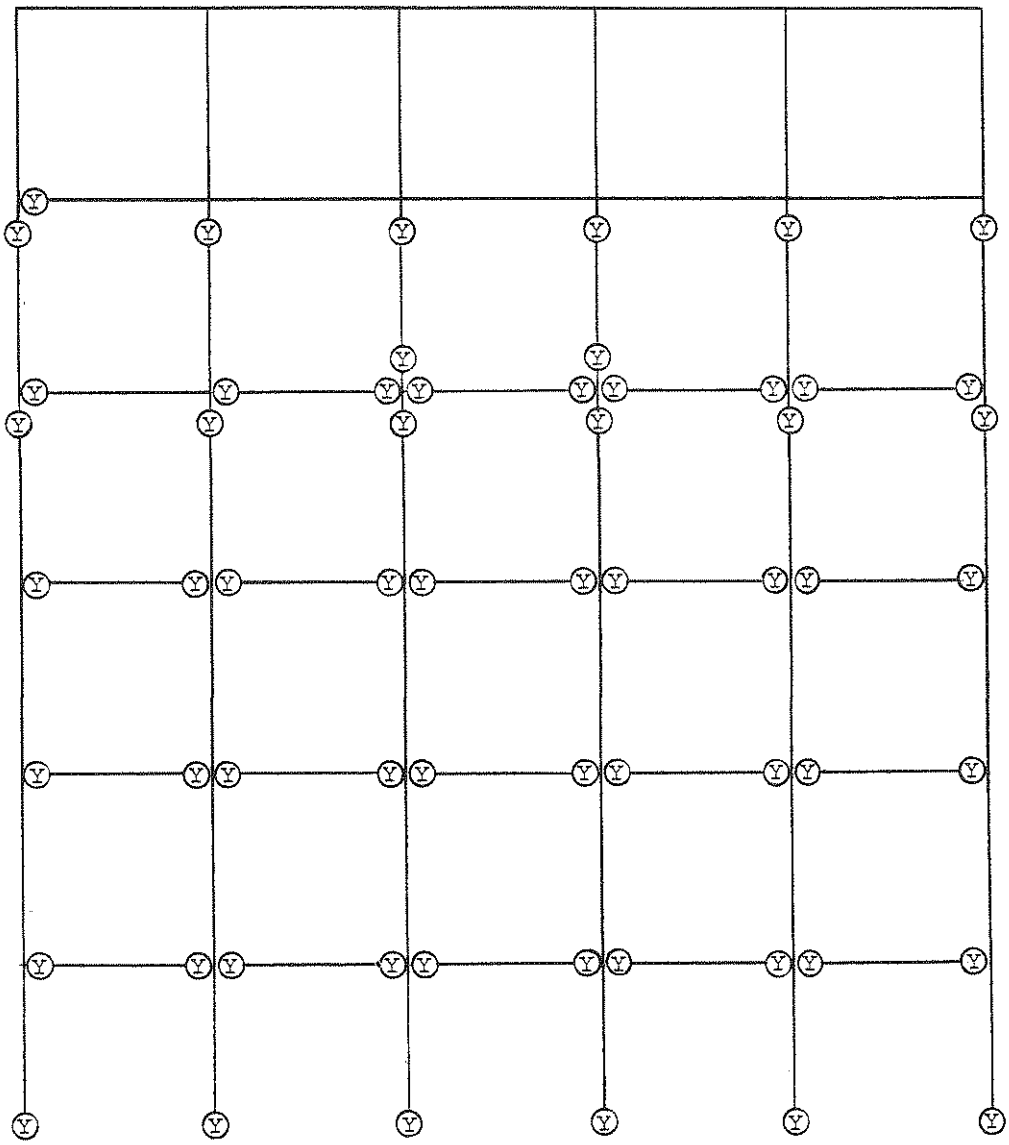

NOTATION:

⊗ = CRACK

Ⓨ = YIELD

Fig. 4.11 (a)
Failure Mode of the Exterior Frame
Frame Structure II

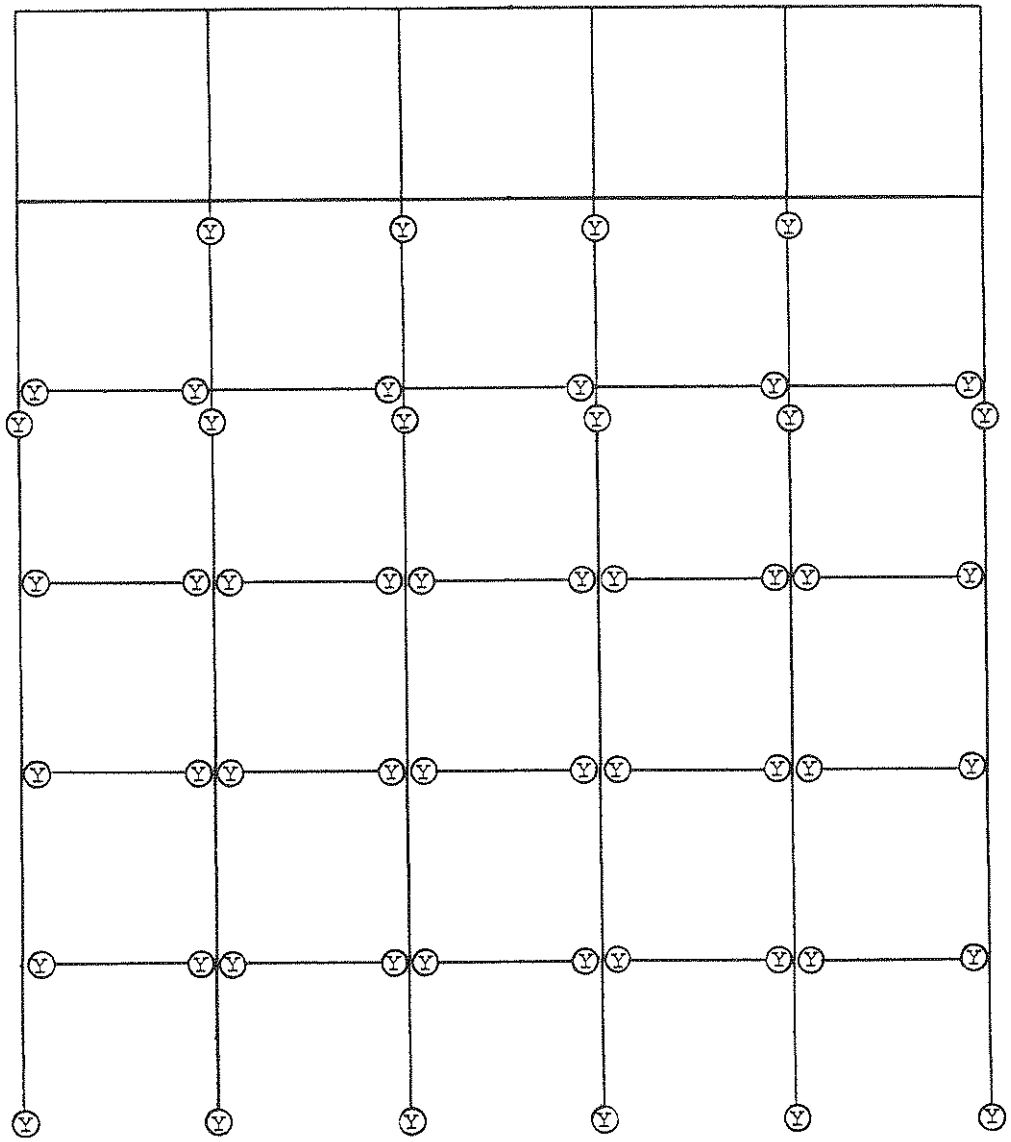

NOTATION:

⊗ = CRACK

Ⓨ = YIELD

Fig. 4.11 (b)
Failure Mode of Interior Frame
Frame Structure II

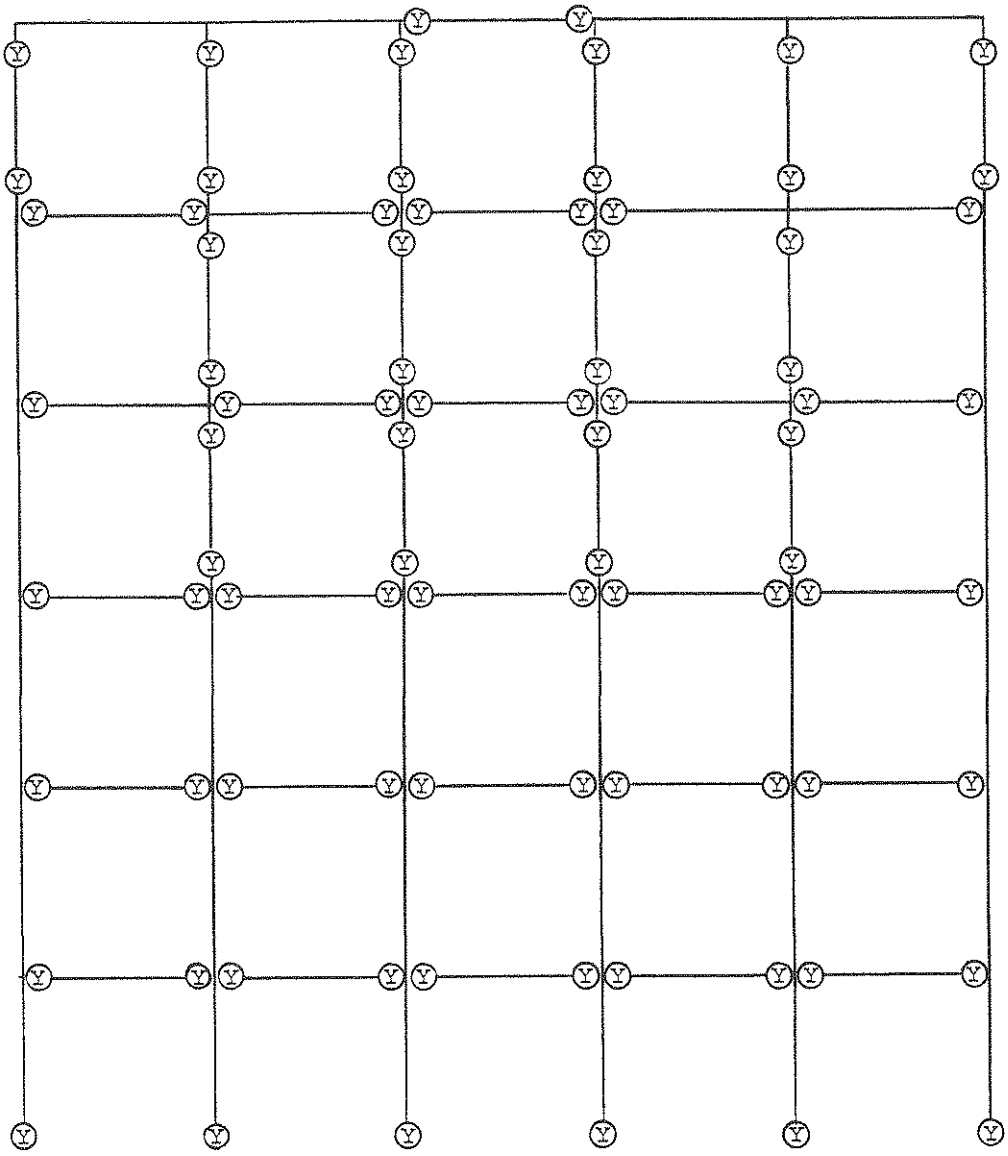

NOTATION:

⊗ = CRACK

Ⓨ = YIELD

Fig. 4.12 (a)
Failure Mode of Exterior Frame
Shear Wall Structure

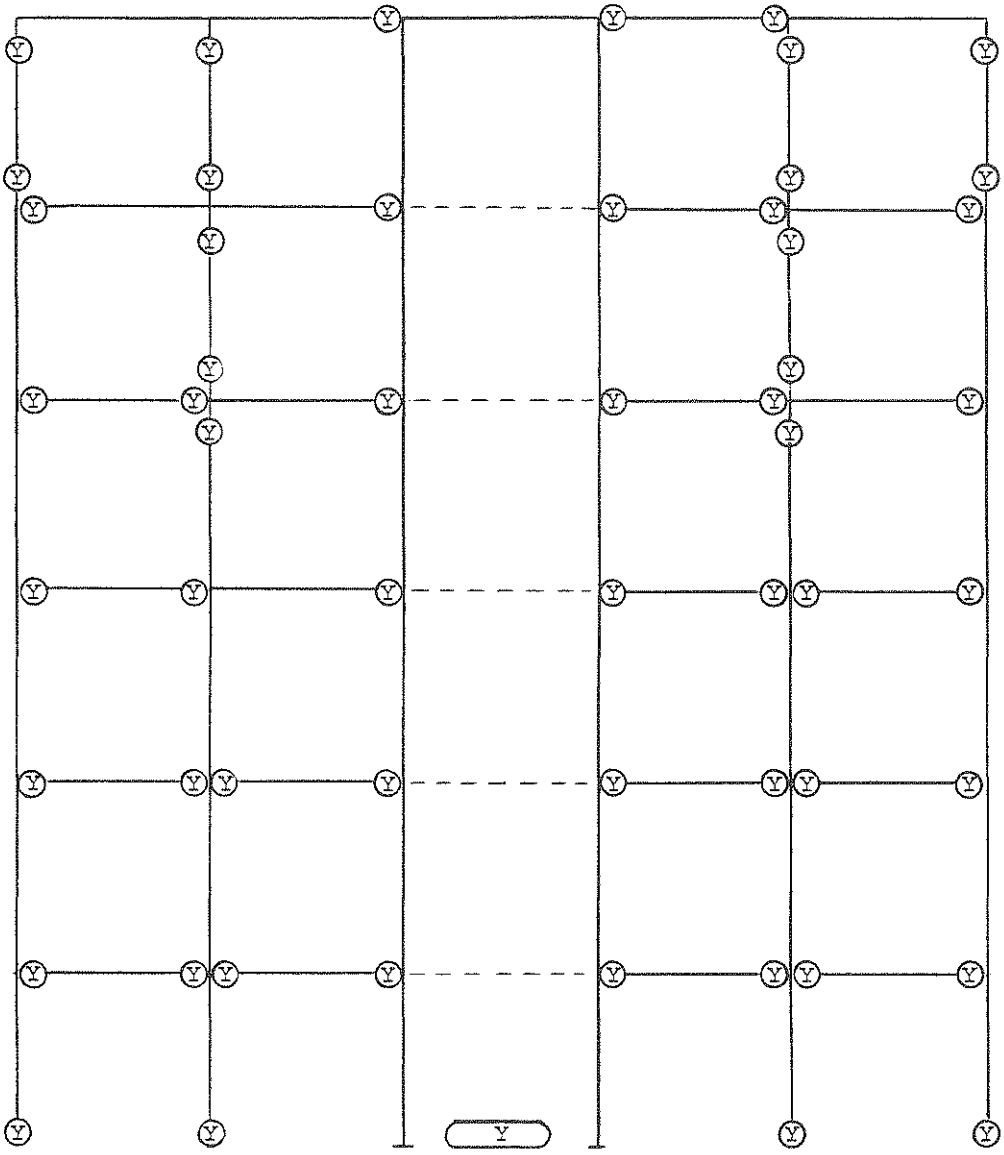

NOTATION:

⊗ = CRACK

Ⓨ = YIELD

Fig. 4.12 (b)
Failure Mode of Interior Frame
Shear Wall Structure

yielded at their connections.

4.5 Component Properties

The component properties produced by the system identification portion of IDARC are summarized in tables 4.1, 4.2 and 4.3. The component properties are calculated from a number of empirical relations that were developed from past studies of component testing [25]. The trilinear envelope curve is then defined from the various component properties.

The properties of the beams are different for the positive and negative behavior because of their unsymmetrical tee shape. Table 4.1 list the properties of the strong and weak beams. The negative moment strength of both types of beams is noticeably larger than the positive moment strength due to the effect of the slab. Additionally, the yield moments of the weak beams were approximately 20% less than the yield moments of the strong beams.

Properties of the exterior and interior columns for all stories are given in tables 4.2(a) and 4.2(b) respectively. Component properties of the columns are identical in both directions because of symmetry. The distribution of column strength throughout the structure's height agrees with the resulting failure modes previously discussed.

Table 4.3 gives the component properties of the shear walls. The cracking moment, yield moment and yield curvature are smaller for the lower level walls than the upper level walls even though the size of the shear wall was uniform throughout the structure. The reduction of strength in the lower level walls is due to the increased axial load and shear span ratio. The properties are calculated after

the static analysis has been performed and the distribution of internal forces in the structure is known, thus the envelope curves developed are for the elements in their working stage.

(1)	Strong Beams (2)	Weak Beams (3)
Initial stiffness (kip/in)	1.88×10^{8}	1.24×10^{8}
Post yielding stiffness (kip/in)	9.39×10^{5}	6.21×10^{5}
Positive cracking moment (in-kip)	1376	1124
Positive yield moment (in-kip)	1529	1249
Positive yield curvatue (radians)	9.56×10^{-5}	1.09×10^{-4}
Negative cracking moment (in-kip)	-4188	-3129
Negative yield moment (in-kip)	-5721	-4626
Negative yield curvature) (radians)	-1.45×10^{-4}	-1.64×10^{-4}

Table 4.1
Component properties of beams

Story level (1)	1 (2)	2 (3)	3 (4)	4 (5)	5 (6)	6 (7)
Axial stiffness (kip/in)	8.67×10^3	7.81×10^3	7.03×10^3	7.03×10^3	5.55×10^3	5.55×10^3
Initial flectural stiffness (kip/in)	5.14×10^7	4.28×10^7	3.23×10^7	3.07×10^7	2.02×10^7	2.02×10^7
Post yielding stiffness (kip/in)	8.21×10^5	6.18×10^5	4.98×10^5	3.43×10^5	2.40×10^5	1.97×10^5
Cracking moment (in-kip)	1587	1315	1077	963	670	607
Yield moment (in-kip)	4004	3153	2711	2150	1711	1586
Yield curvature (radian)	2.59×10^{-4}	3.14×10^{-4}	4.58×10^{-4}	3.76×10^{-4}	3.56×10^{-4}	4.68×10^{-4}

Table 4.2 (a)
Component properties
Interior columns

Story level (1)	1 (2)	2 (3)	3 (4)	4 (5)	5 (6)	6 (7)
Axial stiffness (kip/in)	1.25×10^4	1.25×10^4	8.67×10^3	7.03×10^3	5.55×10^3	5.55×10^3
Initial flectural stiffness (kip/in)	1.11×10^8	1.03×10^8	5.28×10^7	3.07×10^7	2.02×10^7	2.02×10^7
Post yielding stiffness (kip/in)	2.40×10^6	2.46×10^6	1.32×10^6	4.68×10^5	3.27×10^5	2.37×10^5
Cracking moment (in-kip)	3217	3084	1854	1174	795	670
Yield moment (in-kip)	9083	8723	5312	2563	1950	1711
Yield curvature (radian)	2.62×10^{-4}	3.56×10^{-4}	5.27×10^{-4}	4.34×10^{-4}	5.25×10^{-4}	5.00×10^{-4}

Table 4.2 (b)
Component properties
Exterior columns

Story level (1)	1 (2)	2 (3)	3 (4)	4 (5)	5 (6)	6 (7)
Axial stiffness (kip/in)	4.84×10^4	4.84×10^4	4.84×10^4	4.84×10^4	4.84×10^4	4.84×10^4
Initial flectural stiffness (kip/in)	6.89×10^{10}	6.89×10^{10}	6.89×10^{10}	6.89×10^{10}	6.89×10^{10}	6.89×10^{10}
Post yielding stiffness (kip/in)	7.21×10^6	8.98×10^6	4.16×10^7	8.28×10^6	1.50×10^8	1.44×10^8
Cracking moment (in-kip)	58570	67620	76590	84440	99300	110100
Yield moment (in-kip)	146200	169100	191600	211100	248500	275800
Yield curvature (radian)	6.65×10^{-6}	7.09×10^{-6}	7.03×10^{-6}	7.10×10^{-6}	7.20×10^{-6}	8.12×10^{-6}

Table 4.3
Component properties
Shear walls

CHAPTER 5

RESULTS OF MONTE CARLO SIMULATIONS

5.1 Introduction

A number of Monte Carlo simulations were applied to each of the three test structures to provide data that can be used to correlate seismic damage with magnitude and epicentral distance. The Monte Carlo simulation procedure used can be summarized as follows. First a set of twenty accelerograms with the same characteristics, magnitude, epicentral distance and duration, are produced. Each accelerogram in the set will be slightly different from all the others because of the random generation procedure. Next a complete inelastic dynamic analysis is performed for every accelerogram in the set, and the resulting damage is calculated. Finally statistics are performed to determine the mean damage and the expected maximum damage for that particular structure and earthquake characteristics.

The Monte Carlo simulations were performed for a number of earthquakes within the magnitude range of 5 to 7. The upper bound was determined according to Nuttli [23], who stated that a body wave magnitude of 6.5 represents the largest earthquake expected in eastern United States within a one hundred year period. Using equation 3.22, this corresponds to a magnitude of approximately 7. The lower bound was chosen based on the insignificant damage produced by earthquakes with magnitudes less than 5. Therefore the magnitude range represents earthquakes that are likely to occur and that will cause structural damage in the reinforced concrete

structures considered.

Epicentral distances in the range of 20 km to 100 km were considered (approximately 10 to 60 miles). For each magnitude in the range defined above, epicentral distances of 20, 50 and 100 km were considered. Again the upper limit for the epicentral distance was chosen such that distances greater than 100 km did not produce significant structural damage.

The inelastic dynamic analysis performed by IDARC uses a step by step numerical solution procedure [25]. The time step used in the dynamic analysis of all the structures was 0.005 seconds, which corresponds to one one-hundredth of the fundamental natural period of the shear wall structure. The total duration of the analysis was taken as 1.5 times the duration of the strong ground motion, and the damping ratio of the structures was assumed to be 2% of the critical damping.

The distribution of damage indices from the Monte Carlo simulations was assumed to be Gaussian. Figure 5.1 shows the actual distribution of overall damage indices obtained in frame structure I from fifty simulations of magnitude 5.7 and an epicentral distance of 20 km. Statistics of the results produced the mean and standard deviation of 0.164 and 0.055 respectively. These values are slightly higher than those obtained from the first twenty simulations, table 5.3 (3) (4). *The expected maximum damage is considered as a damage level that has a five percent probability of exceedence.* Thus for a Gaussian distribution, the expected maximum damage index is equal to the mean damage index plus 1.65 standard deviations of the damage index, as expressed in equation 5.1.

$$D_{max} = D_{mean} + 1.65\,\sigma_D \tag{5.1}$$

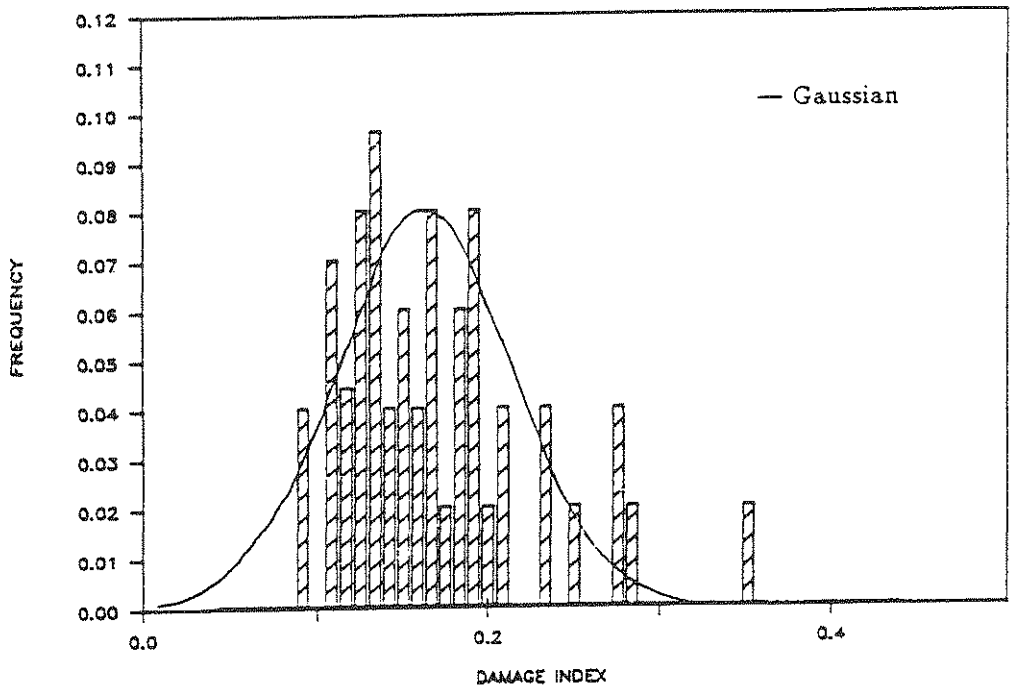

Figure 5.1
Distribution of damage for 50 simulations
Frame structure I
M = 5.7, R = 20 km

5.2 Analysis of Frame Structure I

The results of the Monte Carlo simulations for frame structure I provide a great deal of information on the resulting damage of the structure. For a given set of earthquake characteristics, a single simulation was performed to determine the final damaged state of the structure, i.e. where was the cracking, yielding, etc.. The next twenty simulations were performed for that set of earthquake characteristics to determine the mean and expected maximum damage. After a number of combinations of magnitude and epicentral distances were considered, contour plots of mean and expected maximum damage as a function of magnitude and epicentral distance were developed. Finally the distribution of damage throughout the structure was evaluated to determine the effect of local concentrations of damage in the structure.

5.2.1 Final State of Damaged Structure

In order to get a physical feel of the damaged structure relative to the resulting damage indices, the final state of the damaged structure is considered. A magnitude of 6.2 and epicentral distance of 20 km are chosen such that there is significant damage present, but total collapse of the structure does not occur. A single simulation, that resulted in an overall damage index between the mean and the expected maximum damage, is considered.

A qualitative description of the damage can be made with reference to figure 5.2. A comparison between figures 5.2(a) and 5.2(b) indicates the exterior and interior frames behaved almost identically. There was some minor difference between yielding and cracking in the beams and columns on the upper stories.

From the figures it is evident that all the beams on the first three stories have

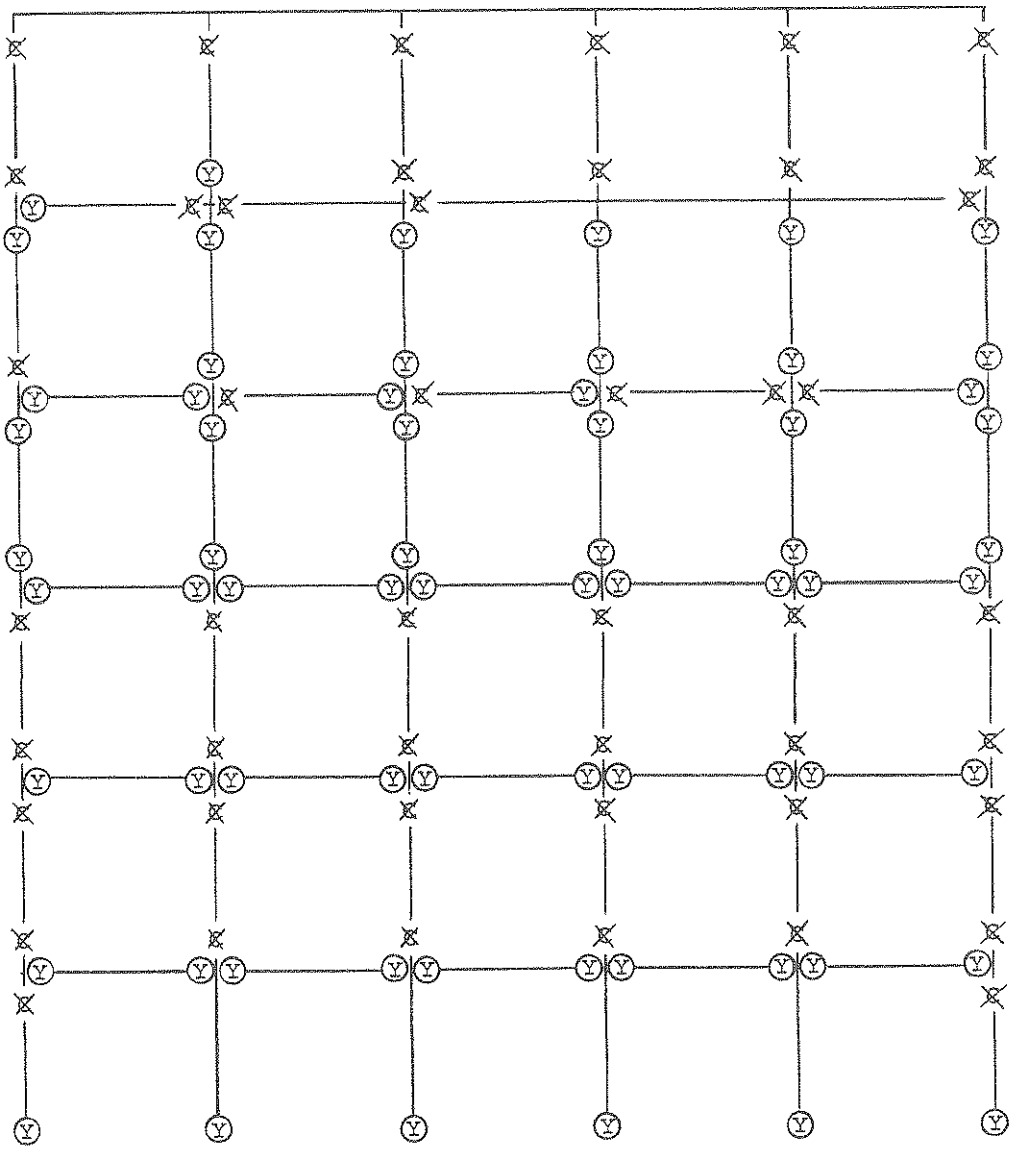

NOTATION:

⊗ = CRACK

Ⓨ = YIELD

Fig. 5.2 (a)
Final State of the Exterior Frame of
Frame Structure I
M = 6.2, R = 20 km

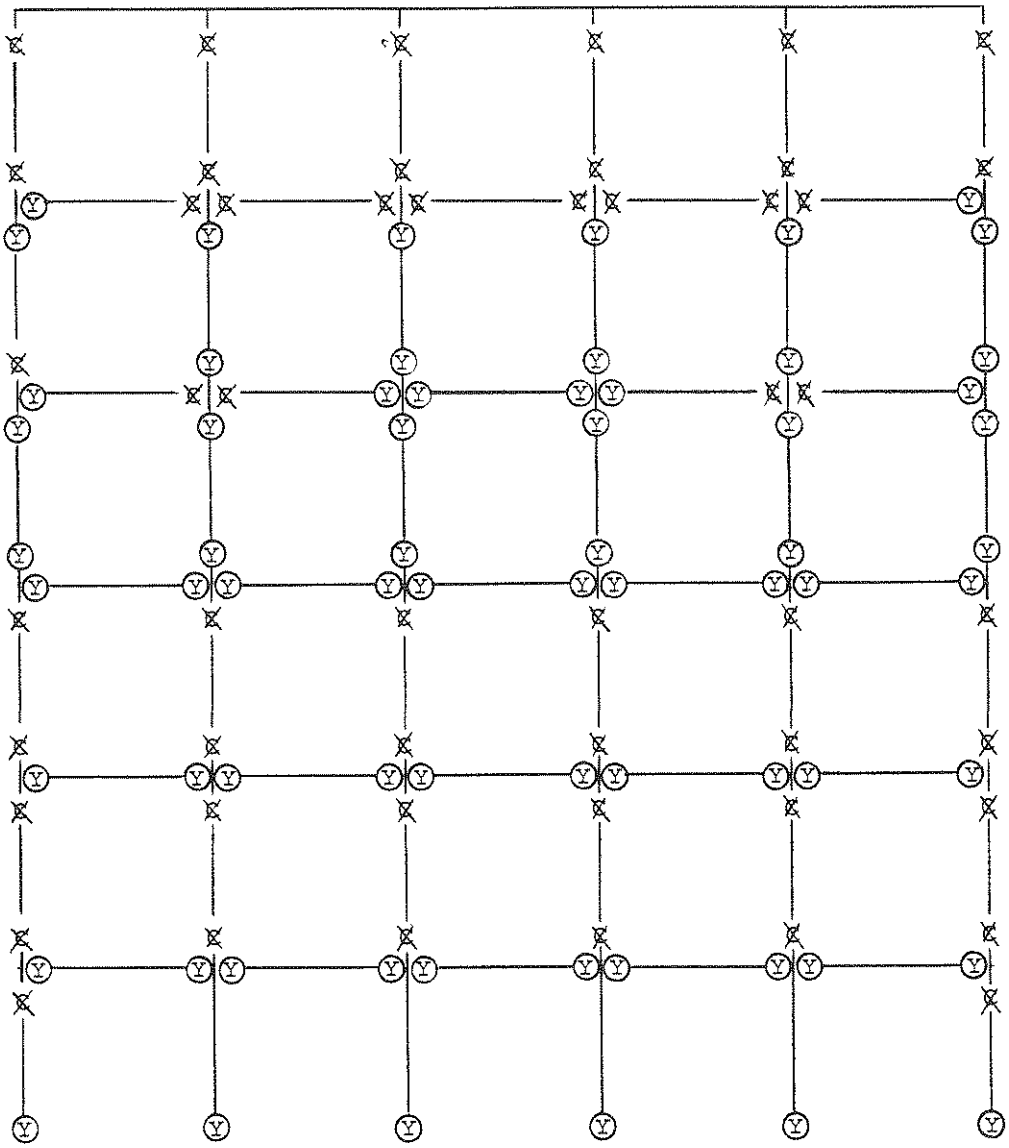

NOTATION:

⊗ = CRACK

Ⓨ = YIELD

Fig. 5.2 (b)
Final State of Interior Frame of
Frame Structure I
M = 6.2, R = 20 km

yielded as a result of the applied earthquake motion. On the fourth and fifth stories there was a combination of yielding and cracking in the beams, whereas the beams remained elastic on the sixth story.

Cracking occurred extensively in the columns on the second, third and sixth stories. On the first story, the columns generally yielded at their connection with the foundation and remained elastic at their connection with the first story beams. There was almost complete yielding at both ends of the columns on the fourth and fifth stories resulting in a panel type mechanism. Table 5.1 presents the maximum story drifts and displacements as a result of the dynamic analysis. Large story drifts are present in the fourth and fifth stories as a result of the extensive yielding in the columns. It is interesting to note the maximum top deformation of the structure was approximately 1.3% of the structures height. The top deformation and the story drifts both exceed the allowable limits defined by the UBC and ATC specifications.

To relate quantitatively the final state of the damaged structure, figure 5.3 represents the resulting damage indices of all the elements in the structure. A comparison between figures 5.3(a) and 5.3(b) indicates the interior frame has been damaged slightly more than the exterior frame.

In spite of the yielding in the beams on the first three stories, the resulting damage is only minor with damage indices ranging from 0.13 to 0.20. The resulting damage in the beams that cracked on the fourth and fifth stories was very minor, and there was no damage in the beams on the sixth story. In all cases, the resulting damage in the beams was repairable.

Damage in the columns on the fourth and fifth stories was severe due to the extensive yielding and large story drifts. The damage indices of these columns were

generally greater than 0.40, thus leaving the columns beyond repairable.

Figure 5.3 represents an enormous amount of data that can not be evaluated in the case of twenty Monte Carlo simulations. In order to reduce the amount of information, damage indices of the individual members are reduced to equivalent damage indices for the vertical and horizontal elements on each story. This is accomplished using the energy ratios discussed in section 2.2, and the resulting story level damage indices are presented in table 5.2. The overall damage index of 0.331 represents the structure as a whole is repairable, but there was number of columns that were actually beyond repair.* The results of the twenty Monte Carlo simulations with this magnitude and epicentral distance considered produced a mean damage index of 0.256 and an expected maximum damage index of 0.388.

5.2.2 Contour Plots

The overall damage indices for frame structure I have been used to construct contour plots of equal damage as a function of magnitude and epicentral distance. From the resulting contour plots, the correlation of damage with distance and magnitude can be deduced, and regions of collapse, severe damage and repairable damage can be defined. The results of the Monte Carlo simulations are tabulated in table 5.3 for frame structure I.

The contour plot developed from the mean overall damage indices of frame structure I is presented in figure 5.4. There is a small region of total collapse of the structure defined by magnitudes greater than 6.8 and distances less than 25 km. In

* This observation needs further investigation, in order to define more clearly the threshold of repairability of the whole structure.

Story No. (1)	Max story drift (inch) (2)	Max drift % story height (3)	Max story disp (inch) (4)	Max disp % total height (5)
1	1.398	0.97	1.398	0.16
2	2.195	1.52	3.591	0.42
3	2.132	1.48	5.709	0.66
4	3.338	2.32	8.313	0.96
5	2.848	1.98	10.580	1.22
6	0.829	0.58	11.580	1.34

Table 5.1
Story drift and displacement
Frame structure I
M = 6.2, R = 20 km

Story No. (1)	Vertical components		Horizontal components	
	Damage index (2)	Energy ratio (3)	Damage index (4)	Energy ratio (5)
1	0.177	0.059	0.183	0.147
2	0.097	0.023	0.209	0.178
3	0.191	0.054	0.143	0.124
4	0.684	0.159	0.114	0.043
5	0.632	0.171	0.047	0.006
6	0.126	0.035	0.004	0.000

Damage index for building 0.331

Table 5.2
Story level damage indices
Frame structure I
M = 6.2, R = 20 km

M (1)	R (km) (2)	Mean damage (3)	STD. (4)	Actual max damage (5)	Expected* max damage (6)
5.0	20	0.064	0.013	0.087	0.085
5.0	50	0.045	0.011	0.067	0.063
5.3	20	0.098	0.016	0.141	0.124
5.3	50	0.054	0.012	0.080	0.074
5.3	100	0.031	0.007	0.050	0.043
5.7	20	0.159	0.051	0.282	0.243
5.7	50	0.081	0.015	0.109	0.106
5.7	100	0.050	0.009	0.066	0.065
6.2	20	0.256	0.080	0.367	0.388
6.2	50	0.132	0.049	0.276	0.216
6.2	100	0.074	0.013	0.098	0.095
6.6	20	0.734	0.331	1.524	1.280
6.6	50	0.285	0.093	0.475	0.438
6.6	100	0.109	0.029	0.165	0.157
7.0	20	1.338	0.538	2.318	2.226
7.0	50	0.516	0.176	0.790	0.806
7.0	100	0.170	0.042	0.273	0.239

* Based on Eq. 5.1

Table 5.3
Overall damage indices from simulations for
Frame structure I

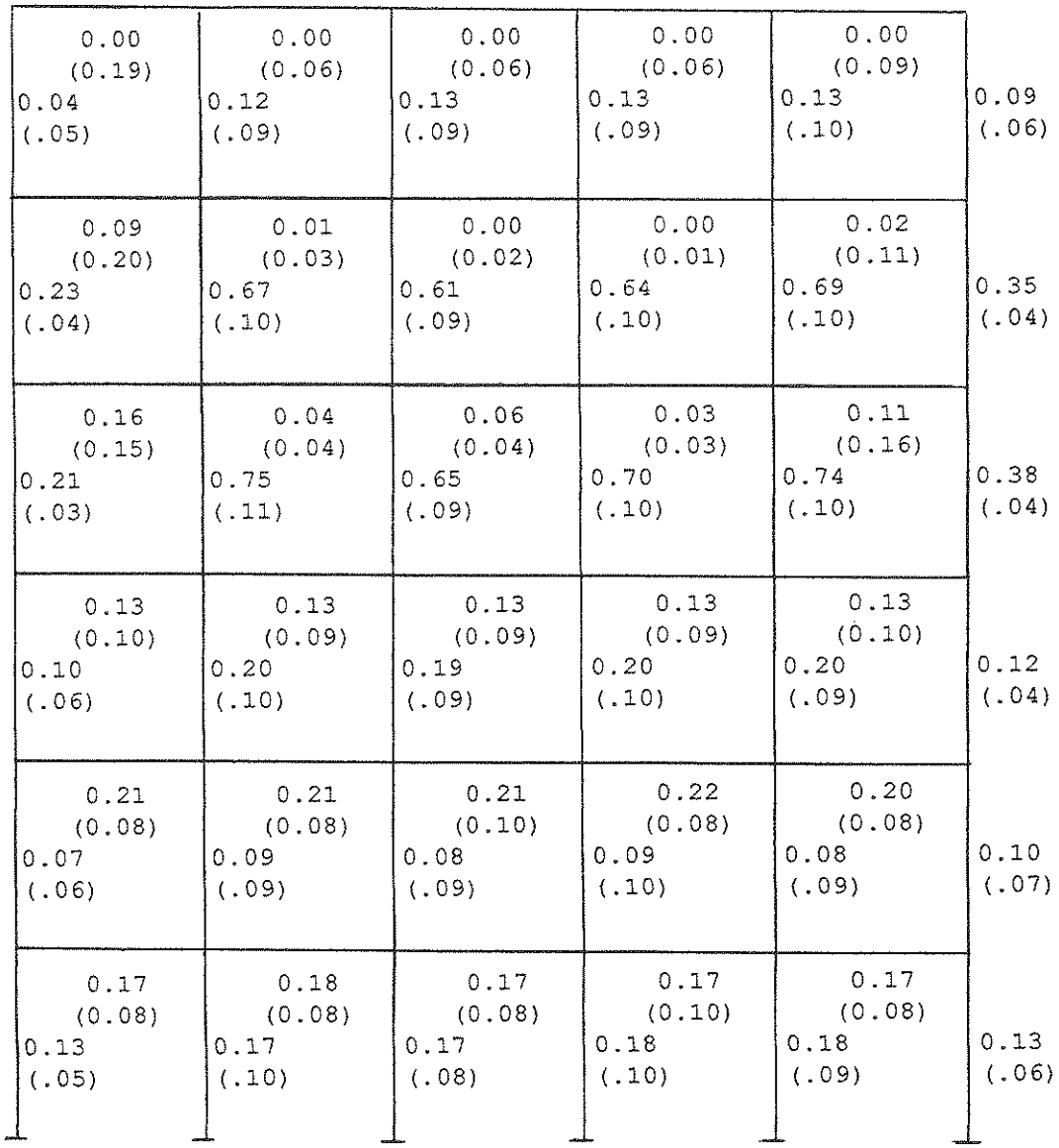

VALUES IN PARANTHESIS INDICATE ENERGY RATIOS

Fig. 5.3 (a)
Damage Indices of Exterior Frame of
Frame Structure I
M = 6.2, R = 20 km

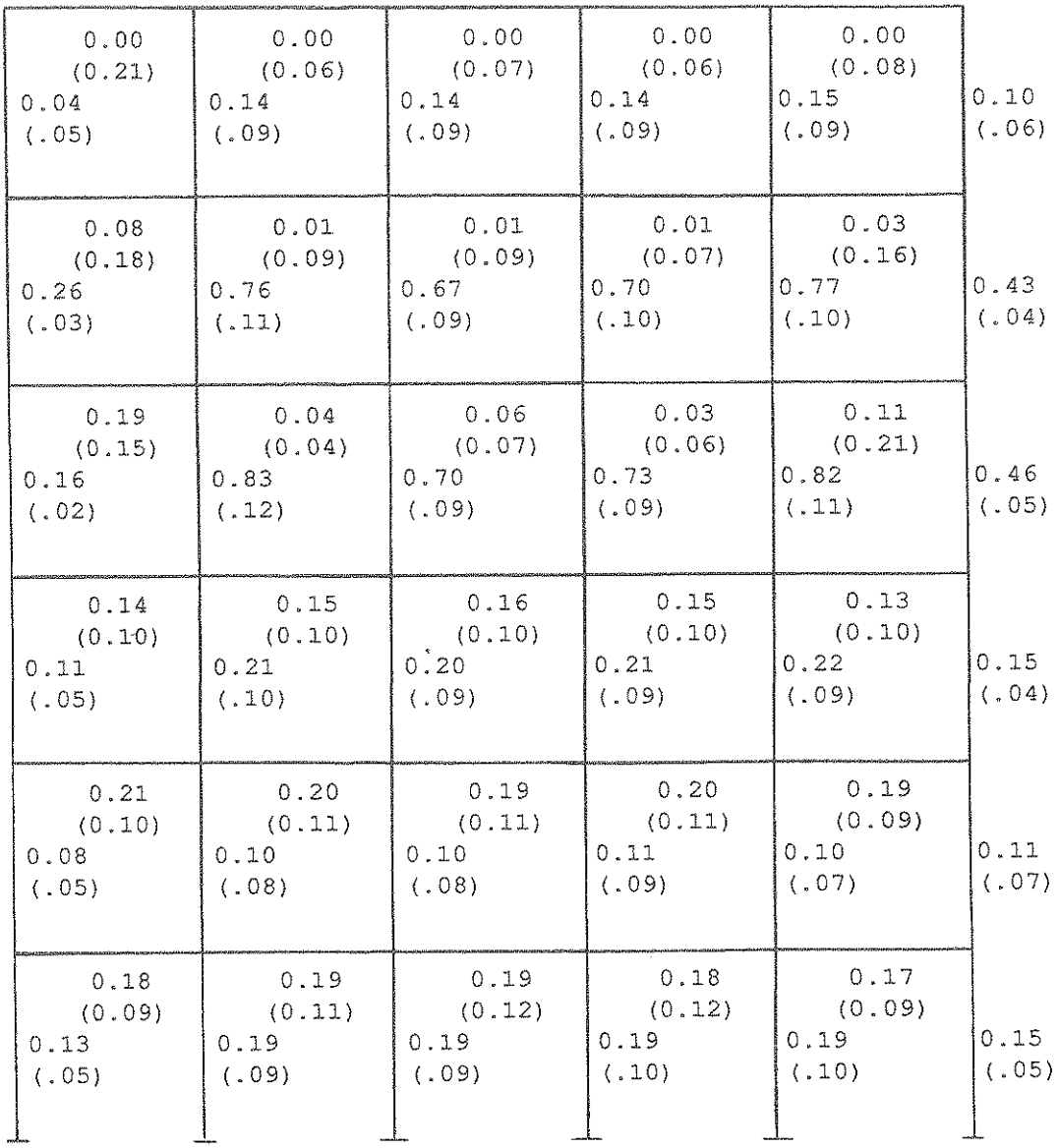

VALUES IN PARANTHESIS INDICATE ENERGY RATIOS

Fig. 5.3 (b)
Damage Indices of the Interior Frame of
Frame Structure I
M = 6.2, R = 20 km

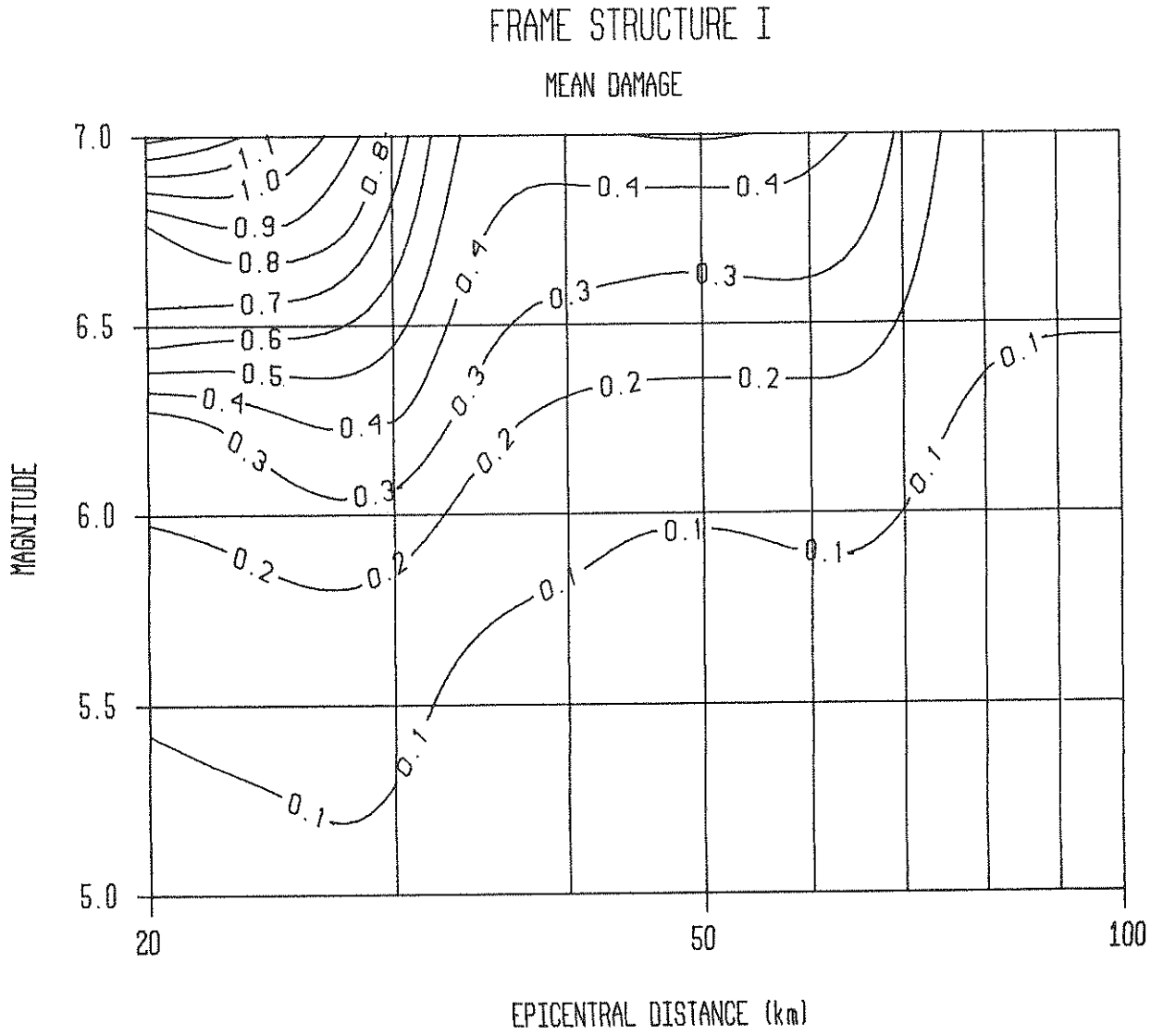

Figure 5.4
Contour Plot of Mean Damage
Frame Structure I

this region the mean overall damage index was greater than or equal to 1.0, which by definition results in total collapse of the structure. Local collapse of the structure at damage indices less than 1.0 will be treated in the next section. There is a large region in which combinations of epicentral distance and magnitude result in severe damage (beyond repair). This region can be defined by magnitudes greater than 6.2 and distances less than 32 km. In addition to the combinations just mentioned, severe damage can occur at distances up to 60 km for magnitudes greater than 6.8. For all distances and magnitudes less than 6.2, the resulting damage was repairable. In this region, there is a substantial reserve capacity of the structure to resist future earthquakes without collapse.

The mean overall damage may not be the best indicator of the seismic risk involved for a given earthquake event. Therefore contours of expected maximum overall damage index were developed. For a given magnitude and epicentral distance combination, there is a 95% probability that the resulting damage will be less than the expected maximum damage. From the resulting contour plot, figure 5.5, the region of total collapse has increased considerably from the mean damage case. Total collapse occurs for magnitudes greater than 6.5 and distances less than 30 km, and irreparable damage occurs at distances less than 70 km and magnitudes greater than 6.5. For distances less than 35 km, severe damage results at magnitudes as low as 6.0. Generally, for all earthquakes with magnitudes less than 6.0, the resulting damage was repairable.

5.2.3 Distribution of Damage in Structure

There is a possibility that concentrations of damage greater than the overall

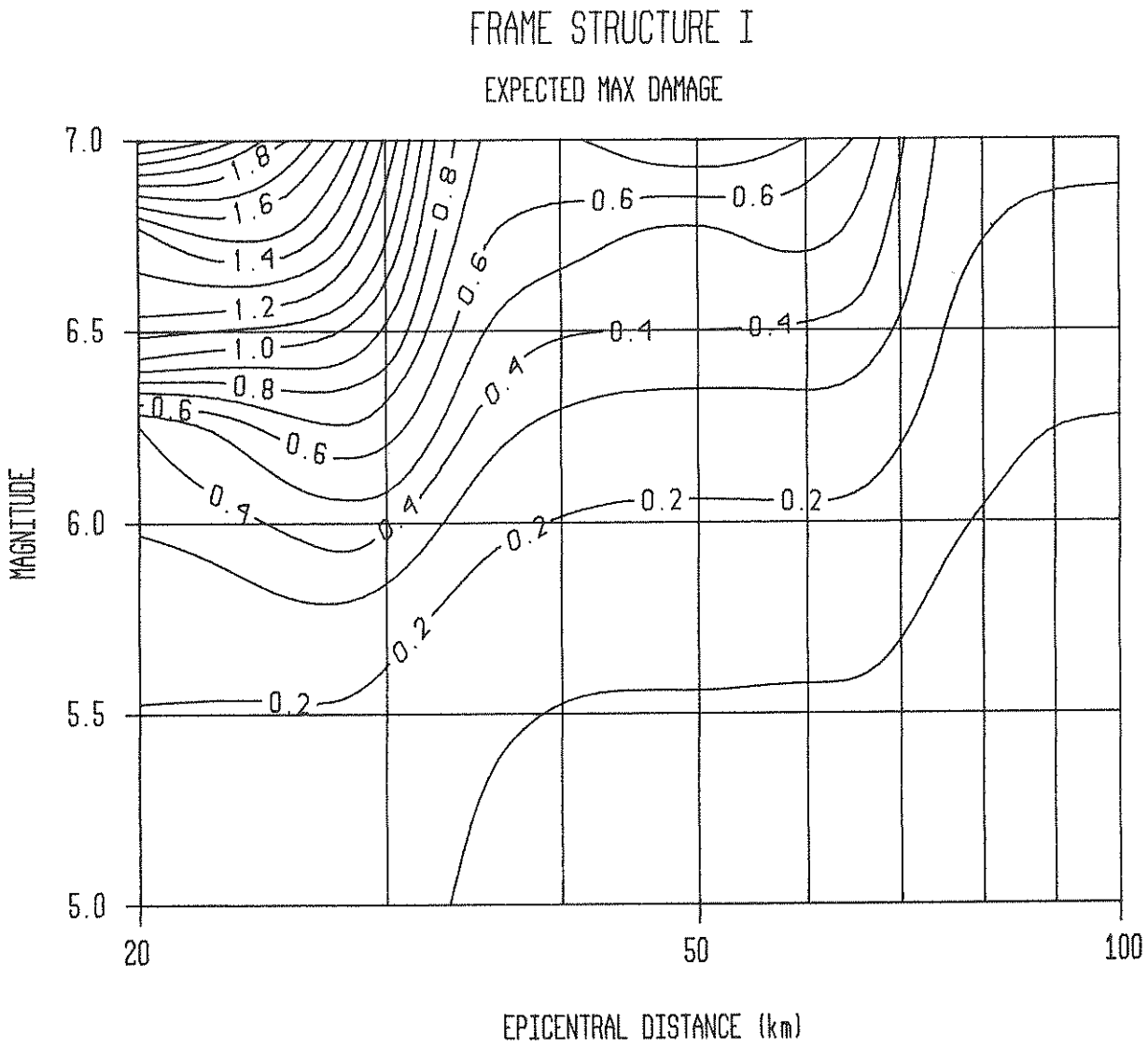

Figure 5.5
Contour Plot of Expected Maximum Damage
Frame Structure I

damage index may occur in the structure. The worst case would be local collapse of a portion of the structure, which may cause progressive building collapse, while the overall damage index indicates only severe damage. Thus the distribution of damage in the vertical elements is considered to relate local concentrations of damage to the overall damage index. Again, both the mean and expected maximum damage will be considered. The damage in the columns has been chosen because collapse of a column may lead to progressive collapse of the structure. Currently the program IDARC [25] does not recognize the effect of local collapse of a column element on the collapse mechanism of the structure.

Figures 5.6 though 5.9 are plots of the distribution of mean and expected maximum damage index in the vertical elements throughout the height of the structure. Each plot is for a constant magnitude with epicentral distances of 20, 50, and 100 km considered. The dashed lines represents the limit of repairable damage, thus any point to the right of the dashed line represents damage that is beyond repair.

The distribution of mean and expected maximum damage in the vertical elements for a magnitude of 5.7 are shown in figures 5.6 (a) and 5.6 (b) respectively. At this magnitude, the mean damage for all distances considered was repairable. If the expected maximum damage is used to evaluate the risk, damage beyond repair was present in the columns on the fourth and fifth stories. The expected maximum overall damage for a magnitude of 5.7 and a distance of 20 km was 0.243, as indicated in table 5.3 (6), which does not predict the concentration of severe damage in the columns on the fourth and fifth stories. For distances of 50 and 100 km, there was not a substantial difference between the mean and expected maximum damage.

If the magnitude is increased to 6.2, at a distance of 20 km, the mean damage

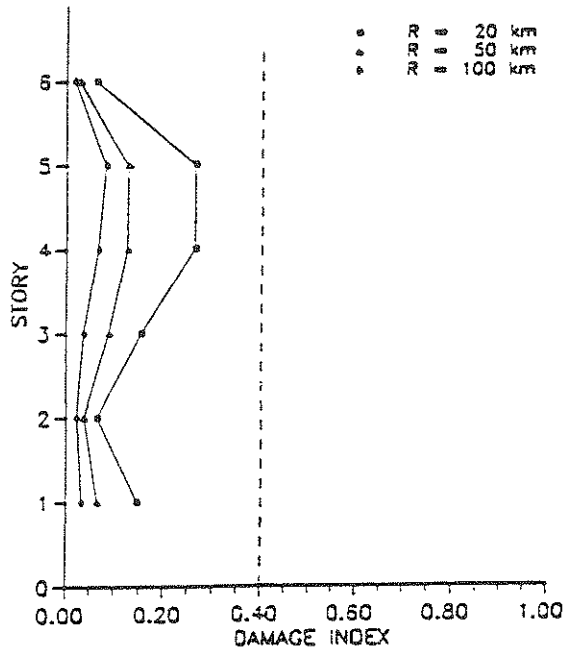

(a) Mean damage

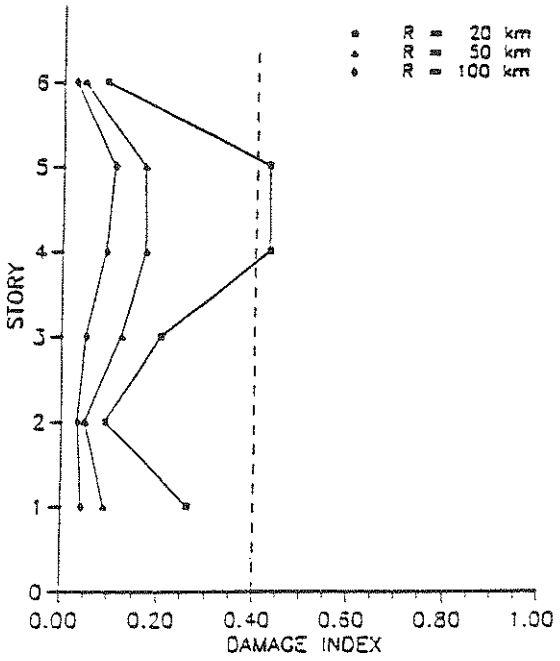

(b) Expected maximum damage

Figure 5.6
Distribution of Damage Frame Structure I
Magnitude = 5.7

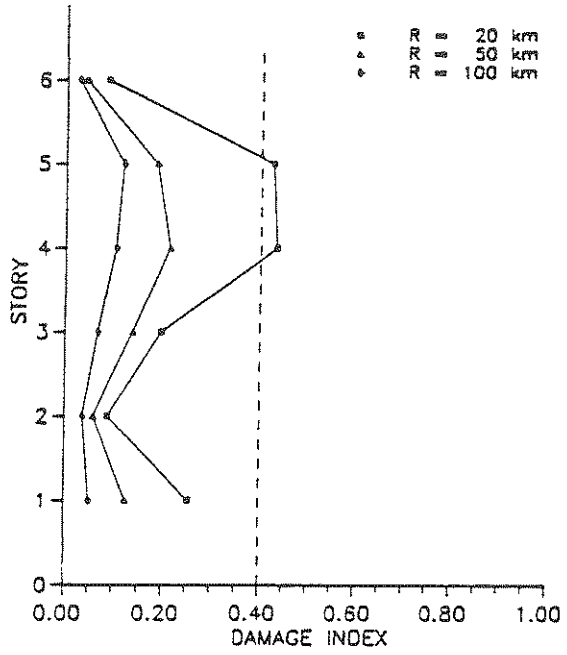

(a) Mean damage

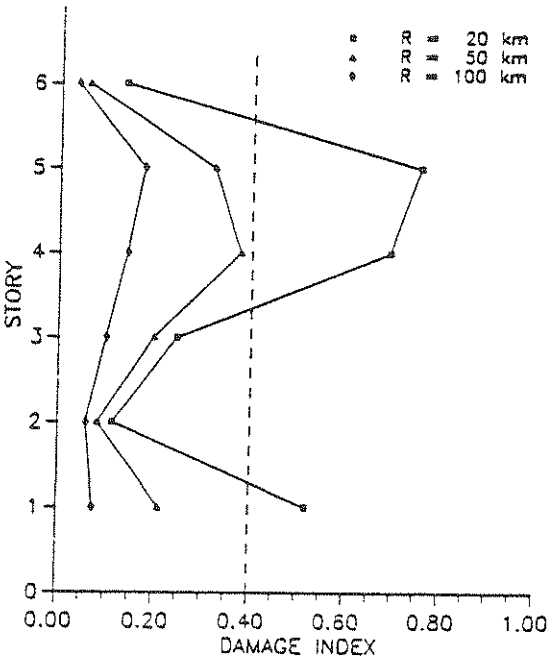

(b) Expected maximum damage

Figure 5.7
Distribution of damage frame structure I
Magnitude = 6.2

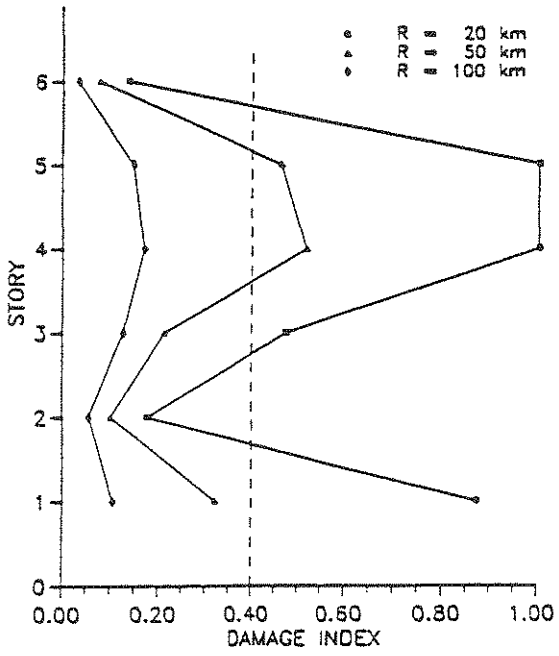

(a) Mean damage

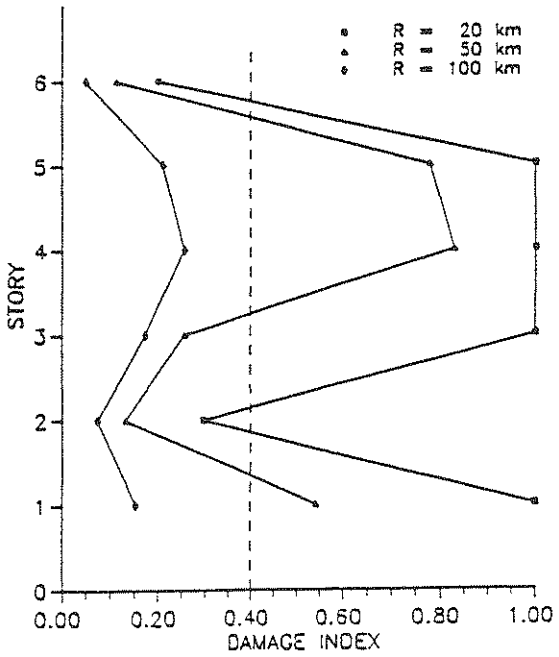

(b) Expected maximum damage

Figure 5.8
Distribution of damage frame structure I
Magnitude = 6.6

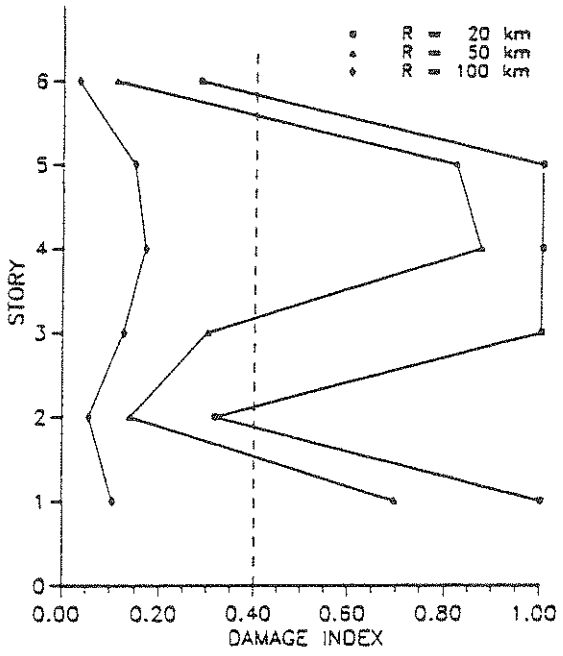

(a) Mean damage

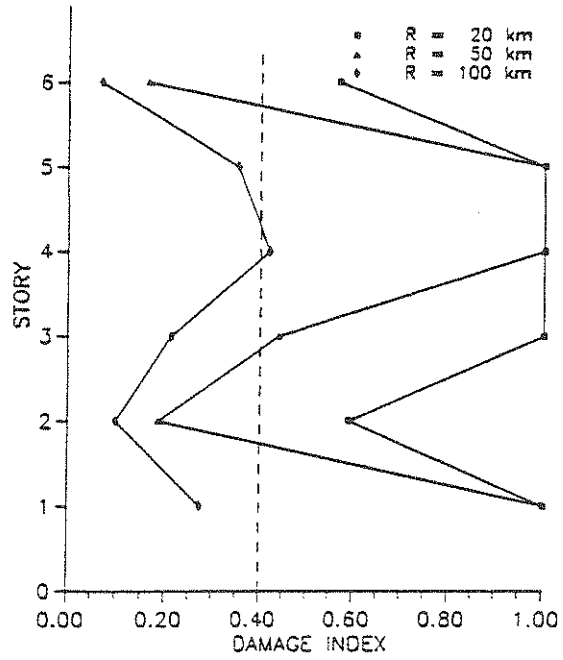

(b) Expected maximum damage

Figure 5.9
Distribution of damage frame structure I
Magnitude = 7.0

index on the fourth and fifth stories was severe, as seen in figure 5.7 (a). Again the overall mean damage index indicates the structure as a whole is repairable, in spite of the local severe damage. The expected maximum damage in the vertical elements is shown in figure 5.7 (b). At distances of 50 and 100 km, the entire structure is repairable, but at 20 km severe damage results in the columns on three stories.

Local collapse of the columns is present for both the mean and the expected maximum damage at magnitudes of 6.6 and 7.0, see figures 5.8 and 5.9. The mean damage in figure 5.8 (a) for a magnitude of 6.6 indicates local collapse in the columns on the fourth and fifth stories at a distance of 20 km, and severe damage at a distance of 50 km. The mean overall damage index for a magnitude of 6.6 and a distance of 20 km was 0.734, table 5.3 (6), which does not indicate total collapse of the structure, but collapse of the columns on the fourth and fifth stories may lead to total collapse of the structure. From figure 5.8 (b) the expected maximum damage at a distance of 20 km results in collapse of the columns on four stories. In this case, the overall expected maximum damage index was greater than 1.0 (as indicated in table 5.3 (6)) and total collapse was predicted.

Figure 5.9 shows the distribution of damage resulting from a magnitude of 7.0. At distances of 20 km, the mean and expected maximum damage indicates local collapse in the columns, whereas at a distance of 50 km the mean indicates severe damage and the expected maximum damage indicates local collapse in the columns. For an epicentral distance of 100 km, only the expected maximum damage in the columns on the fourth story indicates severe damage. For all other magnitudes considered, the resulting damage (mean and expected maximum) was repairable.

The distribution of damage throughout the structure followed the same form

for all the magnitude distance combinations considered. Generally the damage was highest on the fourth and fifth stories due to the weak columns resulting from the gravity load design. The damage in the remaining stories was not as high except at the base where there was a significant amount of yielding present. The comparison of the distribution of damage with the overall damage index indicates the local concentration of damage may be critical in assessing the risk involved.

5.3 Analysis of Frame Structure II

The analysis of frame structure II was performed in a similar manner to that of frame structure I in order to determine the effect of the reduced beam size on the resulting damage. Thus the final state of the damaged structure is analyzed to compare the behavior with that of the frame structure with strong beams. Additionally, contour plots of damage and the distribution of damage in the structure are considered.

5.3.1 Final State of Damaged Structure

To directly compare the behavior of frame structure I and frame structure II, an earthquake with a magnitude of 6.2 and an epicentral distance of 20 km has been chosen as in the case of frame structure I. A representative simulation that resulted in an overall damage index between the mean and the expected maximum is also considered.

The resulting qualitative representation of the damaged state of frame structure II is shown in figure 5.10. A comparison between the final state of the exterior and interior frames, figure 5.10 (a) and 5.10 (b) respectively, indicates that their final

states were almost identical.

Complete yielding of all the beams has occurred on the first four stories, and cracking has occurred in the beams on the fifth story as a result of the applied earthquake motion. As in the case of frame structure I, the beams on the sixth story remained elastic.

Column yielding generally occurred at the base of the first story and at both ends of the columns on the fourth and fifth stories. All the columns on the second, third and sixth stories were cracked due to the earthquake excitation. Story drifts and displacements from this representative earthquake are provided in table 5.4. Note that the story drifts were almost uniform throughout the first five stories, with drifts of approximately 2% of the story height. This uniform drift possibly results from a beam type mechanism forming in the beams on the lower stories. The resulting maximum top deformation was 1.7 % of the structures height.

Damage indices of all the elements are shown in figure 5.11, and provide a quantitative description of the resulting damage. A comparison of figures 5.11 (a) and 5.11 (b) indicates the interior frame was damaged slightly more than the exterior frame, as in the case of frame structure I.

Damage indices of the beams on the first three stories ranged from 0.20 to 0.28, and the resulting damage on the top three stories were generally less than 0.15. Thus all the beams were repairable even though there was extensive yielding present. Damage in the columns on the first and fifth stories was on the border of repairable and severe, whereas the damage on the fourth story was generally severe.

The resulting story level damage indices and overall damage index are summarized in table 5.5 for this representative simulation. The damage of the vertical

Story No. (1)	Max story drift (inch) (2)	Max drift % story height (3)	Max story disp (inch) (4)	Max disp % total height (5)
1	2.397	1.66	2.397	0.28
2	3.181	2.21	5.556	0.64
3	3.751	2.60	9.307	1.08
4	3.762	2.61	13.030	1.51
5	2.037	1.41	14.660	1.70
6	0.417	0.29	15.040	1.74

Table 5.4
Story drift and displacement
Frame structure II
M = 6.2, R = 20 km

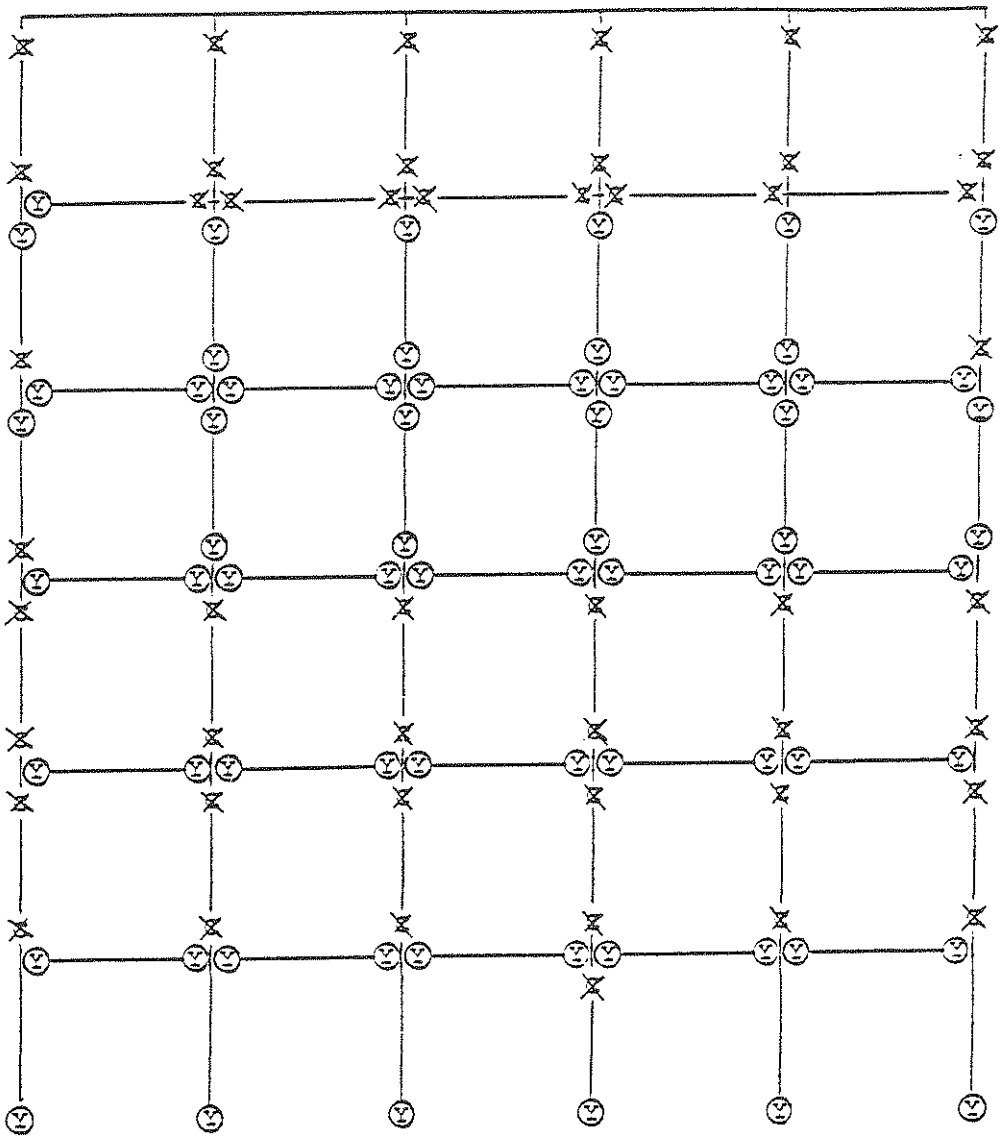

NOTATION:

⧖ = CRACK

Ⓨ = YIELD

Figure 5.10 (a)
Final state of exterior frame
Frame structure II
$M = 6.2$, $R = 20$ km

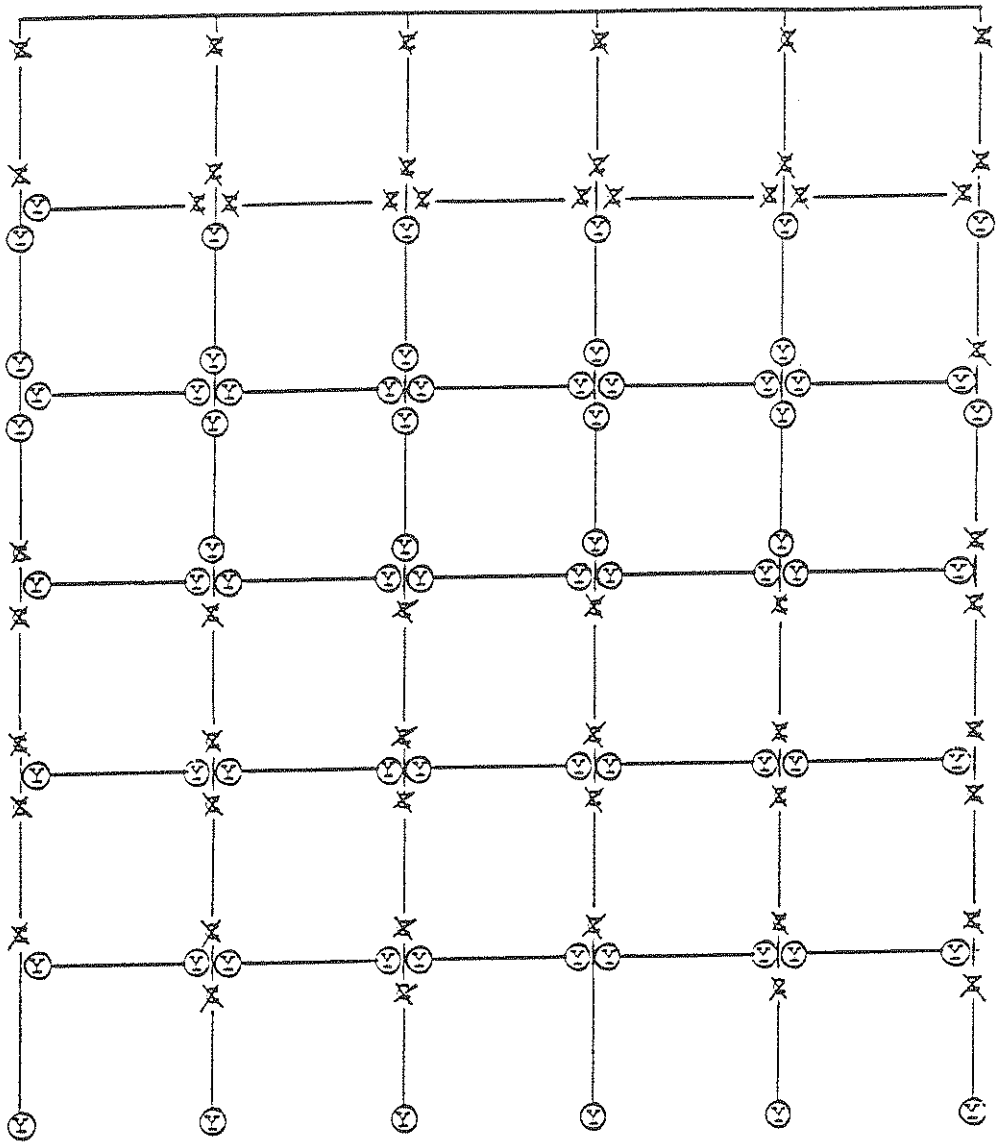

NOTATION:

⊠ = CRACK

Ⓨ = YIELD

Figure 5.10 (b)
Final state of interior frame
Frame structure II
M = 6.2, R = 20 km

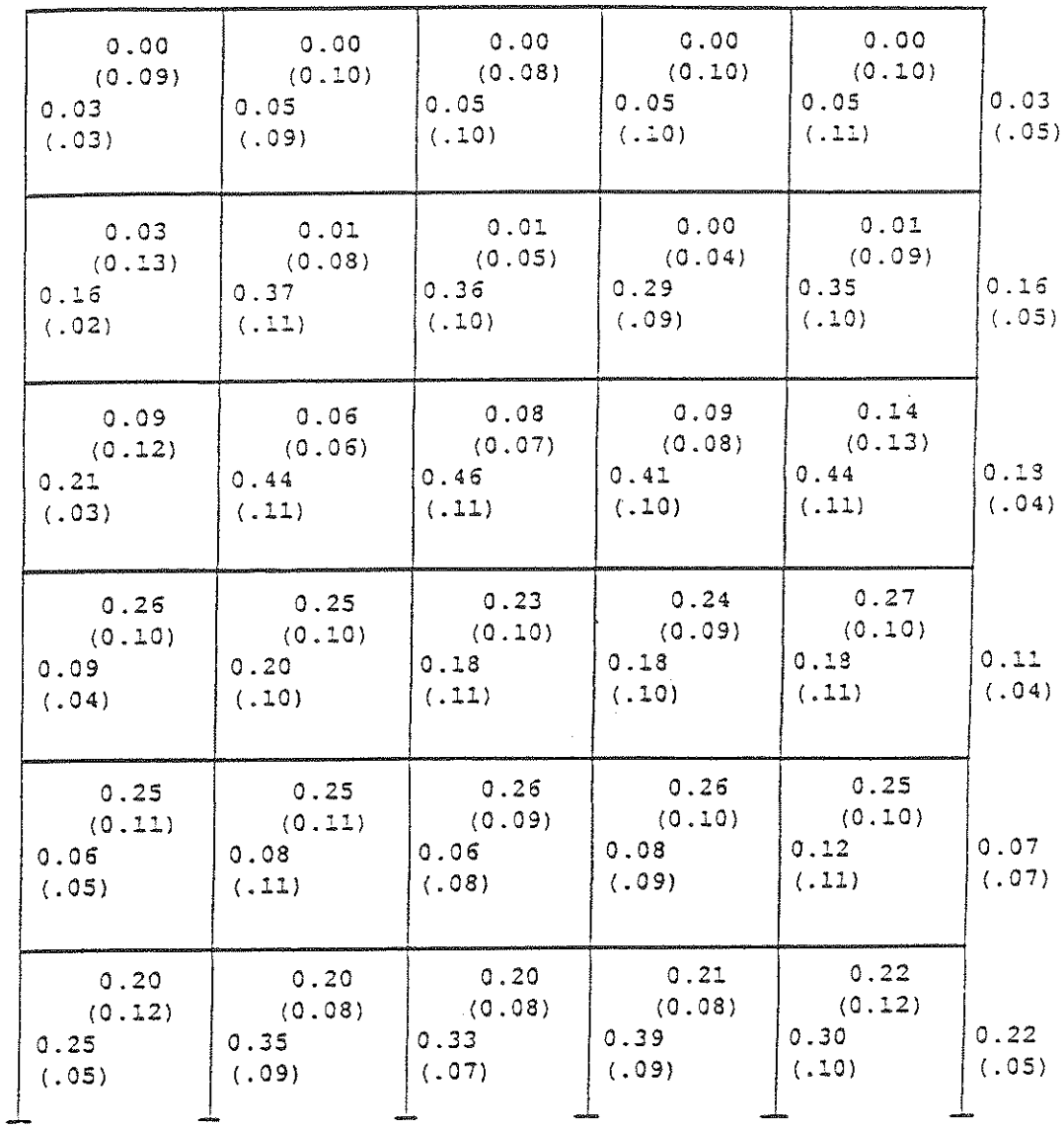

VALUES IN PARANTHESIS INDICATE ENERGY RATIOS

Figure 5.11 (a)
Damage indices of exterior frame
Frame structure II
M = 6.2, R = 20 km

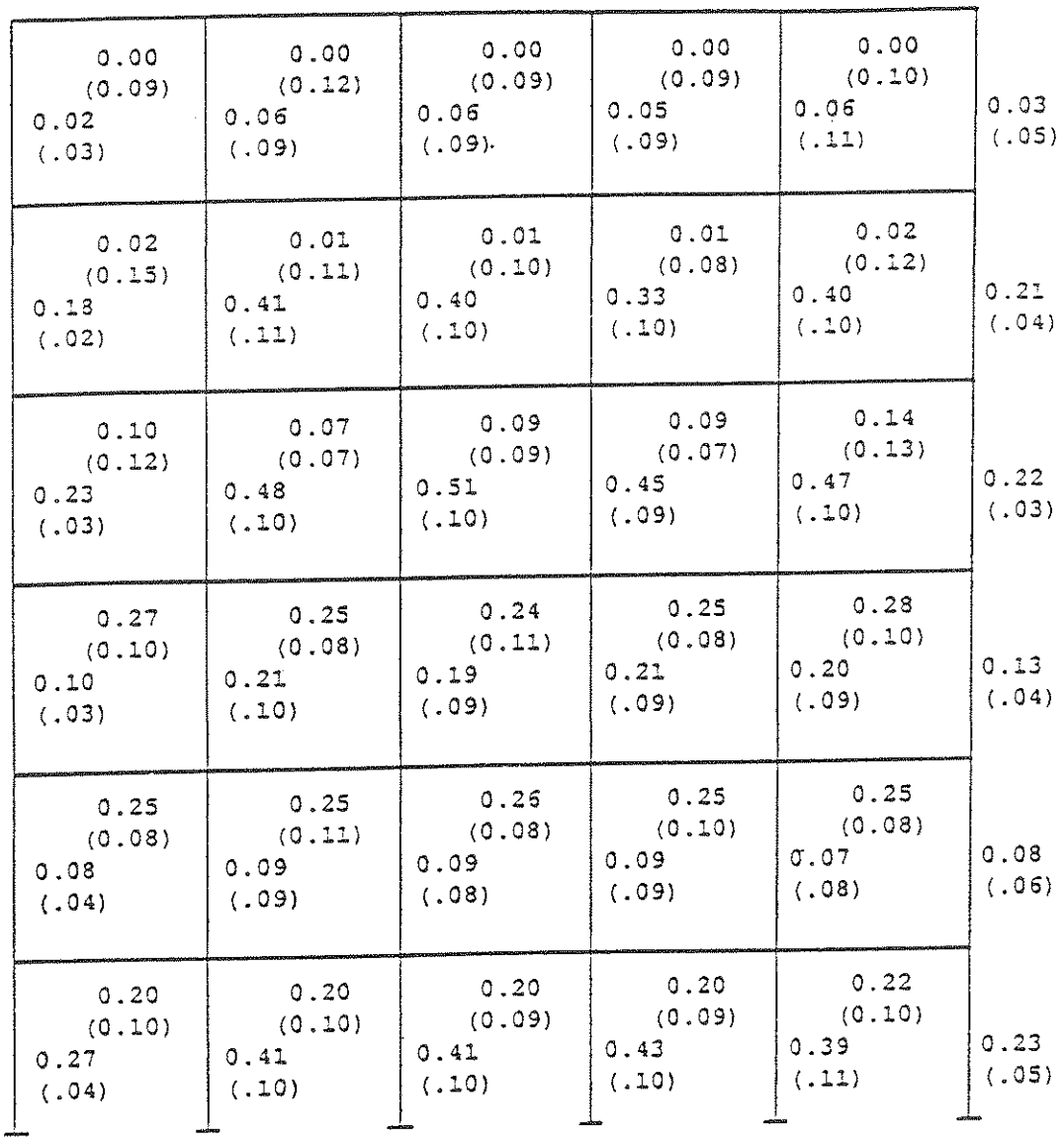

VALUES IN PARANTHESIS INDICATE ENERGY RATIOS

Figure 5.11 (b)
Damage indices of interior frame
Frame structure II
M = 6.2, R =20 km

and horizontal components agree with the previous discussion, and the only severe damage results in the vertical elements on the fourth story. The overall damage index of 0.267 indicates a repairable structure with reserve capacity to resist future earthquakes. The resulting overall damage index was in the range of the mean damage, 0.211, and the expected maximum damage, 0.330, that resulted from the Monte Carlo simulations, table 5.6 (3) (6).

5.3.2 Contour Plots

Contour plots of equal damage as a function of magnitude and epicentral distance have also been developed for frame structure II. Table 5.6 summarizes the results of the Monte Carlo simulations. For this structure, magnitudes less than 5.7 were not considered because the resulting damage was not significant.

The contour plot of the mean overall damage of frame structure II is shown in figure 5.12. Total collapse of the structure only occurs for magnitudes of 7.0 and distances of 20 km. A region of severe damage is present for magnitudes greater than 6.4 and epicentral distances less than 30 km. Severe damage was also present at magnitudes close to 7.0 for a distance of 50 km. Generally, for all distances greater than 30 km, the damage was repairable, except for the large magnitudes previously mentioned. At distances less than 30 km the resulting damage was repairable for all magnitudes less than 6.4.

Again contour plots of the expected maximum overall damage were developed to provide a more realistic assessment of the seismic risk. Figure 5.13 represents the contour plot of the expected maximum damage of frame structure II. From the plot it is evident that a region of total collapse of the structure is present for magnitudes

Story No. (1)	Vertical components		Horizontal components	
	Damage index (2)	Energy ratio (3)	Damage index (4)	Energy ratio (5)
1	0.352	0.099	0.210	0.153
2	0.087	0.019	0.257	0.217
3	0.185	0.048	0.259	0.189
4	0.426	0.110	0.104	0.056
5	0.342	0.090	0.018	0.006
6	0.055	0.013	0.003	0.000

Damage index for building 0.267

Table 5.5
Story level damage indices
Frame structure II
M = 6.2, R = 20 km

M (1)	R (km) (2)	Mean damage (3)	STD. (4)	Actual max damage (5)	Expected* max damage (6)
5.7	20	0.120	0.036	0.205	0.179
5.7	50	0.057	0.014	0.091	0.080
5.7	100	0.027	0.007	0.042	0.039
6.2	20	0.211	0.072	0.374	0.330
6.2	50	0.105	0.034	0.195	0.161
6.2	100	0.055	0.015	0.085	0.079
6.6	20	0.553	0.185	0.935	0.858
6.6	50	0.219	0.095	0.434	0.376
6.6	100	0.074	0.015	0.109	0.100
7.0	20	1.069	0.461	2.236	1.830
7.0	50	0.434	0.188	0.997	0.744
7.0	100	0.127	0.031	0.171	0.178

* Based on Eq. 5.1

Table 5.6
Overall damage indices from simulations for
Frame structure II

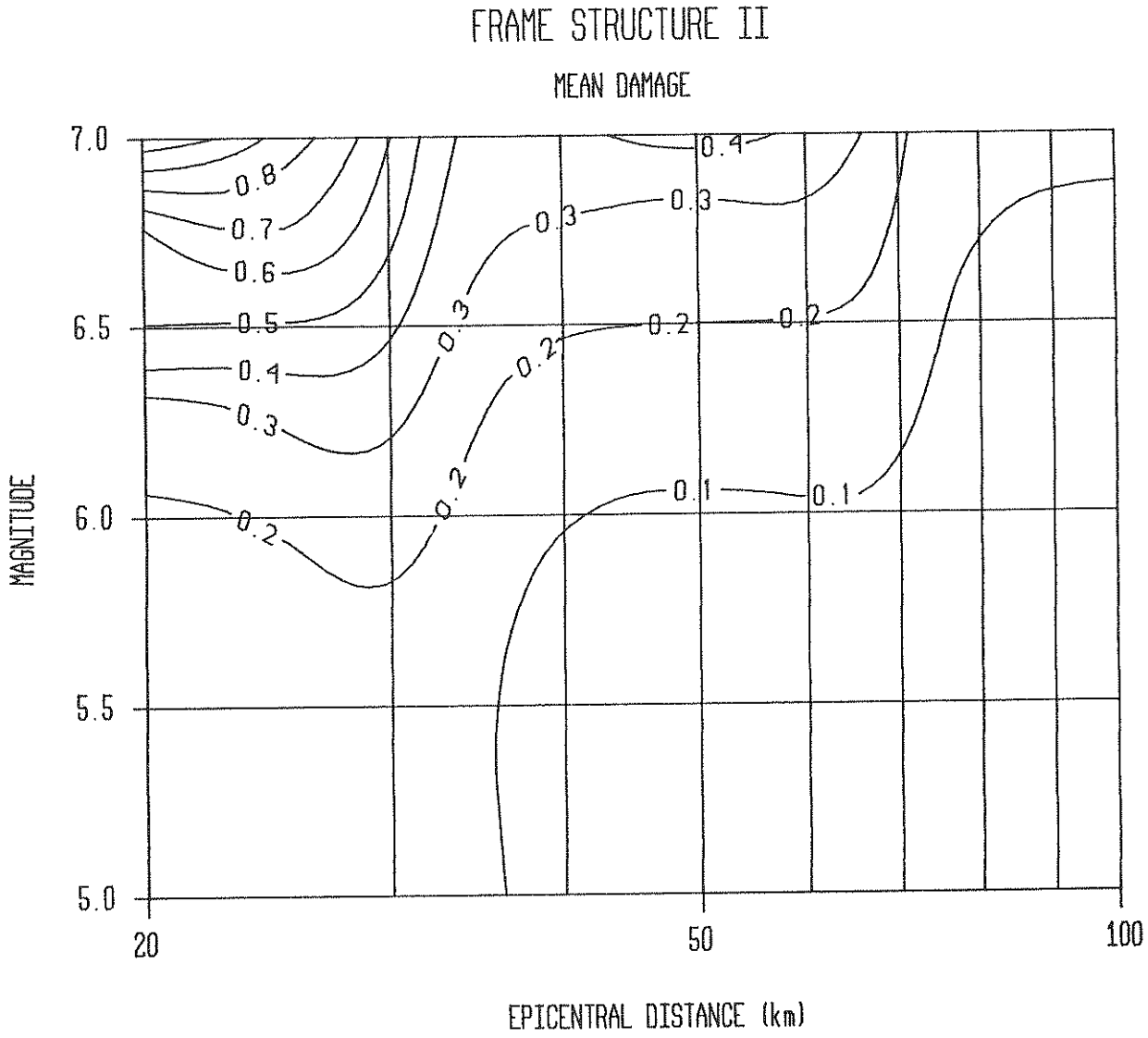

Figure 5.12
Contour Plot of Mean Damage
Frame Structure II

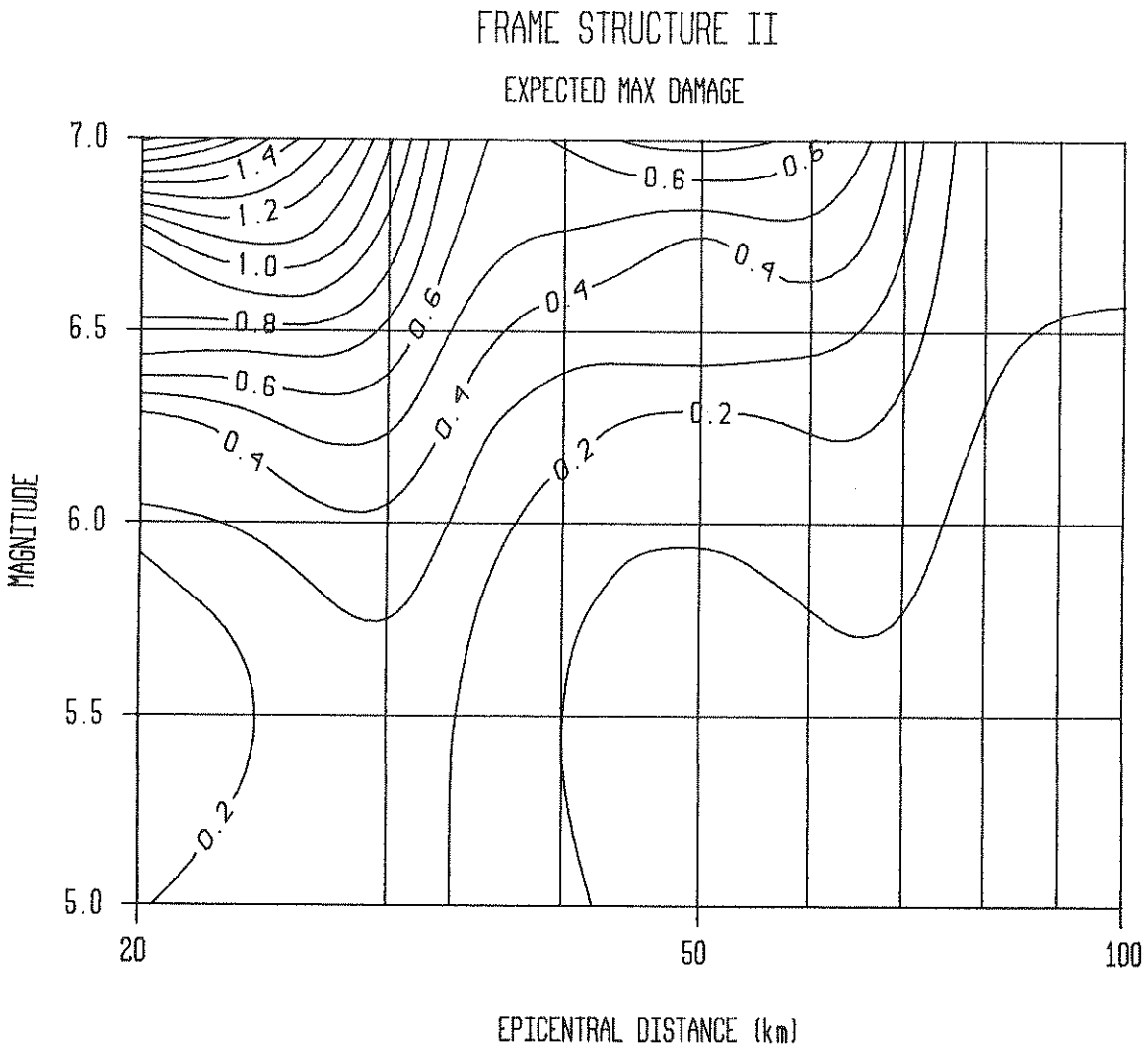

Figure 5.13
Contour Plot of Expected Maximum Damage
Frame Structure II

greater than 6.7 and epicentral distances less than 30 km. The region of severe damage has extended to distances up to 70 km for magnitudes greater than 6.6. Additionally, at distances less than 35 km, severe damage is present for magnitudes as low as 6.0. The region of repairable damage occurs again for magnitudes less than 6.0 and all epicentral distances.

5.3.3 Distribution of Damage in Structure

The distribution of damage in the vertical elements of frame structure II has been considered for the same reasons discussed for frame structure I. Similar plots have been constructed for mean and expected maximum damage, and are shown in figures 5.14 through 5.17.

Plots of the distribution of mean and expected maximum damage for a magnitude 5.7 are shown in figures 5.14 (a) and 5.14 (b) respectively. From these plots, it is evident that both the mean and expected maximum damage are repairable at all distances. When the magnitude is increased to 6.2, the distribution of the resulting mean damage, figure 5.15 (a), still indicates repairable damage throughout the structure. However severe damage results on the first, fourth and fifth stories when the expected maximum damage is considered, figure 5.15 (b).

At magnitudes greater than 6.6, local collapse in the columns is present. The distribution of mean and expected maximum damage for a magnitude of 6.6 are shown in figures 5.16 (a) and 5.16 (b) respectively. Severe damage is present on the first, fourth and fifth stories at a distance of 20 km when the mean damage is considered. The mean damage at 50 and 100 km was in the repairable range for all stories. However when the expected maximum damage is considered at a distance

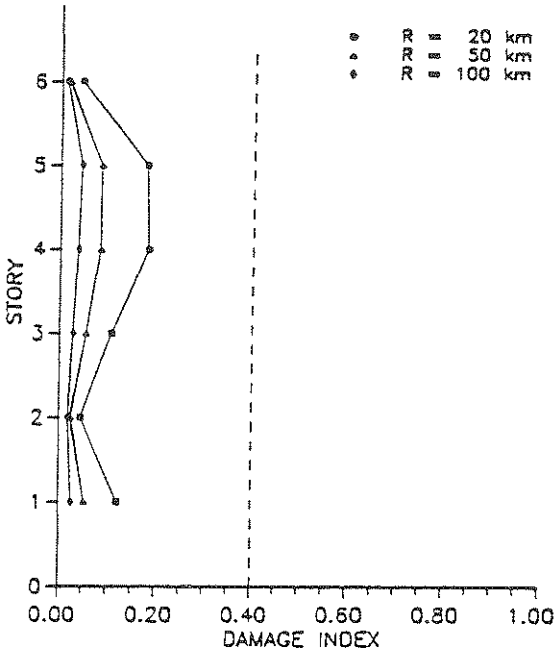

(a) Mean damage

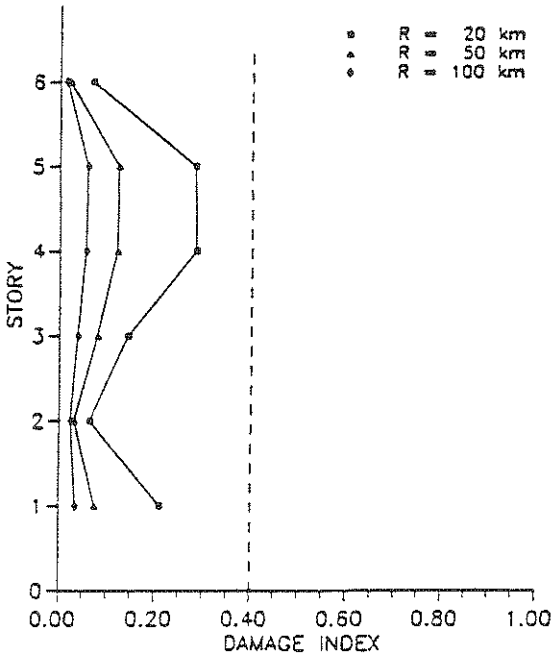

(b) Expected maximum damage

Figure 5.14
Distribution of damage frame structure II
Magnitude = 5.7

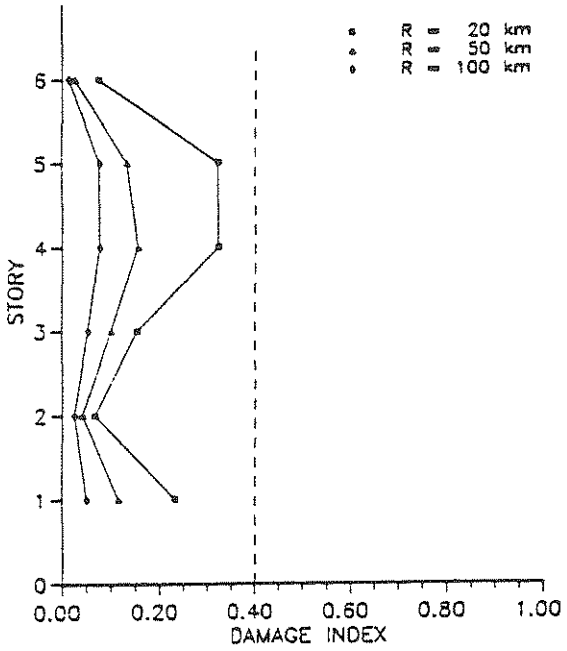

(a) Mean damage

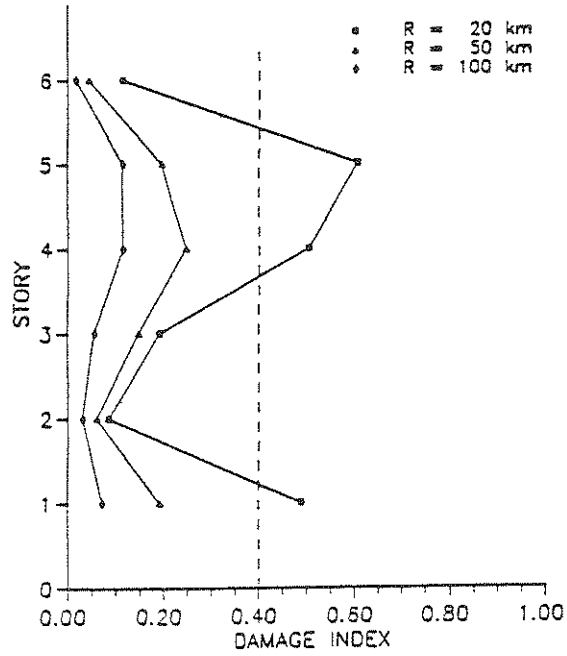

(b) Expected maximum damage

Figure 5.15
Distribution of damage frame structure II
Magnitude = 6.2

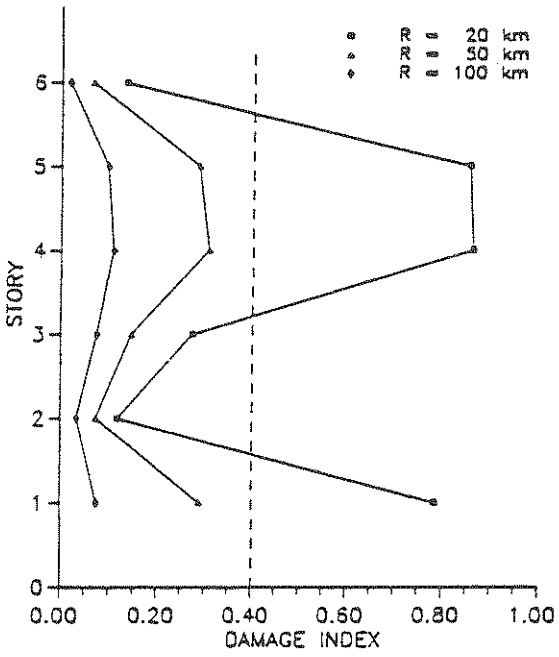

(a) Mean damage

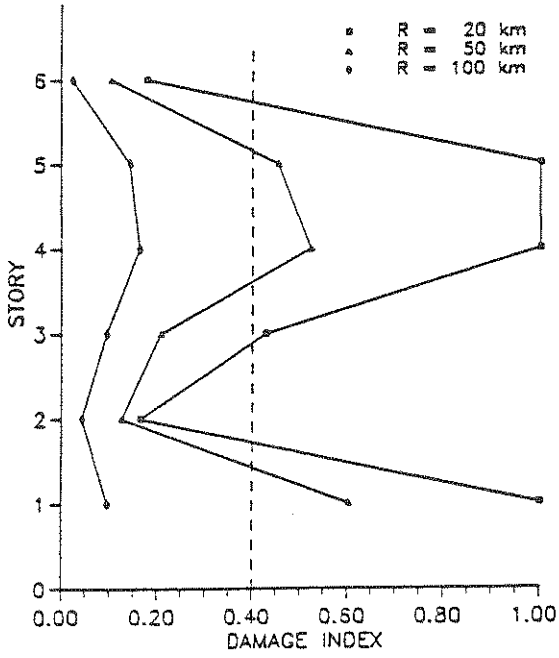

(b) Expected maximum damage

Figure 5.16
Distribution of damage frame structure II
Magnitude = 6.6

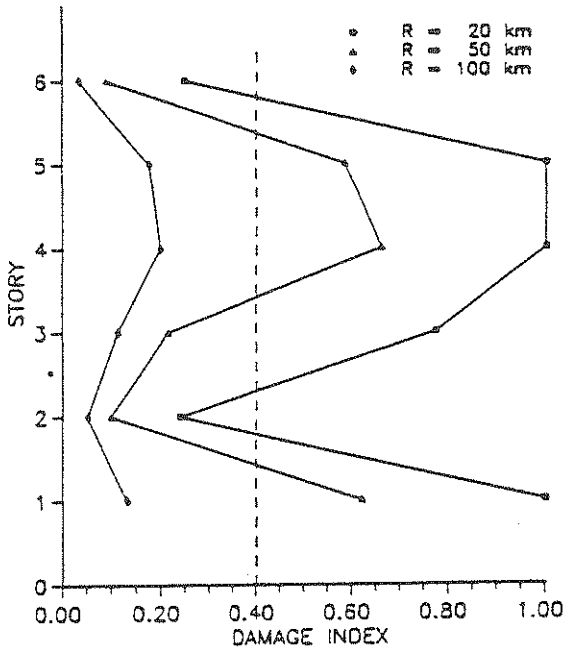

(a) Mean damage

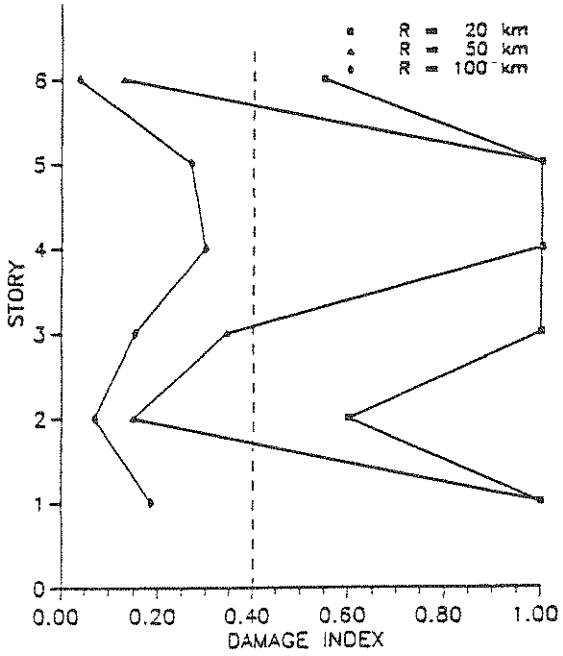

(b) Expected maximum damage

Figure 5.17
Distribution of damage frame structure II
Magnitude = 7.0

of 20 km, collapse results on the first, forth and fifth stories. The resulting overall expected maximum damage index of 0.858, table 5.6 (6), does not indicate total collapse of the structure. Additionally, severe damage was present in the vertical elements on three stories for a distance of 50 km, but the overall expected maximum damage index of the structure was less than 0.4.

The distribution of mean damage for a magnitude of 7.0, figure 5.17 (a), indicates local collapse at 20 km and severe damage at 50 km. When the expected maximum damage is considered, figure 5.17 (b), local collapse occurs at both 20 and 50 km. Generally for all the magnitude and epicentral distance combinations considered, the damage in the vertical elements was highest on the first, fourth and fifth stories. The resulting damage at a distance of 100 km was repairable for all magnitudes in the range considered.

5.4 Analysis of Coupled Frame-Shear Wall Structure

To determine the effect of the shear wall on the resulting damage indices, the analysis of the shear wall structure was performed identically as that of frame structure I. The relation between the final state of the damaged structure and the corresponding damage indices is considered. Contour plots of mean and expected maximum damage were developed and regions of repairable damage, severe damage and collapse are identified. Additionally, the distribution of damage throughout the structure is sought to define the relation between local concentrations of damage and the overall damage index.

5.4.1 Final State of Damaged Structure

A physical description of the resulting damage and its relation to the corresponding damage indices can be obtained from consideration of the final state of the structure. In order to compare the results with frame structure I, the magnitude and epicentral distance were taken as 6.2 and 20 km respectively. A single simulation with a resulting overall damage index between the mean and expected maximum damage is considered.

The final state of the exterior and interior frames of the shear wall structure are shown in figures 5.18 (a) and 5.18 (b) respectively. The exterior frame resulted with cracking of the columns on the first three stories, and a combination of cracking and yielding of the columns on the fourth and fifth stories. There was complete yielding of all the columns on the sixth story. Almost all the beams in the exterior frame have yielded, except on the sixth story, where some remained elastic or cracked.

The beams and columns of the interior frame containing the shear wall behaved similarly to the exterior frame. The shear wall resulted in yielding and cracking on the first three stories, with yielding on the first story occurring both at the base and mid-height of the wall. The shear wall generally cracked at the ends and remained elastic at the center on the top three stories.

A beam type mechanism is predominate due to the extensive yielding of the beams. This evident from the distribution of story drifts, table 5.7, which are approximately uniform throughout the structure. Additionally the top deformation was 1.4% of the structures height.

A quantitative description of the final damaged state of the structure can be

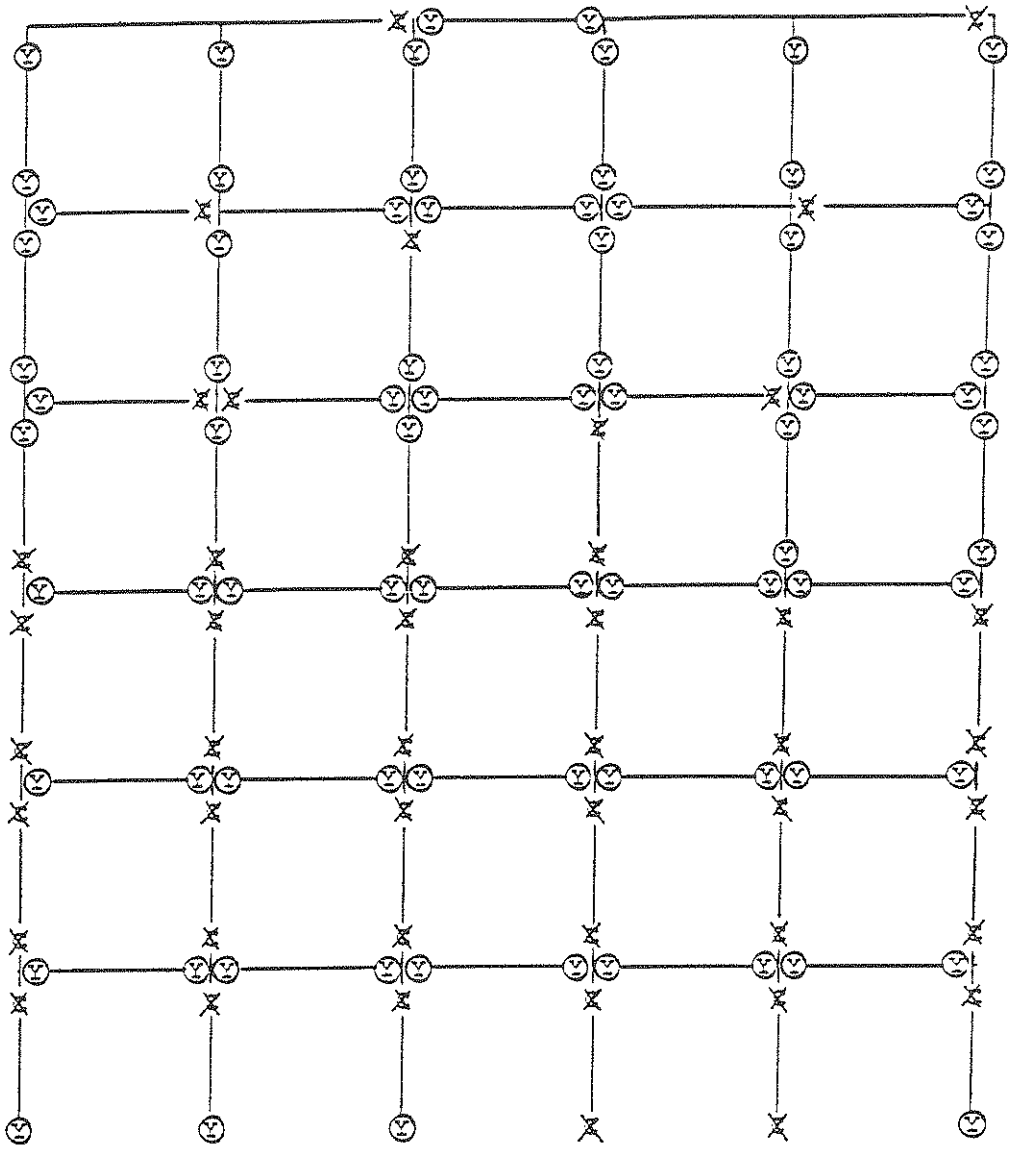

NOTATION:

= CRACK

= YIELD

Figure 5.18 (a)
Final state of exterior frame
Shear wall structure
M = 6.2, R = 20 km

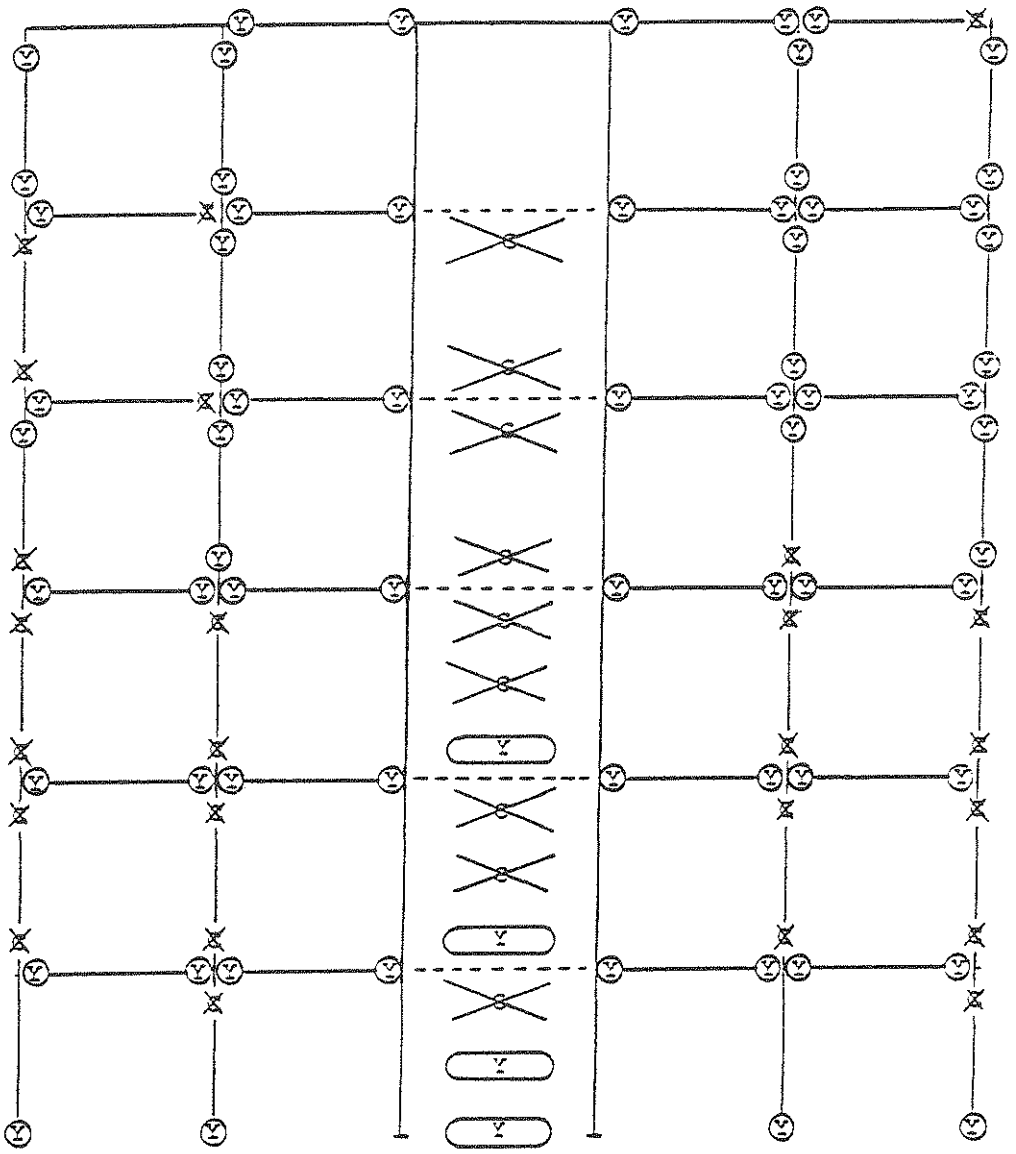

NOTATION:

= CRACK

= YIELD

Figure 5.18 (b)
Final state of interior frame
Shear wall structure
$M = 6.2$, $R = 20$ km

made with reference to figures 5.19 (a) and 5.19 (b). The resulting damage of the beams was highest in the interior frame for the beams connected to the shear wall, but all the beams were in the repairable range. Damage indices of the columns were generally in the repairable range, with the exception of a few columns on the fifth story. Damage of the shear wall was significant on the first three stories with severe damage resulting on the first story.

The resulting story level damage indices are presented in table 5.8 for the horizontal and vertical elements. Severe damage results only in the vertical elements on the first story, although the damage on the fifth story was close to the limit of repairable damage. The overall damage index of the structure of 0.259 indicates the structure as a whole is repairable, but severe damage occurred in the shear wall on the first story. The resulting mean and expected maximum overall damage indices were 0.222 and 0.338 respectively for the earthquake characteristics considered, table 5.9 (3) (6).

5.4.2 Contour Plots

The results of the Monte Carlo simulations for the shear wall structure are given in table 5.9, and have been used to construct contour plots of mean and expected maximum damage versus magnitude and epicentral distance. From these plots regions of repairable damage, severe damage and collapse are defined.

The resulting contour plot of mean damage of the shear wall structure is shown in figure 5.20. From the plot, it is evident that the damage is localized to large magnitudes and small distances. With the addition of the shear wall to frame structure I, the region of total collapse was eliminated. Severe damage was confined

Story No. (1)	Max story drift (inch) (2)	Max drift % story height (3)	Max story disp (inch) (4)	Max disp % total height (5)
1	1.492	1.04	1.492	0.17
2	1.868	1.30	3.341	0.39
3	1.748	1.19	5.018	0.59
4	1.747	1.19	6.692	0.77
5	1.735	1.20	8.377	0.97
6	1.708	1.19	10.040	1.16

Table 5.7
Story drift and displacement
Shear wall structure
M = 6.2, R = 20 km

Story No. (1)	Vertical components		Horizontal components	
	Damage index (2)	Energy ratio (3)	Damage index (4)	Energy ratio (5)
1	0.538	0.151	0.192	0.140
2	0.297	0.061	0.196	0.147
3	0.141	0.039	0.150	0.104
4	0.276	0.069	0.114	0.060
5	0.354	0.080	0.096	0.040
6	0.258	0.089	0.097	0.020

Damage index for building 0.259

Table 5.8
Story level damage indices
Shear wall structure
M = 6.2, R = 20 km

M	R (km)	Mean damage	STD.	Actual max damage	Expected* max damage
(1)	(2)	(3)	(4)	(5)	(6)
5.0	20	0.039	0.008	0.058	0.052
5.3	20	0.062	0.018	0.102	0.092
5.3	50	0.027	0.009	0.060	0.042
5.7	20	0.120	0.062	0.350	0.222
5.7	50	0.047	0.018	0.109	0.077
5.7	100	0.022	0.003	0.029	0.027
6.2	20	0.222	0.070	0.354	0.338
6.2	50	0.063	0.023	0.130	0.101
6.2	100	0.035	0.010	0.060	0.052
6.6	20	0.526	0.212	0.981	0.912
6.6	50	0.108	0.040	0.249	0.174
6.6	100	0.046	0.013	0.071	0.067
7.0	20	0.820	0.362	1.545	1.417
7.0	50	0.220	0.065	0.375	0.327
7.0	100	0.085	0.034	0.164	0.141

* Based on Eq. 5.1

Table 5.9
Overall damage indices from simulations for
Shear wall structure

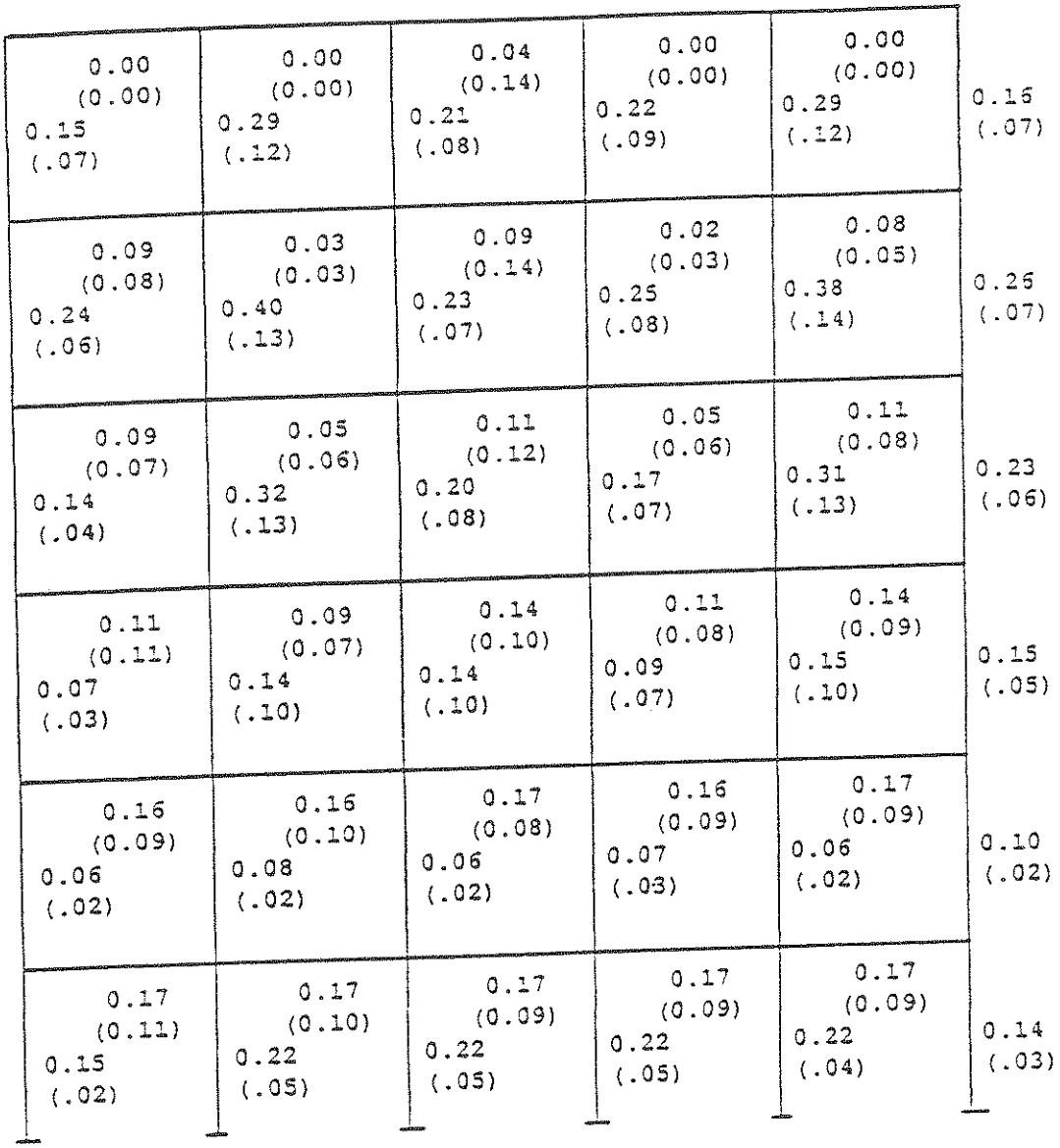

VALUES IN PARANTHESIS INDICATE ENERGY RATIOS

Figure 5.19 (a)
Damage indices of exterior frame
Shear wall structure
M = 6.2, R = 20 km

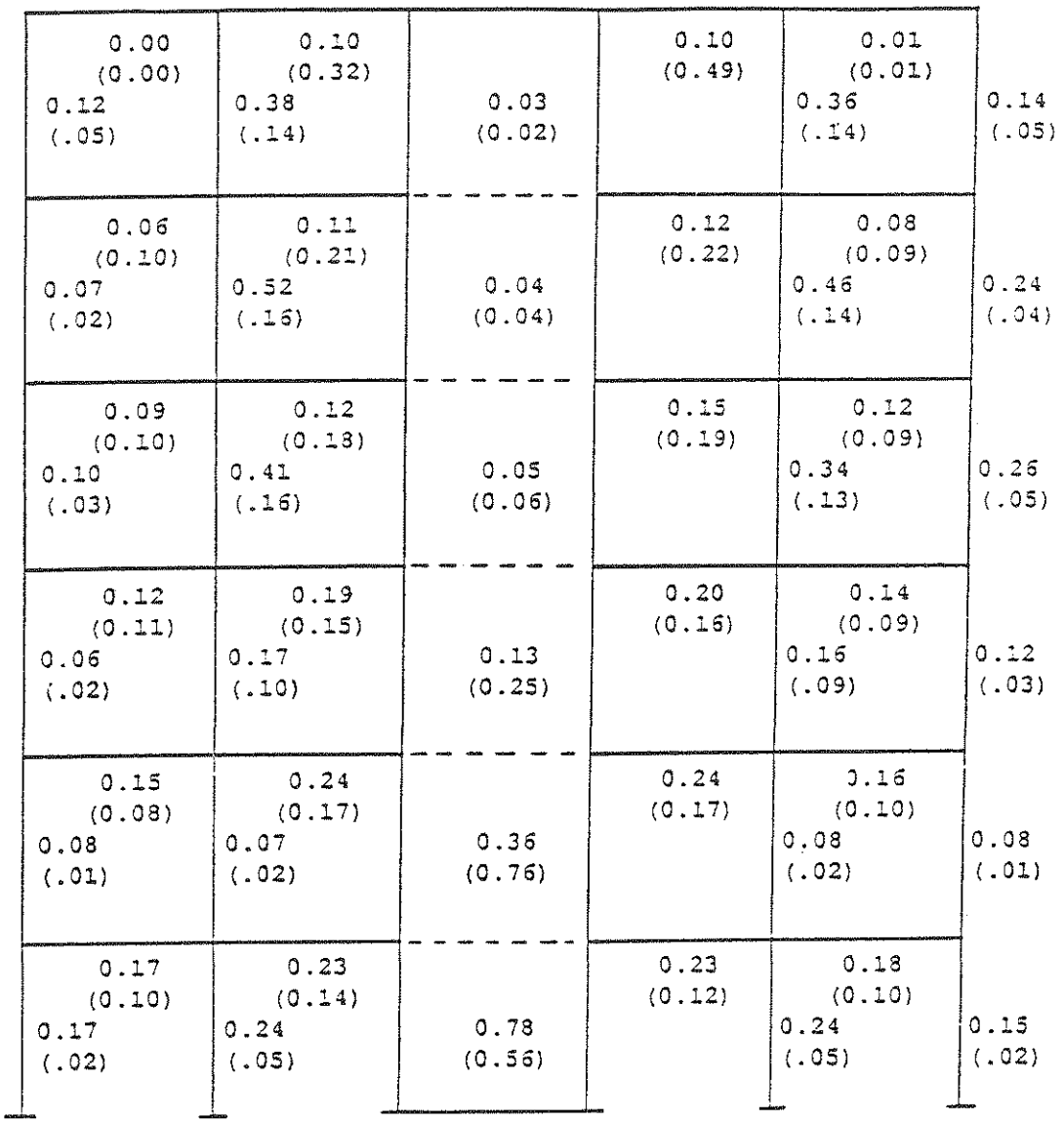

VALUES IN PARANTHESIS INDICATE ENERGY RATIOS

Figure 5.19 (b)
Damage indices of interior frame
Shear wall structure
M = 6.2, R =20 km

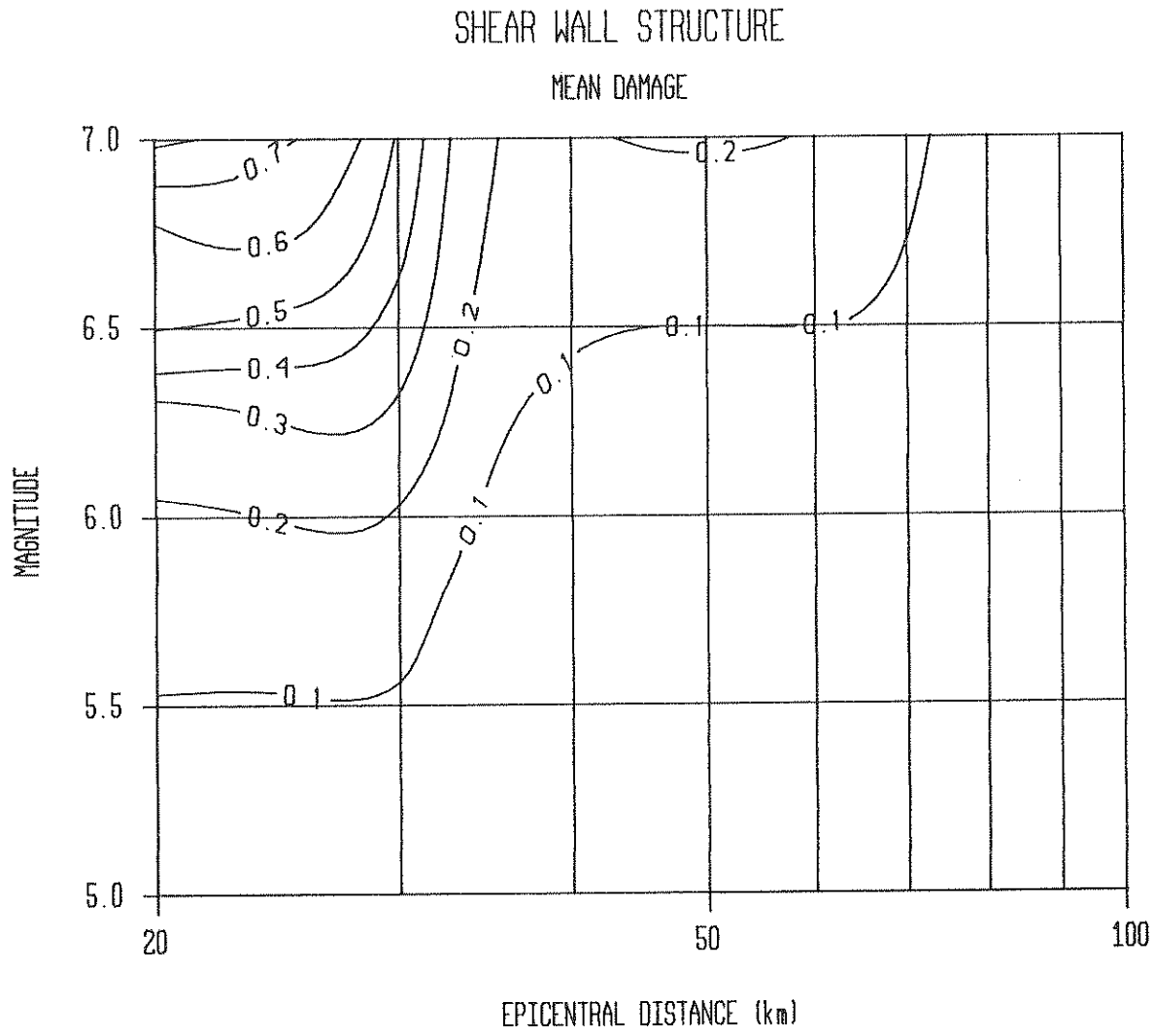

Figure 5.20
Contour Plot of Mean Damage
Shear Wall Structure

to magnitudes greater than 6.4 and epicentral distances less than 30 km. The resulting damage was repairable for all magnitudes in the range considered when the epicentral distance was greater than 30 km. Additionally, the resulting damage at distances less than 30 km was repairable for magnitudes less than 6.4.

The expected maximum damage of the shear wall structure as a function of magnitude and epicentral distance is shown in figure 5.21. A small region of total collapse is present for magnitudes greater than 6.8 and distances less than 28 km. The overall expected maximum damage also predicts magnitude and epicentral distance combinations that result in severe damage. This region is defined for magnitudes greater than 6.6 and epicentral distances less than 32 km. As in the case of the overall mean damage index, the significant expected maximum damage was confined to large magnitudes and short distances. For all magnitudes and epicentral distances greater than 25 km, the resulting damage was repairable. Additionally, the expected maximum damage was repairable for magnitudes less than 6.2 at all distances.

5.4.3 Distribution of Damage in Structure

To evaluate the relation between concentrations of damage in the structure to the overall damage index, the distribution of damage throughout the structure is considered. The distribution of mean and expected maximum damage indices in the vertical elements can be compared to the resulting distribution of damage in frame structure I to determine the effect of the shear walls on the resulting damage. Magnitudes in the range of 5.7 to 7.0 are considered each with epicentral distances of 20, 50 and 100 km.

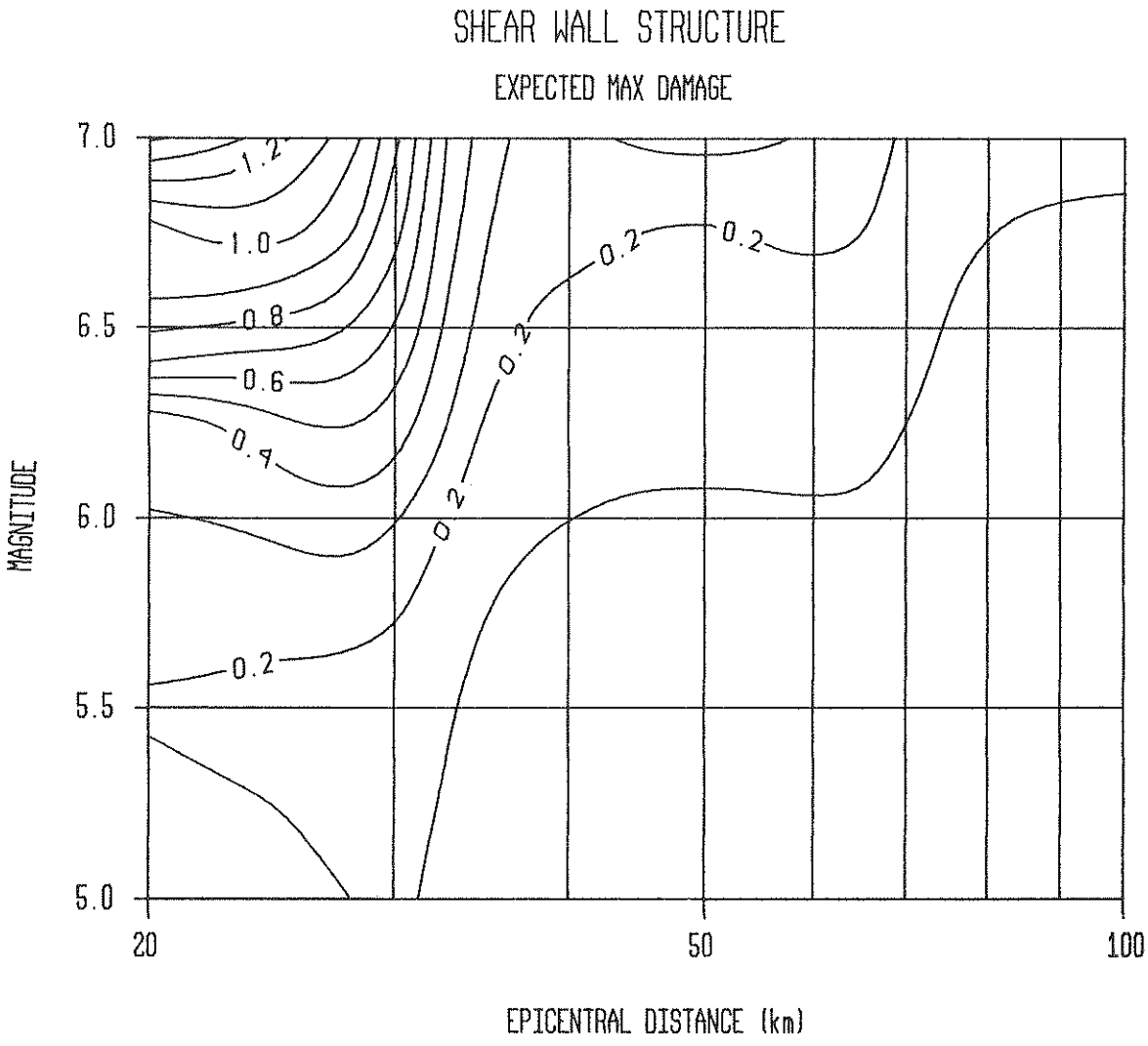

Figure 5.21
Contour Plot of Expected Maximum Damage
Shear Wall Structure

The resulting distribution of mean and expected maximum damage in the vertical elements of the shear wall structure for a magnitude of 5.7 are shown in figures 5.22 (a) and 5.22 (b) respectively. The distribution of mean damage indicates repairable damage at all distances, with the highest damage occurring on the first story. When the expected maximum damage is considered, the damage on the first story becomes severe at a distance of 20 km. At distances of 50 and 100 km, there was not a significant difference between the mean and the expected maximum damage in the upper stories.

With the magnitude increased to 6.2, the concentration of mean damage occurred on the first two stories, figure 5.23 (a), at a distance of 20 km. Additionally, severe damage results on the first story. The expected maximum damage indicates severe damage on the first two stories at a distance of 20 km. The resulting mean and expected maximum damage at 50 and 100 km were again almost identical, and repairable at all stories.

The distribution of mean and expected maximum damage for a magnitude of 6.6 are shown in figures 5.24 (a) and 5.24 (b) respectively. The mean damage shows the same trend as before with the concentration of highest damage on the first two stories, but now local collapse occurs on the first story for a distance of 20 km. Additionally, the damage at all other stories has increased a considerable amount from the lower magnitudes, and severe damage results on the fifth story. Again at distances of 50 and 100 km, the resulting damage was repairable throughout all the vertical elements in the structure. The resulting expected maximum damage at a distance of 20 km was severe at all stories, with collapse of the vertical elements on the first two stories. The resulting damage in the first story at a distance of 50 km

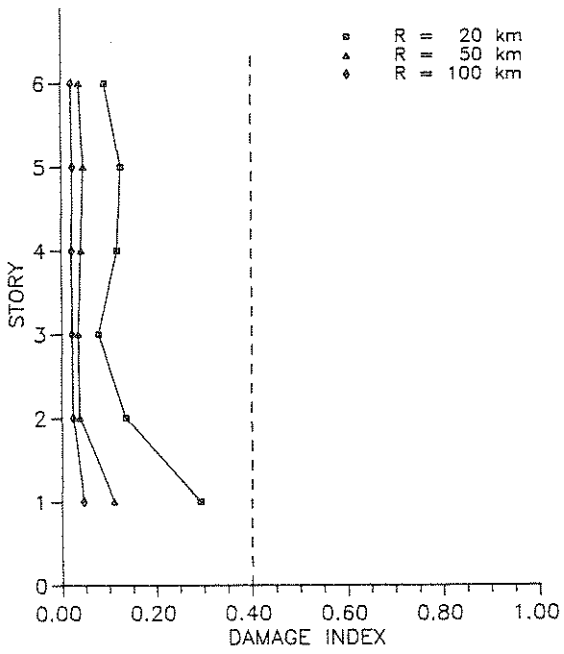

(a) Mean Damage

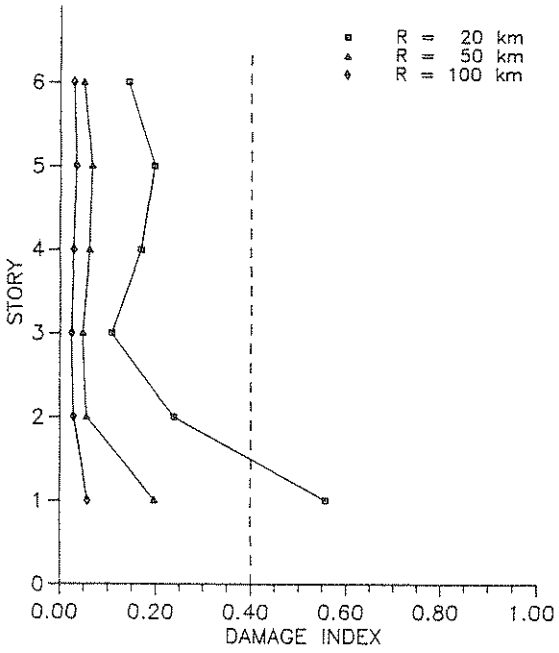

(b) Expected Maximum Damage

Figure 5.22 Distribution of Damage Shear Wall Structure; Magnitude = 5.7

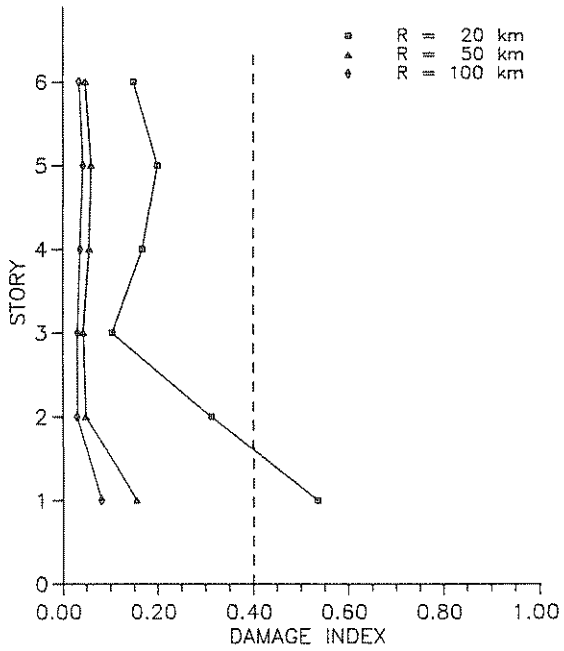

(a) Mean Damage

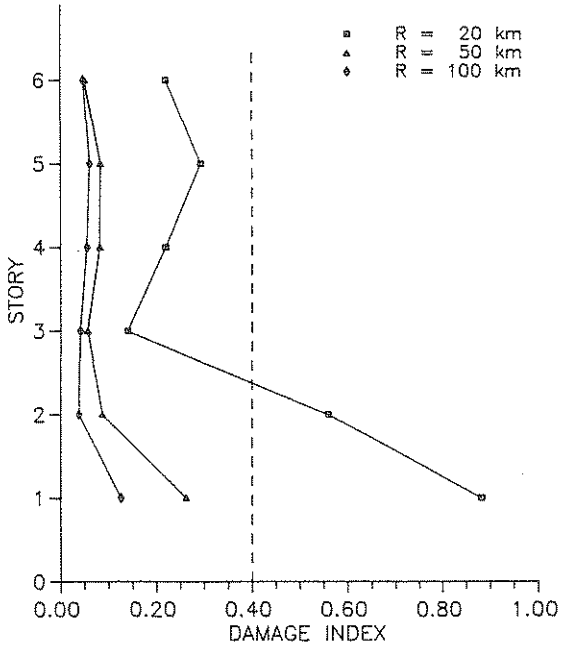

(b) Expected Maximum Damage

Figure 5.23 Distribution of Damage Shear Wall Structure; Magnitude = 6.2

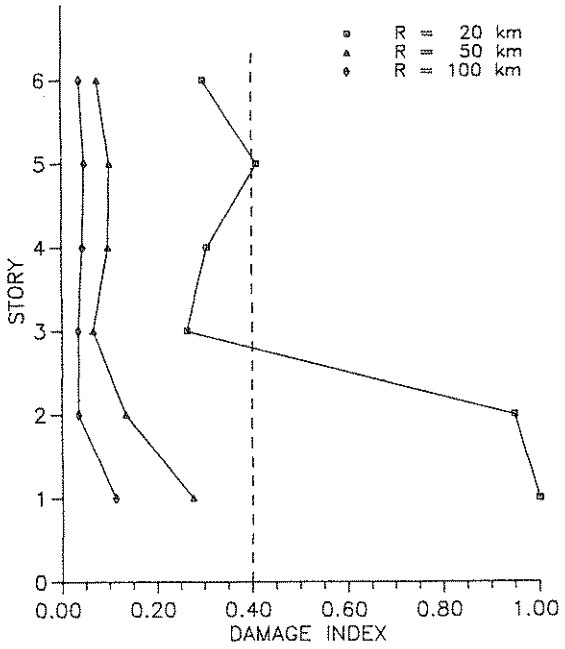

(a) Mean Damage

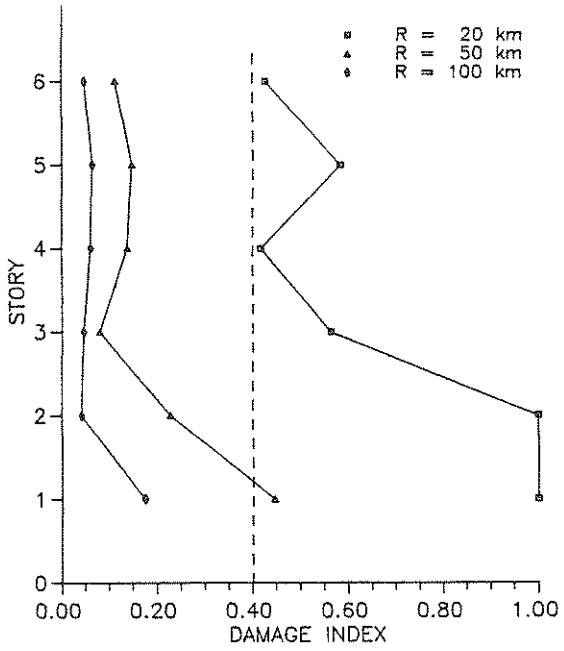

(b) Expected Maximum Damage

Figure 5.24 Distribution of Damage Shear Wall Structure; Magnitude = 6.6

was now in the severe range.

The resulting mean damage index for a magnitude of 7.0 and a distance of 20 km was 0.820, table 5.9 (3), which does not indicate total collapse of the structure. The distribution of mean damage for this case, figure 5.25 (a), indicates local collapse on the first two stories and severe damage on all other stories except the third. Thus the distribution of damage in the overall risk assessment proves to be crucial. Severe damage also results in the vertical elements on the first story at a distance of 50 km. The expected maximum damage for a magnitude of 7.0 is shown in figure 5.25 (b). At a distance of 20 km, the entire distribution of damage indices is well to the right of the repairable damage limit, with local collapse on the first two stories. The overall expected maximum damage index of the structure for this case was greater than 1.0, indicating total collapse of the structure. Thus the overall damage index may predict collapse when the distribution of damage throughout all the vertical elements is relatively high. At a distance of 50 km, severe damage results on the first two stories and the remaining stories are repairable. For all the cases considered, both the mean and expected maximum damage at a distance of 100 km were repairable.

The distribution of damage in the coupled frame shear wall structure showed a slightly different trend than found in the previous two frame structures. The largest damage indices now occur on the first story, and there is a slight increase in the damage on the fourth and fifth stories. The opposite trend was found in the frame structures. That is, the highest damage was on the fourth and fifth stories, and there was a slight increase in the damage on the first story.

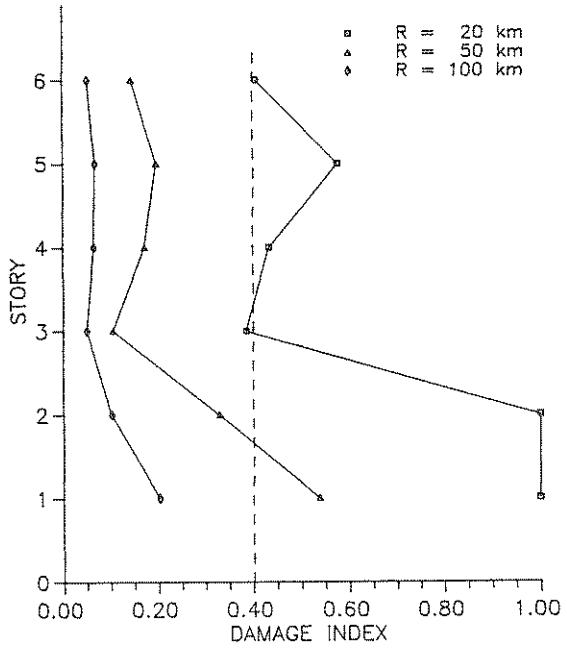

(a) Mean Damage

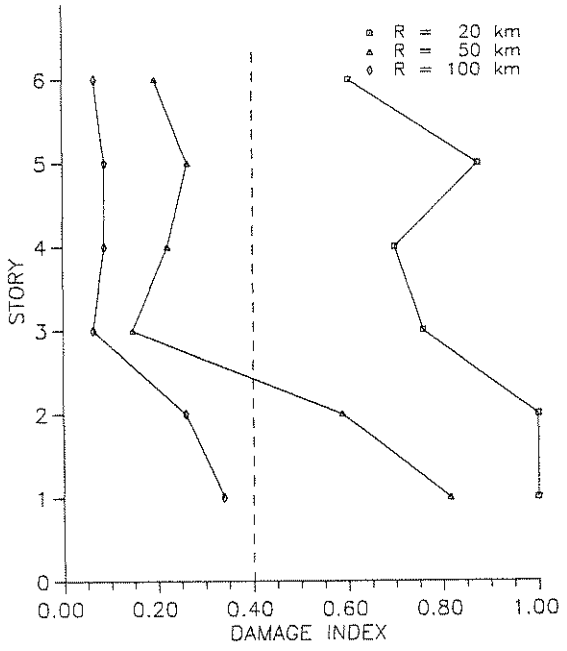

(b) Expected Maximum Damage

Figure 5.25 Distribution of Damage Shear Wall Structure; Magnitude = 7.0

5.5 Empirical Equations for Damage

For practical purposes, a simplified expression is desired to relate the overall damage index of the structure to the prescribed earthquake characteristics. The form of the relation desired is a constant multiplied by a function of magnitude and epicentral distance, where the constant depends on the structure. Thus the resulting damage of a structure, and the corresponding seismic risk, can be easily assessed for a given earthquake magnitude and epicentral distance.

Several forms of the functional relation of magnitude and epicentral distance were considered and regression analysis was performed to fit the function to the data obtained from the Monte Carlo simulations. The form of the equation that fit best for all structures is expressed as

$$D = k\left(\frac{10^{\beta M}}{R^{\alpha}}\right) \tag{5.2}$$

for M nondimensional and R in kilometers. Regression analysis of the mean and expected maximum overall damage index for the three test structures resulted with $\beta \approx 0.6$ and $\alpha \approx 1.0$. Thus a single function of magnitude and epicentral distance can be used for all cases. This equation is expressed as

$$D = k\left(\frac{10^{0.6M}}{R}\right) \tag{5.3}$$

with α and β constant for all structures. The coefficient k was determined to produce the best fit with the available data from the Monte Carlo simulations. The resulting k values and their corresponding coefficients of variation from the regression analysis are presented in table 5.10.

(1)	Mean k_{mean} (2)	c.o.v. (3)	Expected Max k_{max} (4)	c.o.v. (5)	k_{max}/k_{mean} (6)
Frame structure I	1.48×10^{-3}	0.193	2.23×10^{-3}	0.218	1.51
Frame structure II	1.08×10^{-3}	0.188	1.75×10^{-3}	0.257	1.62
Shear wall structure	0.84×10^{-3}	0.272	1.36×10^{-3}	0.314	1.62

Table 5.10
Regression coefficients for
damage function

It is interesting to note that the ratio k_{max}/k_{mean} was approximately constant for all three structures as shown in table 5.10 (6). Furthermore, this ratio was almost identical to the number of standard deviations added to the mean to obtain the expected maximum damage. The expected maximum damage was defined as having a 5% probability of exceedence, and for a Gaussian distribution, this corresponds to the mean plus 1.65 standard deviations (see Eq. 5.1). The ratio of k_{max}/k_{mean} was 1.62 for both frame structure II and the shear wall structure, and was slightly less for frame structure I. Thus damage with a different probability of exceedence can be easily approximated from the k coefficient of the mean damage.

Contour plots of the mean overall damage of the three structures were developed from the empirical damage function defined by equation 5.3. Figure 5.26 represents the contour plot developed from equation 5.3 for frame structure I with $k = 1.48\text{x}10^{-3}$. The contours of equal damage in figure 5.26 compare well with those of figure 5.4 developed from the actual data. The predicted damage was slightly lower than the actual damage, but the regions of collapse, severe damage and repairable damage were generally the same.

The resulting contours of mean overall damage from equation 5.3 for frame structure II and the shear wall structure are shown in figures 5.27 and 5.28 respectively. The comparison of the predicted and actual damage was the same as frame structure I, with the predicted damage slightly less than the actual damage. Generally the contour plots developed from equation 5.3 produce approximately straight lines of equal damage, whereas the contours of actual damage showed a considerable amount of curvature. This difference between the two results from the number of data points used. The plots of the actual damage from the Monte

Carlo simulations were developed from approximately fifteen data points, and intermediate points were interpolated by the software from adjacent points using an inverse distance formulation. The contour plots of damage from equation 5.3 were developed with forty data points and the amount of interpolation between data points was reduced. Therefore the contour plots developed from equation 5.3 may give a better representation of the damage as a function of magnitude and epicentral distance. The empirical damage function generally overestimated the overall damage index for magnitudes less than 6.0, and underestimated the overall damage index for magnitudes greater than 6.0. The actual difference between the predicted overall damage index and the actual overall damage index for all magnitudes was not substantial.

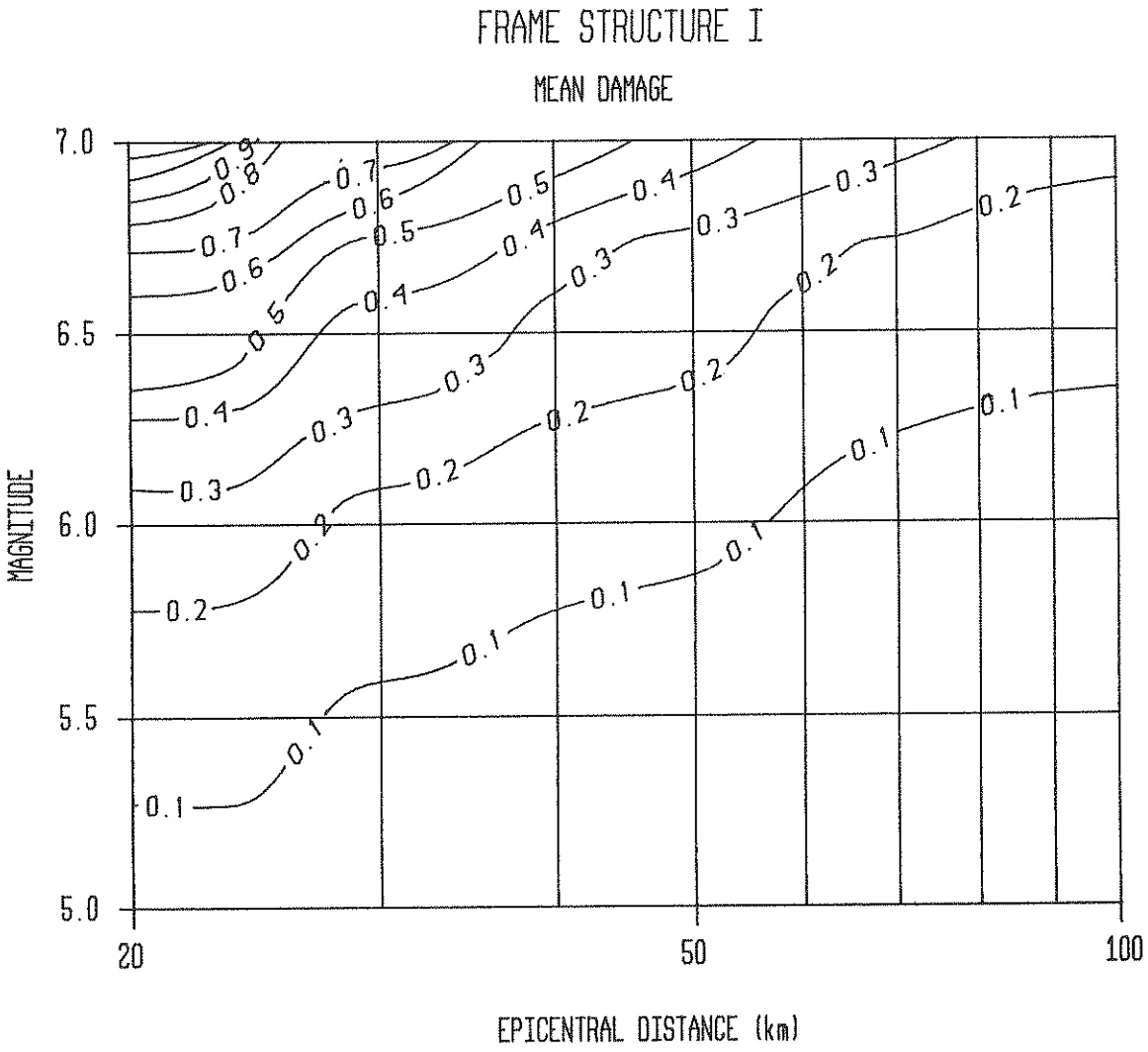

Figure 5.26
Contour Plot of Mean Damage from Empirical Equation
Frame Structure I

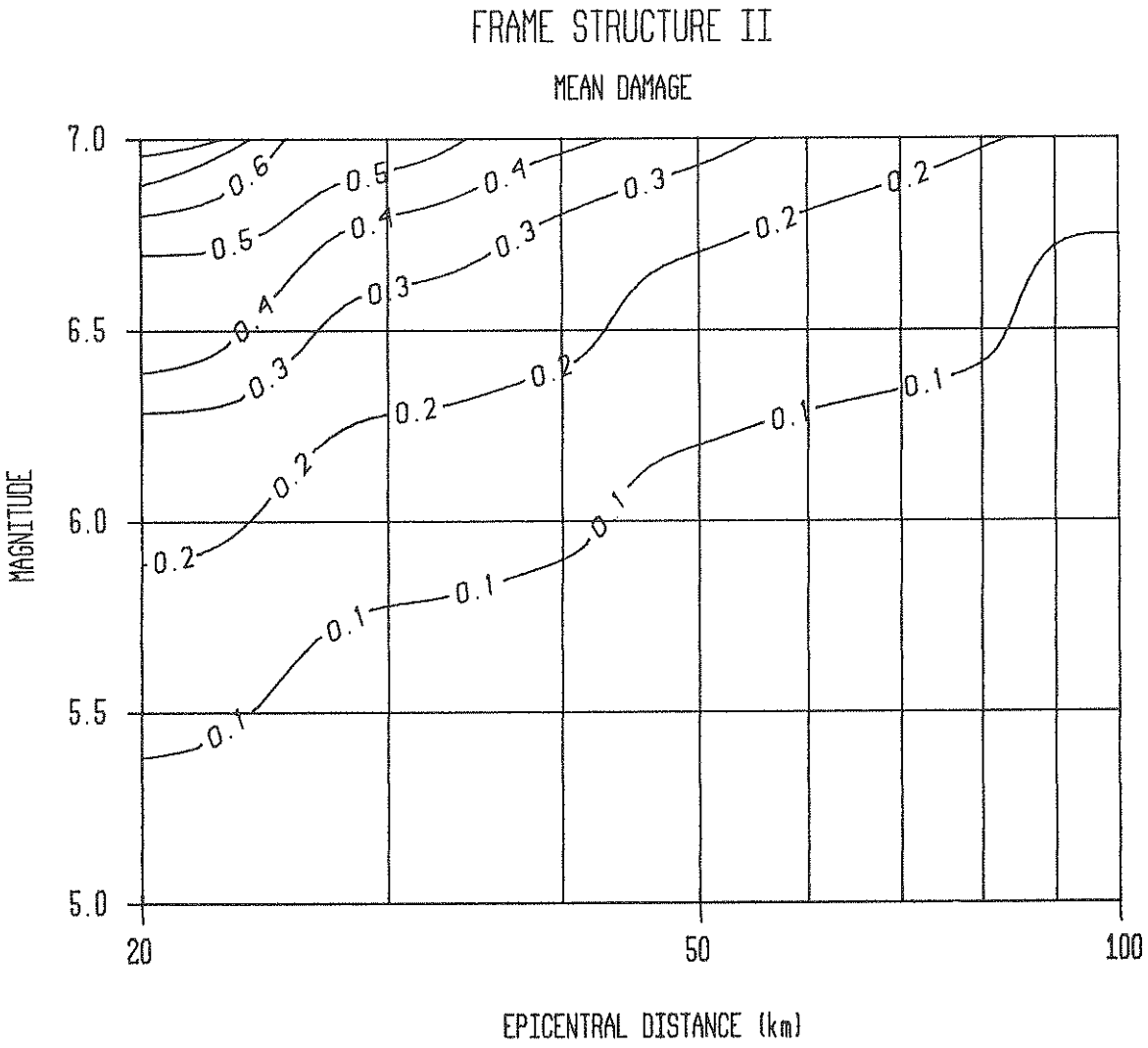

Figure 5.27
Contour Plot of Mean Damage from Empirical Equation
Frame Structure II

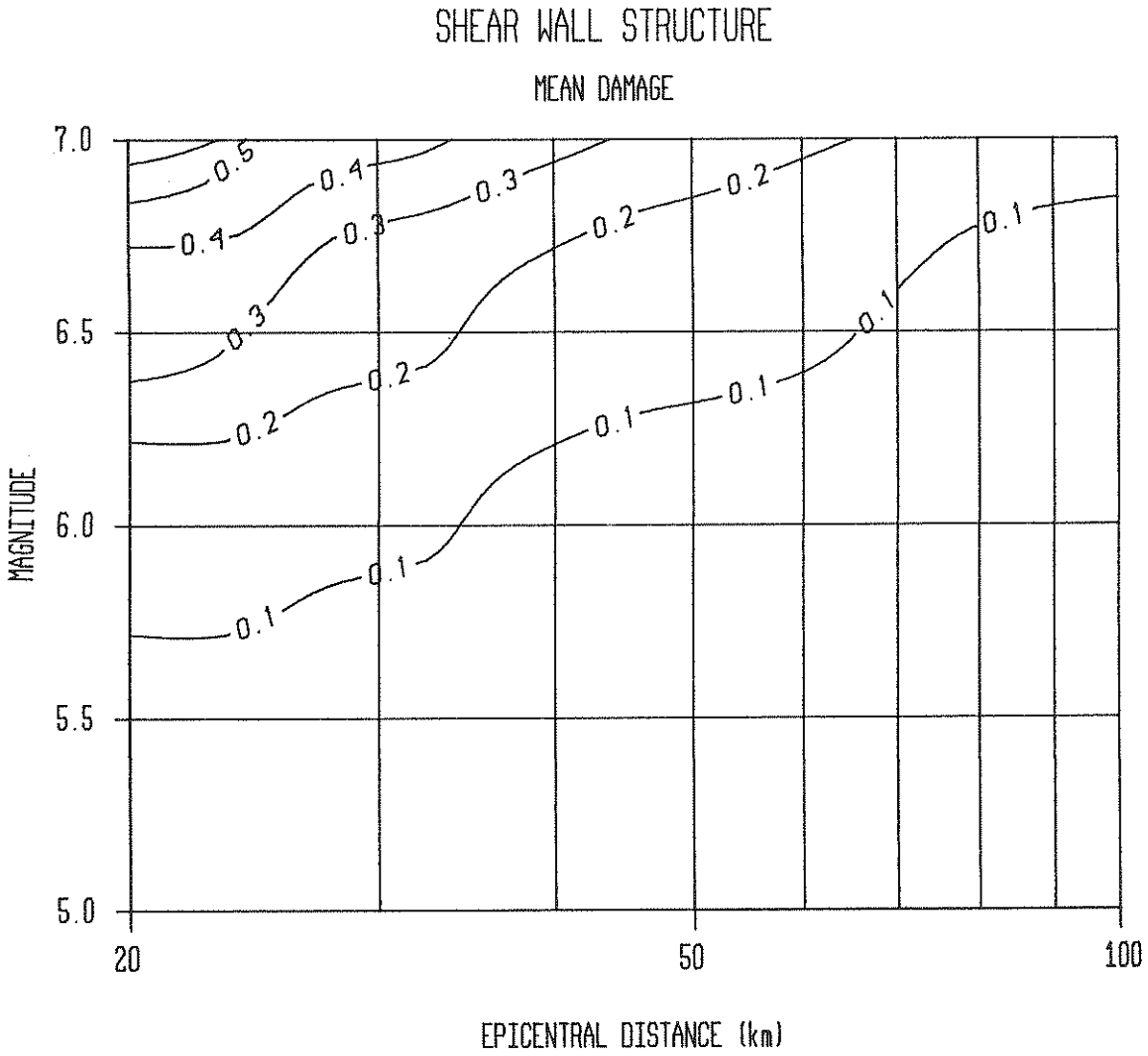

Figure 5.28
Contour Plot of Mean Damage from Empirical Equation
Shear Wall Structure

CHAPTER 6

DISCUSSION AND CONCLUSIONS

6.1 General

The primary purpose of this research was to assess the seismic hazard associated with reinforced concrete structures in the eastern United States. For this purpose, damage of the structure was considered as an indicator of the risk involved if an earthquake of considerable size occurs. The structures considered were designed for gravity loads according to the ACI 318/83 building code, with no consideration to seismic loads.

Simulated earthquake motion was used for the analysis because of the absence of recorded accelerograms of eastern United States earthquakes. The ground motion was modeled as a nonstationary random process with spectral characteristics determined from attenuation relations for eastern North American earthquakes. A Monte Carlo simulation technique was used along with the program IDARC [25] to determine the resulting damage indices due to various different earthquakes.

The results of the study were used to develop the correlation of the damage index with earthquake characteristics for different types of structural configurations. An equation was developed to relate damage as a function of magnitude and epicentral distance, and can be used to assess the risk involved for a prescribed earthquake event. Additionally, the distribution of damage in the structure was considered to determine the effect of local concentrations of damage on the overall damage index.

6.2 Correlation of Damage, Magnitude and Distance

Monte Carlo simulations were performed for a number of combinations of magnitude and epicentral distance which resulted in significant damage. Statistics of the simulation results provide the mean and standard deviation of the damage index. These values can be used to define an expected maximum damage index that has a prescribed probability of exceedence, for this study a 5% probability of exceedence was considered. Additionally, the resulting overall damage and the local distribution of damage in the structure were considered.

6.2.1 Overall Damage

The correlation of the mean and expected maximum damage with magnitude and epicentral distance was developed in chapter five for each of the three test structures. From the contour plots developed regions of collapse, severe damage and repairable damage were defined. All three test structures showed a similar correlation between the resulting damage index and earthquake characteristics.

The contour plots of mean damage generally showed a small region of collapse for magnitude epicentral distance combinations in the range of 7.0 and 20 km. The region of severe damage generally resulted for magnitudes greater than 6.5 at close distances, and for larger magnitudes at increased distances. In all cases, no severe damage was present for epicentral distances greater than 60 km. Furthermore damage of the structures was repairable for all distances when the magnitude was approximately less than 6.4.

When the expected maximum damage was considered, the contour plots followed the same trend as the mean damage, but with increased damage indices at

all points. The region of collapse generally extended to magnitudes as low as 6.7 with distances up to 30 km. For magnitudes greater than 6.2 and close distances, severe damage resulted, but severe damage did not occur at any magnitudes when the epicentral distance was greater than 70 km. As in the case of the mean, the resulting damage was repairable at magnitudes less than 6.2.

Generally the damage index followed an "exponential " function of magnitude when the epicentral distance was constant. That is, at low magnitudes the increase in damage due to a small increase in magnitude was small, but at large magnitudes a small increase in magnitude produced a considerable increase in the resulting damage index. For a constant magnitude, the damage appeared to vary as the inverse of the epicentral distance. The empirical equation developed to define the correlation between damage, magnitude and distance exhibits the characteristics mentioned above. Note that the damage in equation 5.3 is related to ten raised to the power of magnitude, thus the desired relation between damage and magnitude is obtained. Additionally the regression analysis resulted with damage inversely proportional to the epicentral distance. The difference between the mean and the expected maximum damage was a change in the coefficient k multiplying the function of magnitude and epicentral distance.

6.2.2 Local Damage

A comparison of concentrations of local damage with the overall damage index is necessary to accurately assess the risk involved. The distribution of mean and expected maximum damage in the vertical elements was treated in chapter five for the three test structures. In many instances damage indices in the vertical elements

on a given story exceeded 1.0 indicating local collapse, while the overall damage index only indicated severe damage. Local collapse of the columns on a given story may lead to progressive collapse of the structure, and thus needs to be considered.

The highest concentration of damage in the two frame structures occurred in the columns on the fourth and fifth stories. This occurred because the gravity load design produced flexible columns in the upper stories of the structure. The large damage index was primarily cause by the ductility component of equation 2.1 due to large inter story drifts. The highest concentrations of damage in the shear wall structure occurred on the first story. This resulted because the increased stiffness of the shear wall attracted loads at the base of the structure.

From the plots of the distribution of damage in the structure and the results of the Monte Carlo simulations, the correlation between the overall damage index and the maximum damage index of the vertical elements can be made. The largest damage in frame structure I was approximately 1.75 times the overall damage index, thus local collapse of the vertical elements may occur at an overall damage index of 0.57. For frame structure II, the highest damage in the vertical elements was found to be 1.50 times the overall damage index. In this case, a damage index of 0.67 could produce local collapse in some of the columns. The relationship between the highest damage index in the vertical elements and the overall damage index was roughly 2.5 for the shear wall structure. Therefore an overall damage index of approximately 0.40 could result in collapse of the vertical elements on the first story. In all three structures, the correlation between the overall damage index and the peak damage index of the vertical elements was valid for both the mean and expected maximum damage indices.

An interesting observation can be made from the plots of the distribution of damage throughout the structures presented in chapter five. Mainly, the distribution of damage and the flexural behavior of the vertical elements of the structure are related. It is a well known fact that a frame structure behaves in shear with its floors remaining level when the structure deforms, and a shear wall behaves in flexure similar to a cantilever beam [19]. When there is a coupled frame shear wall structure, the system behaves in a combination of shear and flexure.

The interaction of frames and shear walls has been studied in the past, and the effect of the interaction of the two systems on the distribution of bending moment in the structure has been developed [30]. Figure 6.1 (a) shows the distribution of the flexural moment in the vertical elements for a shear wall structure and a coupled frame shear wall system. The dotted line represents the pure shear wall acting alone, and the solid line represents the coupled system. Note that the moment distribution has shifted to the right for the coupled frame shear wall structure. If the shear wall is removed, the flexural moment distribution shifts further to the right reducing the moment at the base and increasing the moment in the upper stories. This is evident from figure 6.1 (c) which represents the flexural moment in a strong shear frame.

The correlation of the damage index and the absolute value of the flexural behavior of the shear wall structure can be made with reference to figures 6.1 (b) and (e). From the figures, it is evident that the absolute value of the flexural moment has the same shape as the distribution of damage. Taking the absolute value of the moment for the comparison is justified because damage is quantified by an index which is always a positive quantity. The absolute moment is largest at

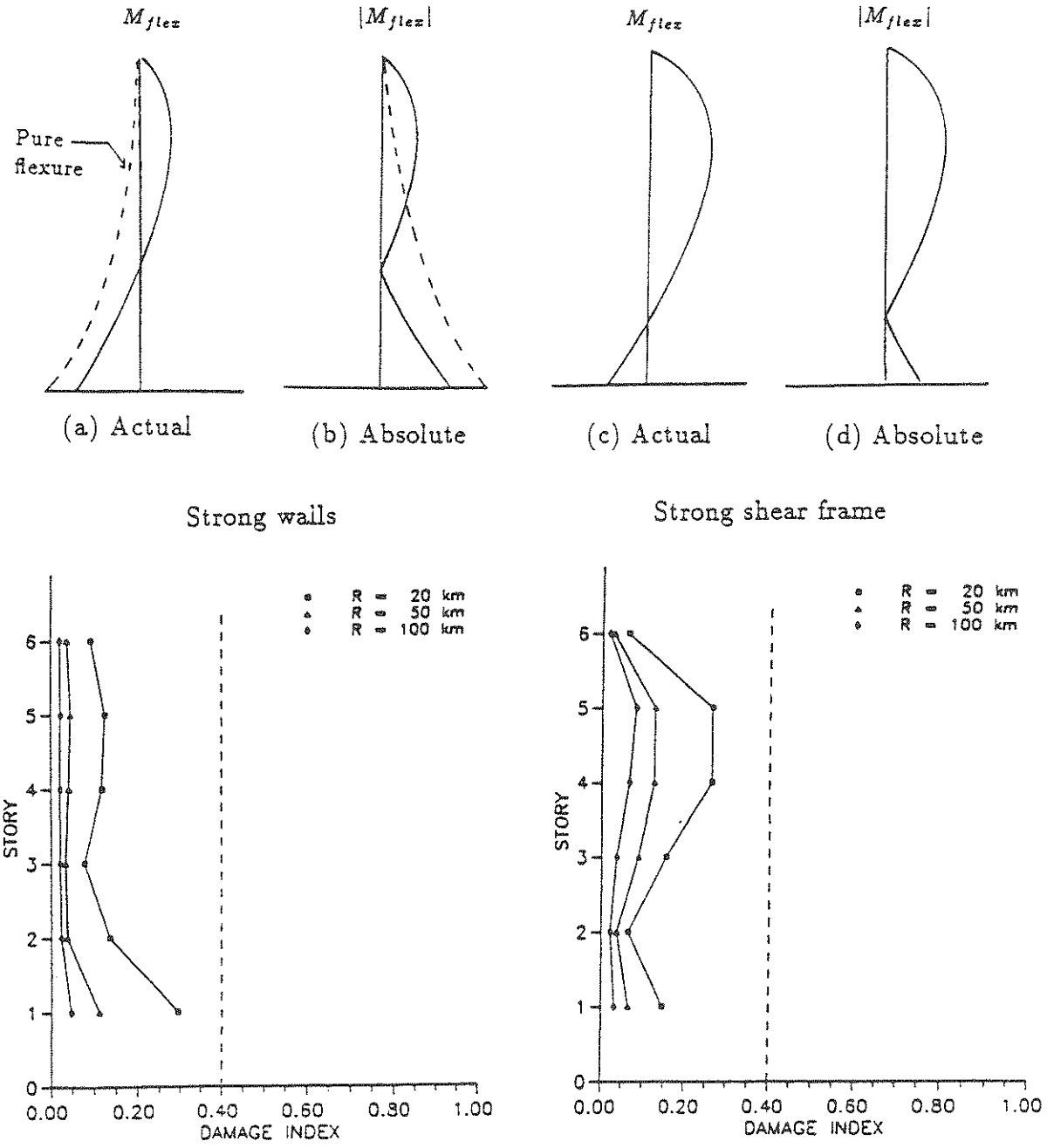

Figure 6.1
Flexural Moment Distribution and Damage Indices
in the Vertical Elements

the base and has a slight increase in the upper stories, this is the exact distribution of the damage index in the vertical elements discussed in section 5.4.3.

Similarly, the same correlation can be made for the frame structures with reference to figures 6.1 (d) and (f). In this case, the absolute value of the moment is largest in the upper stories and shows a slight increase at the base of the structure. Again this is exactly the way the damage index was distributed in the vertical elements of the frame structures. This correlation between the flexural moment distribution and the damage index indicates that the damage model and its implication in the program IDARC [25] adequately predicts the behavior of frame and coupled frame shear wall structures. It shows also that the damage index is strongly influenced by the flexural system (vertical elements such as columns and shear walls).

6.3 Comparison of Results

To assess the seismic hazard associated with different types of reinforced concrete structures, three test structures were considered - two frame structures and one coupled frame shear wall structure. The design of frame structure I was performed for gravity loads and resulted in "weak columns" and "strong beams". To determine the effect of member sizes on the resulting damage, frame structure II was designed identical to frame structure I, but with "weak beams". A shear wall was added to frame structure I to determine the damage associated with a coupled frame shear wall structure.

6.3.1 Failure Modes and Story Drift

A comparison of the failure modes of frame structure I and frame structure

II, figures 4.10 and 4.11 respectively, indicates that the reduced beam size caused only minor differences in the ultimate state of the structure. Mainly, the reduced beam sized caused increased yielding in the beams on the fourth floor and decreased yielding of the columns on the fifth story. The resulting mean story drifts from the Monte Carlo simulations for frame structure I and frame structure II are presented in tables 6.1 and 6.2 respectively. The story drifts are expressed as a percent of the story height, and all earthquakes had an epicentral distance of 20 km. Generally the story drifts of frame structure II were larger than the drifts of frame structure I, but the distribution of the drifts throughout the structure was the same for both frame structures. The largest drifts occurred on the fourth story because of the extensive yielding in the columns. The larger drifts of frame structure II were most likely caused by an increased flexibility of the structure resulting from weaker beams.

The effect of the shear wall on the failure mode of the structure can be made with reference to figures 4.10 and 4.12. The shear wall caused increased yielding in the beams and columns on the upper stories, but the wall itself remained elastic. Mean story drifts of the shear wall structure are presented in table 6.3, and are generally uniform throughout of the height of the structure with a slight increase in the drifts at the base of the structure. Even though the columns on the upper stories yield in the failure mode, the shear wall remained elastic and the upper stories deform elastically. Comparison of the drifts of the shear wall structure to frame structure I indicates the addition of the shear wall significantly reduced the drifts on the fourth and fifth stories.

Story (1)	M = 5.7 (2)	M = 6.2 (3)	M = 6.6 (4)	M = 7.0 (5)
6	0.3	0.4	0.6	1.2
5	0.8	1.3	3.8	6.7
4	1.0	1.6	4.9	8.7
3	1.0	1.6	4.1	7.5
2	1.0	1.4	3.9	7.0
1	0.9	1.1	3.0	5.9

Table 6.1
Mean story drifts (% of story height)
Frame structure I
Epicentral distance = 20 km

Story (1)	M = 5.7 (2)	M = 6.2 (3)	M = 6.6 (4)	M = 7.0 (5)
6	0.3	0.4	0.7	1.4
5	0.7	1.3	3.4	6.8
4	1.0	1.9	4.5	9.6
3	1.1	1.9	4.4	8.5
2	1.0	1.7	4.2	8.1
1	0.7	1.2	3.6	6.7

Table 6.2
Mean story drifts (% of story height)
Frame structure II
Epicentral distance = 20 km

Story (1)	M = 5.7 (2)	M = 6.2 (3)	M = 6.6 (4)	M = 7.0 (5)
6	0.4	0.7	1.4	2.1
5	0.4	0.7	1.4	2.1
4	0.4	0.7	1.4	2.1
3	0.4	0.7	1.5	2.2
2	0.4	0.8	1.9	2.6
1	0.4	0.8	1.7	1.7

Table 6.3
Mean story drifts (% of story height)
Shear wall structure
Epicentral distance = 20 km

6.3.2 Overall Damage

The effect of the reduced beams and the addition of the shear wall on the overall damage index can be deduced from a comparison of the test structures. Additionally, the seismic risk associated with each type of design can be concluded from the resulting damage indices.

A comparison of the overall damage of frame structure I and frame structure II indicates that the reduced beam size caused a decrease in the overall damage index. The mean and expected maximum overall damage index were reduced by approximately 25% when the "weak beams" were used. This was generally true for all magnitudes and epicentral distance combinations in the range considered.

The effect of the shear wall on the overall damage index can be determined from a comparison of the results of frame structure I and the shear wall structure. At epicentral distances close to 20 km the addition of the shear wall resulted in a 25% reduction in the overall damage index, but at larger epicentral distances the addition of the shear wall reduced the damage by approximately 50%. This large reduction in damage almost completely eliminated the damage for epicentral distances greater than 40 km, thus reducing the seismic risk.

A reduction in the overall damage index of the structure was seen for both modifications of frame structure I. The effect of the weak beams and the addition of the shear wall on the overall damage index was almost identical for earthquakes with epicentral distances less than 40 km. The shear wall resulted in a much higher reduction in the overall damage index than the weak beams when earthquakes with epicentral distances greater than 40 km were considered.

6.3.3 Local Damage

In section 6.2.2, the correlation between the overall damage index and the maximum damage in the vertical elements was found. The distribution of damage in the frame structures resulted with the maximum damage in the columns on the fourth and fifth stories and a slight increase in the damage on the first story. The largest story drifts occurred on the third, fourth and fifth stories, and the column sizes were 20, 18 and 16 inch square on these respective floors. Therefore the combination of large drifts and reduced column size resulted in large concentrations of damage on the fourth and fifth stories. The distribution of damage in the shear wall structure resulted in the highest damage at the base of the structure and a slight increase of the damage in the upper stories.

Frame structure I was found to have a peak damage in the vertical elements that was 1.75 times the overall damage index of the structure. When the beam size was reduced, the peak damage was only 1.50 times the overall damage index. Additionally, the overall damage index was reduced by 25%, therefore the reduced beam size had the effect of a 35% reduction in the peak damage of the vertical elements. This resulted because the weak beams allowed more flexibility in the joints, and thus reduced the amount of rotation taken by the ends of the columns. Therefore the damage in the columns decreased, and the damage in the beams increased slightly with the combined effect of reducing the overall damage index.

With the addition of the shear wall to frame structure I, the overall damage index was reduced from 25% to 50% depending on the epicentral distance, but the peak damage in the structure was 2.5 times the overall damage index. Therefore

at close epicentral distances, the peak damage in the vertical elements was greater than the peak damage in the vertical elements of frame structure I. For earthquakes with large epicentral distances, the addition of the shear wall reduced the peak damage in the vertical elements by 30%. If the damage of the shear wall on the first story could be controlled for earthquakes with small epicentral distances, the addition of the shear wall would be justifiable. An increase in the thickness of the shear wall on the first story will reduce the large concentrations of damage that were present. This is evident from table 6.4 which presents the distribution of damage in the vertical elements of the shear wall structure for varying wall thickness on the first story. The original thickness of six inches was not changed in the upper stories.

6.4 Conclusions

The results of this study can be used to assess the seismic hazard associated with reinforced concrete structures in the eastern United States. The structures considered were six stories and were primarily designed for gravity loads. If it is assumed that the design details were made adequately, analysis showed that the structures would satisfy the earthquake loads for seismic zone 2 of UBC [39] or a seismicity index of 2 according to ATC 03/06 [2]. The results of the Monte Carlo simulations showed that the structures would suffer only minor damage for any earthquake with a magnitude less than 6.0, and would be generally repairable. This magnitude limit was determined from consideration of the expected maximum overall damage of the structure. Additionally, any earthquake with an epicentral distance greater than 70 km would not produce severe damage.

There is a significant seismic hazard associated with the reinforced concrete

Story (1)	$t = 6''$ (2)	$t = 8''$ (3)	$t = 10''$ (4)
1	0.536	0.448	0.332
2	0.296	0.176	0.202
3	0.142	0.136	0.149
4	0.271	0.247	0.214
5	0.352	0.317	0.281
6	0.251	0.253	0.220
overall	0.260	0.227	0.189

Table 6.4
Variation of damage in the vertical elements of the shear wall structure with thickness of the wall on the first story
M = 6.2, R = 20 km

structures considered if an earthquake with a magnitude greater than 6.0 and an epicentral distance less than 70 km occurs. Irreparable damage would result in portions of the structure and there would be a possibility of total collapse of the structure.

When the initial design of the structure was modified with weaker beams, there was a decrease in the resulting damage, but the seismic hazard was still present for the magnitude epicentral distance combinations previously defined. The addition of the shear wall eliminated the seismic hazard associated with earthquakes that have epicentral distances greater than 40 km, but the hazard was still present for epicentral distances less than 40 km.

The results of the Monte Carlo simulations were used to develop an empirical equation to predict the resulting damage as a function of magnitude and epicentral distance. The dependence of the damage index on magnitude and epicentral distance was found to be the same for the three test structures considered. Therefore with adjustment of a constant k, the damage can be predicted for structures of different size and configuration. Additional studies could provide an empirical relationship between the coefficient k and the number of stories, the relative stiffness of the beams to columns, or several other parameters.

The accuracy of the results obtained depend on a number of factors. Due to the lack of actual recorded accelerograms for earthquakes in the eastern United States with large magnitudes, *simulated ground motion was used in the study.* If an actual accelerogram was available with a magnitude greater than 6.0, the corresponding damage could be calculated and compared to the predicted results. Furthermore, the program IDARC [25] assumes the reinforcement at the joints has adequate

development, suitable confinement and proper joint details to *provide the required ductility that was prescribed.* If the structure is constructed without proper joint details, the resulting damage would be larger and the associated seismic risk would increase.

The results of this study can be used for risk assessment of existing structures or for the study of test structures. The empirical relation can provide a method for quick assessment of expected damage in existing buildings, newly designed buildings or experimental models.

REFERENCES

1. Amin, M., and Ang, A.H.-S., "A Nonstationary Stochastic Model for Strong Motion Earthquakes," Struct. Res. Series 306, Univ. Ill. Dept. of Civil Engineering, April 1966.
2. Applied Technology Council,"Tentative Provisions for the Development of Seismic Regulations for Buildings," Special Publication No. 510, U.S. National Bureau of Standards, U.S. Government Printing Office, Washington, D.C., 1978.
3. Atkinson, G.M.,"Implications of Eastern Ground Motion Characteristics for Seismic Hazard Assessment in Eastern North America," Proceedings from the Symposium on Seismic Hazards, Ground Motion, Soil-Liquefaction and Engineering Practice in Eastern North America, Technical Report NCEER 87-0025, December, 1987.
4. Banon, H., Biggs, J.M., and Irvine, H.M.,"Seismic Damage in Reinforced Concrete Frames," Journal of Structural Engineering, Proc., ASCE, Vol. 107, No. ST9, Sept. 1981, pp 1713-1729.
5. Banon, H., and Veneziano, D., "Seismic Safety of Reinforced Concrete Members and Structures," Earthquake Engineering and Structural Dynamics, Vol. 10, 1982, pp. 179-193.
6. Bolt, B.B., "Duration of Strong Ground Motion," Proc. 5th WCEE, Vol. 1, Rome, 1973.
7. Boore, D. M., "Quantitative Ground Motion Estimates," Proceedings from the Symposium on Seismic Hazards, Ground Motion, Soil-Liquefaction and Engineering Practice in Eastern North America, Technical Report NCEER 87-0025, December, 1987.
8. Building Code Requirements for Reinforced Concrete, ACI Standards 318-83, American Concrete Institute, Detroit, Michigan, 1983.
9. Bycroft, G.N.,"White Noise Representation of Earthquakes," Journal of Engineering Mechanics Division, Proc., ASCE, Vol. 86, No. EM2, April 1960, pp 1-16.

10. Chang, F.K., and Franklin, A.G., "PGA, RMSA, PSDF, Duration and MMI," Ground Motions and Engineering Seismology, Developments in Geotechnical Engineering, Vol. 44, Elsevier Computational Mechanics Publications, 1987.
11. Chung, D.H., and Bernreuter, D.L., "Regional Relationships Among Earthquake Magnitude Scales," Seismic Safety Margins Research Program, NUREG/CR-1457, Lawrence Livermore Laboratory, Livermore, Calif., 1980.
12. Chung, Y.S., Meyer, C., and Shinozuka, M., "Seismic Damage Assessment of Reinforced Concrete Members," Technical Report NCEER-87-0022, Oct. 1987.
13. Clough, R.W., and Penzien, J. ,Dynamics of Structures, McGraw-Hill Book Co. Inc., New York, N.Y., 1975.
14. DiPasquale, E., and Cakmak, A.S., "Detection and Assessment of Seismic Structural Damage," Technical Report NCEER-87-0015, August 1987.
15. Dorby, Idriss, Chang, and Ng, "Influence of Magnitude, Site Conditions and Distance on Significant Duration of Earthquakes," Proc. 6th WCEE, Vol. 1, New Dehlhi, India, 1977.
16. Hammersley, J.M. and Handscomb, D.C.,Monte Carlo Methods, Halsted Press, A Division of John Wiley & Sons, Inc., New York, 1964.
17. Housner, G.W., and Jennings, P.C., "Generation of Artificial Earthquakes," Journal of Engineering Mechanics Division, Proc. ASCE, Vol. 90, No. EM1, 1964, pp 113-150.
18. Iwan, W.D., "A Model for the Dynamic Analysis of Deteriorating Structures," Proc. of 5th WCEE, Rome 1973.
19. Khan, F.R., and Sbarounis, J.A., "Interaction of Shear Walls and Frames," Journal of the Structural Division, Proc., ASCE, Vol. 90, No. ST3, June, 1964.
20. Lomnitz, C., and Rosenblueth, E., Seismic Risk and Engineering Decisions, Elsevier Scientific Publications Co., New York, N.Y., 1976.
21. Meyer, C., and Roufaiel, M.S.L., "Reliability of Damaged Reinforced Concrete Frames," Proc. 8th WCEE, Vol. 4, San Fran., Calif., 1984.
22. Newmark, N., and Rosenblueth, E., Fundamentals of Earthquake Engineering, Prentice Hall, 1974.

23. Nuttli, O.W., and Herrmann, R.B.,"Scaling and Attenuation Relationships for Strong Motion in Eastern North America," Proc. 8th WCEE, Vol. 2, San Fran., Calif., 1984, pp 305-310.

24. Nuttli, O.W., and Herrmann, R.B., "Ground Motion Relations for Eastern North American Earthquakes," Ground Motion and Engineering Seismology, Developments in Geotechnical Engineering, Vol. 44, Elsevier Computational Mechanics Publications, 1987.

25. Park, Y.J., Reinhorn, A.M., and Kunnath, S.K., "IDARC: Inelastic Damage Analysis of Frame Shear-Wall Structure," Technical Report NCEER 87-0008, July 1987.

26. Park, Y.J., Ang, A.H-S., and Wen, Y.K., 'Seismic Damage Analysis and Damage-Limiting Design of R/C Buildings," Civil Engineering Studies, SRS No. 516, University of Illinois, Urbana, October 1984.

27. Park, Y.J., and Ang, A.H-S., "Mechanistic Seismic Damage Model for Reinforced Concrete," Journal of Structural Engineering, ASCE, Vol. 3, No. 4, April 1985, pp 722-739.

28. Park, Y.J., Ang, A. H-S., and Wen, Y.K., "Seismic Damage Analysis of Reinforced Concrete Buildings," Journal of Structural Engineering, ASCE, Vol. 3, No. 4, April 1985, pp 740-757.

29. Pfaffinger, D.D.,"Calculation of Power Spectra from Response Spectra," Journal of Engineering Mechanics Division, ASCE, Vol. 109, No. 1, 1983, pp 357-372.

30. Rosman, R., "Laterally Loaded Systems Consisting of Walls and Frames," Tall Buildings : The Proceedings of a Symposium on Tall Buildings with Particular Reference to Shear Wall Structures, University of Southampton, April 1966.

31. Roufaiel, M.S.L., and Meyer, C., "Analytical Modeling of Hysteretic Behavior of R/C Frames," Journal of Structural Engineering, ASCE, Vol. 113, No. 3, March 1987.

32. Safak, E., "A Band-Limited, Windowed, White-Noise Process for Modeling Earthquake Motion," Ground Motions and Engineering Seismology, Developments in Geotechnical Engineering, Vol. 44, Elsevier Computational Mechanics Publications, 1987.

33. Schrieder, The Monte Carlo Method, Pergaman Press, 1966.
34. Shinozuka, M.,"Monte Carlo Solution of Structural Dynamics," Computers and Structures, Vol. 2, 1972. pp 874-885.
35. Shinozuka, M., and Sato, Y., "Simulation of Nonstationary Random Processes," Journal of Engineering Mechanics Division, ASCE, Vol. 93, No. EM1, Feb. 1967.
36. Somerville, P., "Source Scaling Relations of Large Eastern North American Earthquakes and Implications for Strong Ground Motion," Proceedings from the Symposium on Seismic Hazards, Ground Motion, Soil-Liquefaction and Engineering Practice in Eastern North America, Technical Report NCEER 87-0025, December, 1987.
37. Stephens, J.E., and Yao, J.T.P.,"Damage Assessment Using Response Measurements," Journal of Structural Engineering, ASCE, Vol. 113, No. 4, April 1987, pp 787-801.
38. Takeda, T., Sozen, M.A., and Nielsen, N.N., "Reinforced Concrete Response to Simulated Earthquakes," Journal of Structural Engineering, ASCE, Vol. 96., No. ST12, Dec. 1970, pp 2557-2573.
39. Uniform Building Code, International Conference of Building Officials, 5360 South Workman Mill Road, Whittier, Calif., 1985.
40. Vanmarcke, E.H., and Shih-Shenc, P.L., "Strong-Motion Duration and RMS Amplitude of Earthquakes Records," Bulletin of the Seismological Society of America, Vol. 70, No. 4, August 1980, pp 1293-1307.
41. Seidel, M.J., "Damage Assessment of Reinforced Concrete Structures in Eastern United States," M.S. Thesis, State University of New York at Buffalo, June 1988.
42. Kunnath, S.K., "Analytical Modeling of Inelastic Seismic Response of R/C Structures," ASCE, Journal of Structural Engineering, May 1988 (Submitted).

NATIONAL CENTER FOR EARTHQUAKE ENGINEERING RESEARCH
LIST OF PUBLISHED TECHNICAL REPORTS

The National Center for Earthquake Engineering Research (NCEER) publishes technical reports on a variety of subjects related to earthquake engineering written by authors funded through NCEER. These reports are available from both NCEER's Publications Department and the National Technical Information Service (NTIS). Requests for reports should be directed to the Publications Department, National Center for Earthquake Engineering Research, State University of New York at Buffalo, Red Jacket Quadrangle, Buffalo, New York 14261. Reports can also be requested through NTIS, 5285 Port Royal Road, Springfield, Virginia 22161. NTIS accession numbers are shown in parenthesis, if available.

NCEER-87-0001 "First-Year Program in Research, Education and Technology Transfer," 3/5/87, (PB88-134275/AS).

NCEER-87-0002 "Experimental Evaluation of Instantaneous Optimal Algorithms for Structural Control," by R.C. Lin, T.T. Soong and A.M. Reinhorn, 4/20/87, (PB88-134341/AS).

NCEER-87-0003 "Experimentation Using the Earthquake Simulation Facilities at University at Buffalo," by A.M. Reinhorn and R.L. Ketter, to be published.

NCEER-87-0004 "The System Characteristics and Performance of a Shaking Table," by J.S. Hwang, K.C. Chang and G.C. Lee, 6/1/87, (PB88-134259/AS).

NCEER-87-0005 "A Finite Element Formulation for Nonlinear Viscoplastic Material Using a Q Model," by O. Gyebi and G. Dasgupta, 11/2/87, (PB88-213764/AS).

NCEER-87-0006 "Symbolic Manipulation Program (SMP) - Algebraic Codes for Two and Three Dimensional Finite Element Formulations," by X. Lee and G. Dasgupta, 11/9/87, (PB88-219522/AS).

NCEER-87-0007 "Instantaneous Optimal Control Laws for Tall Buildings Under Seismic Excitations," by J.N. Yang, A. Akbarpour and P. Ghaemmaghami, 6/10/87, (PB88-134333/AS).

NCEER-87-0008 "IDARC: Inelastic Damage Analysis of Reinforced Concrete-Frame Shear-Wall Structures," by Y.J. Park, A.M. Reinhorn and S.K. Kunnath, 7/20/87, (PB88-134325/AS).

NCEER-87-0009 "Liquefaction Potential for New York State: A Preliminary Report on Sites in Manhattan and Buffalo," by M. Budhu, V. Vijayakumar, R.F. Giese and L. Baumgras, 8/31/87, (PB88-163704/AS).

NCEER-87-0010 "Vertical and Torsional Vibration of Foundations in Inhomogeneous Media," by A.S. Veletsos and K.W. Dotson, 6/1/87, (PB88-134291/AS).

NCEER-87-0011 "Seismic Probabilistic Risk Assessment and Seismic Margins Studies for Nuclear Power Plants," by Howard H.M. Hwang, 6/15/87, (PB88-134267/AS).

NCEER-87-0012 "Parametric Studies of Frequency Response of Secondary Systems Under Ground-Acceleration Excitations," by Y. Yong and Y.K. Lin, 6/10/87, (PB88-134309/AS).

NCEER-87-0013 "Frequency Response of Secondary Systems Under Seismic Excitation," by J.A. HoLung, J. Cai and Y.K. Lin, 7/31/87, (PB88-134317/AS).

NCEER-87-0014 "Modelling Earthquake Ground Motions in Seismically Active Regions Using Parametric Time Series Methods," G.W. Ellis and A.S. Cakmak, 8/25/87, (PB88-134283/AS).

NCEER-87-0015 "Detection and Assessment of Seismic Structural Damage," by E. DiPasquale and A.S. Cakmak, 8/25/87, (PB88-163712/AS).

NCEER-87-0016 "Pipeline Experiment at Parkfield, California," by J. Isenberg and E. Richardson, 9/15/87, (PB88-163720/AS).

NCEER-87-0017 "Digital Simulation of Seismic Ground Motion," by M. Shinozuka, G. Deodatis and T. Harada, 8/31/87, (PB88-155197/AS).

NCEER-87-0018 "Practical Considerations for Structural Control: System Uncertainty, System Time Delay and Truncation of Small Control Forces," J. Yang and A. Akbarpour, 8/10/87, (PB88-163738/AS).

NCEER-87-0019 "Modal Analysis of Nonclassically Damped Structural Systems Using Canonical Transformation," by J.N. Yang, S. Sarkani and F.X. Long, 9/27/87, (PB88-187851/AS).

NCEER-87-0020 "A Nonstationary Solution in Random Vibration Theory," by J.R. Red-Horse and P.D. Spanos, 11/3/87, (PB88-163746/AS).

NCEER-87-0021 "Horizontal Impedances for Radially Inhomogeneous Viscoelastic Soil Layers," by A.S. Veletsos and K.W. Dotson, 10/15/87, (PB88-150859/AS).

NCEER-87-0022 "Seismic Damage Assessment of Reinforced Concrete Members," by Y.S. Chung, C. Meyer and M. Shinozuka, 10/9/87, (PB88-150867/AS).

NCEER-87-0023 "Active Structural Control in Civil Engineering," by T.T. Soong, 11/11/87, (PB88-187778/AS).

NCEER-87-0024 "Vertical and Torsional Impedances for Radially Inhomogeneous Viscoelastic Soil Layers," by K.W. Dotson and A.S. Veletsos, 12/87, (PB88-187786/AS).

NCEER-87-0025 "Proceedings from the Symposium on Seismic Hazards, Ground Motions, Soil-Liquefaction and Engineering Practice in Eastern North America, October 20-22, 1987, edited by K.H. Jacob, 12/87, (PB88-188115/AS).

NCEER-87-0026 "Report on the Whittier-Narrows, California, Earthquake of October 1, 1987," by J. Pantelic and A. Reinhorn, 11/87, (PB88-187752/AS).

NCEER-87-0027 "Design of a Modular Program for Transient Nonlinear Analysis of Large 3-D Building Structures," by S. Srivastav and J.F. Abel, 12/30/87, (PB88-187950/AS).

NCEER-87-0028 "Second-Year Program in Research, Education and Technology Transfer," 3/8/88, (PB88-219480/AS).

NCEER-88-0001 "Workshop on Seismic Computer Analysis and Design of Buildings With Interactive Graphics," by J.F. Abel and C.H. Conley, 1/18/88, (PB88-187760/AS).

NCEER-88-0002 "Optimal Control of Nonlinear Flexible Structures," J.N. Yang, F.X. Long and D. Wong, 1/22/88, (PB88-213772/AS).

NCEER-88-0003 "Substructuring Techniques in the Time Domain for Primary-Secondary Structural Systems," by G. D. Manolis and G. Juhn, 2/10/88, (PB88-213780/AS).

NCEER-88-0004 "Iterative Seismic Analysis of Primary-Secondary Systems," by A. Singhal, L.D. Lutes and P. Spanos, 2/23/88, (PB88-213798/AS).

NCEER-88-0005 "Stochastic Finite Element Expansion for Random Media," P. D. Spanos and R. Ghanem, 3/14/88, (PB88-213806/AS).

NCEER-88-0006 "Combining Structural Optimization and Structural Control," F. Y. Cheng and C. P. Pantelides, 1/10/88, (PB88-213814/AS).

NCEER-88-0007 "Seismic Performance Assessment of Code-Designed Structures," H.H-M. Hwang, J-W. Jaw and H-J. Shau, 3/20/88, (PB88-219423/AS).

NCEER-88-0008 "Reliability Analysis of Code-Designed Structures Under Natural Hazards," H.H-M. Hwang, H. Ushiba and M. Shinozuka, 2/29/88.

NCEER-88-0009 "Seismic Fragility Analysis of Shear Wall Structures," J-W Jaw and H.H-M. Hwang, 4/30/88.

NCEER-88-0010 "Base Isolation of a Multi-Story Building Under a Harmonic Ground Motion - A Comparison of Performances of Various Systems," F-G Fan, G. Ahmadi and I.G. Tadjbakhsh, 5/18/88.

NCEER-88-0011 "Seismic Floor Response Spectra for a Combined System by Green's Functions," F.M. Lavelle, L.A. Bergman and P.D. Spanos, 5/1/88.

NCEER-88-0012 "A New Solution Technique for Randomly Excited Hysteretic Structures," G.Q. Cai and Y.K. Lin, 5/16/88.

NCEER-88-0013 "A Study of Radiation Damping and Soil-Structure Interaction Effects in the Centrifuge," K. Weissman, supervised by J.H. Prevost, 5/24/88, to be published.

NCEER-88-0014 "Parameter Identification and Implementation of a Kinematic Plasticity Model for Frictional Soils," J.H. Prevost and D.V. Griffiths, to be published.

NCEER-88-0015 "Two- and Three-Dimensional Dynamic Finite Element Analyses of the Long Valley Dam," D.V. Griffiths and J.H. Prevost, 6/17/88, to be published.

NCEER-88-0016 "Damage Assessment of Reinforced Concrete Structures in Eastern United States," A.M. Reinhorn, M.J. Seidel, S.K. Kunnath and Y.J. Park, 6/15/88.